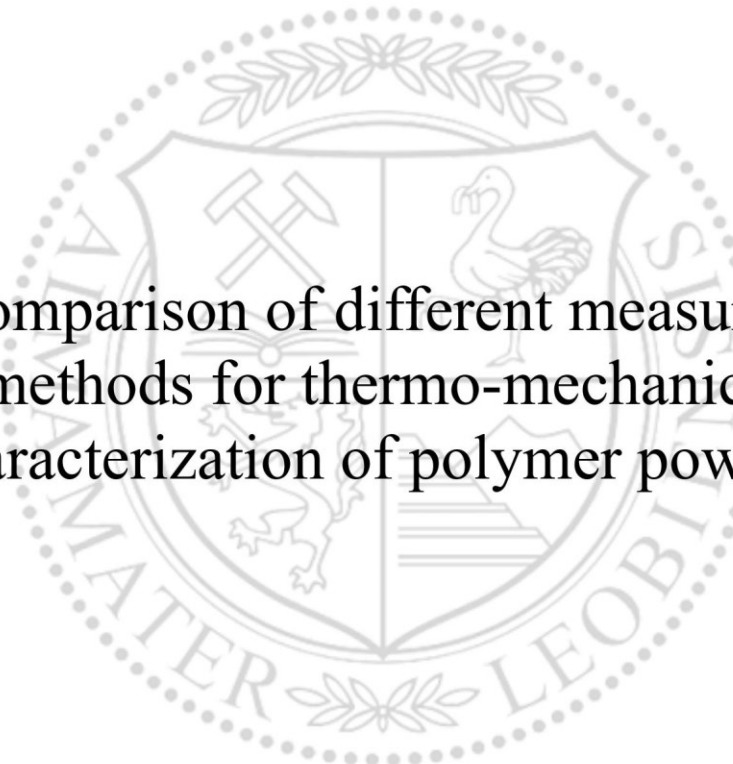Chair of Materials Science and Testing of Polymers

Master's Thesis

Comparison of different measuring methods for thermo-mechanical characterization of polymer powders

Thomas Tröscher, BSc

May 2023

ACKNOWLEDGEMENT

KURZFASSUNG

In der heutigen Industrie sind Polymerpulver in vielen verschiedenen Anwendungen anzutreffen. Einige Beispiele dafür sind, die Herstellung von Schleifmittel, das Drucken eines Prototyps mittels additiver Fertigung und das Beschichten von Metalloberflächen. Ebenfalls haben sich Polymerpulver für einige Kunststoffarten als bevorzugter Feedstock etabliert. Sowohl Polyvinylchlorid als auch Spezialanwendungen aus Polytetrafluorethylen sind ursprünglich in pulvriger Form den Verarbeitungsmaschinen zuzuführen. Die verarbeitungstechnischen und anwendungstechnischen Eigenschaften sind hierbei hinsichtlich ihrer Temperaturabhängigkeit kritisch zu Beurteilen. Eigenschaften wie die Fließfähigkeit, Kohäsion und der effektive innere Reibungswinkel der Pulver scheinen in starker Verbindung zum thermomechanischen Zustand zu stehen. Somit ist die Bestimmung von Übergangstemperaturen wie die Glasübergangstemperaturen oder die Nebenerweichungstemperaturen für Polymerpulver unumgänglich.

Ziel dieser Masterarbeit ist die Ermittlung thermomechanischer Eigenschaften verschiedenerer Kunststofftypen im pulverförmigen Zustand und der Vergleich der Ergebnisse mit konventionellen Prüfmethoden wie Differential scanning calorimetry (DSC) und Dynamisch Mechanische Analyse (DMA) von Festkörpern. Hierzu wurden sowohl die DMA von Pulverproben mit Verwendung eines speziellen Behälters („Powder Pocket") für die Dual Cantilever Anordnung als auch Methoden der Pulverrheologie herangezogen. Die Methoden zur Probenvorbereitung sowie zur Durchführung der Messungen wurde im Laufe der Arbeit optimiert. Hierzu wurden Parameter wie das Festspannmoment, das Füllvolumen, die Verteilung des Pulvers und das Material der Powder Pocket variiert, sowie eine geeignete Vorkomprimierung gefunden.

Die Wahl des Metalls der Powder Pocket und das Füllvolumen scheinen den größten Einfluss auf die Messqualtät zu haben. Die Empfindlichkeit des Messsignals ist vergleichbar mit DSC, jedoch konnten zusätzliche Übergänge bei PA12 und im Tieftemperaturbereich von PTFE gemessen werden, die mittels DSC nicht möglich waren. Mithilfe pulverrheologischer Methoden konnten thermische Übergänge nur grob ermittelt werden. Jedoch konnte der Einfluss von Übergangstemperaturen auf die Veränderung von praxisrelevanten Pulvereigenschaften gezeigt werden.

ABSTRACT

Polymer powders play a vital role in the current industry and are used in various applications. A few examples are the fabrication of abrasives, printing a prototype via additive manufacturing and coating metal surfaces. Polymer powders became the feedstock of choice for several polymer types. Commonly used Polyvinylchloride, as well as the more specialized Polytetrafluoroethylene, are fed to processing machines as powders. Critically evaluating the thermal dependency of properties, relevant for production and application is a key requirement. Properties like the flowability, cohesion and effective angle of internal friction appear to be connected to the thermo mechanical state of powders. Therefore, determining transition temperatures like the glass transition temperature or second order relaxation temperatures is of utmost importance.

The aim of this master thesis is the determination of thermomechanical properties of different types of polymer powders and compare them to conventional testing methods, such as Differential scanning calorimetry and Dynamic Mechanical Analysis (DMA) of solid samples. Polymer powders were tested via DMA, here a special container ("Powder Pocket") allowed for a measurement in a Dual Cantilever setup. A second characterization method evaluated was connected to powder rheological properties. Over the course of this thesis, the sample preparation and the conduct of the measurement were optimized. For this purpose, several different parameters were evaluated such as, the tightening torque, the sample volume and distribution, the material of the Powder Pocket and a compression step before measuring.

The metal of the Powder Pocket and the sample volume had the biggest influence on the measurement. The sensitivity regarding the measurement is comparable with DSC. However, with powder DMA, additional transition temperatures could be detected in PA12 and the low temperature range of PTFE. Powder rheological methods could only roughly determine the transition temperature of powders. Nonetheless, the connection of process relevant properties and their change at transition temperatures was observed.

CONTENT

SYMBOLS AND ABBREVIATIONS

Units:

°C	Degree Celsius
K	Celvin
Pa	Pascal
J	Joule
g	Gram
l	liter
min	minute
m	meter
Hz	Hertz

Symbols

T_g	Glass transition Temperature [°C]
ΔT_g	Difference between two Tgs (usually solid-powder) [°C]
T_{gg}	Secondary Relaxation Temperature [°C]
Tm	Melting Temperature [°C]
Tc	Crystalline Transition Temperature [°C]
σ	Stress [Pa]
ε	Strain [1]
E'	Storage Modulus [MPa]
E''	Loss Modulus [MPa]
Tan δ	Loss Factor
k	Slope of the linearized yield locus[1]
d	Intercept of the linearized yield locus with the y-axis [Pa]
R	Radius of the big Mohr's Circle [Pa]
x_0	Horizontal position of the Center of small Mohr Circle [Pa]
σ_M	Center of big Mohr Circle [Pa]
σ_P	Preshear normal stress [Pa]
τ_P	Preshear shear stress [Pa]
σ_1	Major Principle Stress [MPa]
σ_2	Minor Principle Stress [MPa]
σ_c	Unconfined Yield Strength [MPa]

ff	Flow Function [1]
c	Cohesion [Pa]
φ_{lin}	Angle of linearized yield locus [°]
φ_{ef}	Effective angle of internal friction [°]
X_c	Degree of crystallinity [%]
ΔH_m	Melting enthalpy [J/g]

Abbreviations:

DMA	Dynamic Mechanical Analysis
DSC	Differential Scanning Calorimetry
PVC	Polyvinyl chloride
E-PVC	Emulsion Polyvinyl chloride
S-PVC	Suspension Polyvinyl chloride
PA12	Polyamide 12
PA11	Polyamide 11
TPE	Thermoplastic Elastomer
TPE-U	Thermoplastic Elastomer Urethane Type
TPE-S	Thermoplastic Elastomer Styrene Type
TPE-O	Thermoplastic Elastomer Olefine Type
MPR	Melt processible rubber
MDI	Methylene diphenyl diisocyanate
HDI	Hexamethylene diisocyanate
PTFE	Polytetrafluoroethylene
$PTFE_{Tg}$	Polytetrafluoroethylene (temperature range close to glass transition)
$PTFE_{Tc}$	Polytetrafluoroethylene (temperature range close to crystalline transition)
$PTFE_{Tgg}$	Polytetrafluoroethylene (temperature range close to secondary relaxation)
PVDF	Polyvinylidene fluoride
SLS	Selective Laser Sintering
EVA	Evaporation Unit
CTD	Convection Temperature Device
MCR	Modular Compact Rheometer
GCU	Gas Chiller Unit
CTL	Cantilever
DoE	Design of Experiment

LIST OF FIGURES

1 INTRODUCTION

Polymers are most commonly processed in a granulate form allowing for efficient and clean production. However, prior to being granulated, polymers tend to be powders. The finished product of polymerization methods such as solution polymerization[1,2], emulsion polymerization[2] , suspension polymerisation[3] and gas phase polymerization[4] are powders which are usually directly compounded to granulate. In specific cases, the polymer powder remains in powder form as it is advantageous or necessary for its application, such as powder coating in the automotive[5] and furniture[6] industry, producing prototypes via additive manufacturing[7] and in the medical field[8].

Knowing the essential properties of the powder is inevitable for some applications. Well-established methods can be found for testing properties connected to the geometry of the powder particles, such as the determination of the bulk density, particle size distribution and specific surface. The bulk density is obtained via gravimetrical measurement of a known volume. Particle size distributions are determined via screening methods. The method generally depends on the range of particle sizes that should be screened for. Large particles ($\varnothing$ ~ 1 mm) are measured via sieves or image analysis, while small particles ($\varnothing$ ~ 10 nm) are measured via dynamic light scattering. The specific surface is determined via Brunauer–Emmett–Teller measurements which rely on the adsorption of an inert gas (usually nitrogen). In contrast, mechanical tests, especially thermo-mechanical tests, are more niche and focus mainly on the flowability and friction of particles. Those tests are essential for the design of storage and transportation methods of powders. For example, bridging is a big problem in hoppers caused by strong cohesion and friction between particles.[9–11]

These properties are suspected of changing with a change in the polymer's morphology and state, particularly above the glass transition temperature. Therefore, the determination of transition temperatures must be conducted on the polymer powders themselves. Currently, the most common way of analyzing transition temperatures in powders is Differential scanning calorimetry (DSC). This test is of thermal nature and is, therefore also applicable for the determination of thermal phenomena of the polymer. The characteristic temperatures can deviate from a temperature measured by thermo-

mechanical tests, which is closely related and more relevant to the application. A method described by Lee[9] called "Non-isothermal dynamic extrusion rheometer" uses a plunger to apply a force on the powder while continuously heating the sample. The material is pushed through a small gap when reaching its melting temperature, but changes in the material response can be measured before flowing occurs. Other methods use a metal container (powder pocket) that holds the powder in place, making Dynamic Mechanical Thermal Analysis (DMA) possible. In this master thesis, the thermo-mechanical characterization of various polymer types in powder form was conducted with a Powder Pocket system designed by Anton Paar in order to investigate the applicability and significance of this method. The results of these measurements were used for the adjustment and evaluation of further tests regarding powder-specific properties and their change caused by transition temperatures. A further objective of the thesis is the comparison and discussion of the thermo-mechanical results by DMA to other conventionally used powder characterization methods such as DSC and powder rheological shear tests.[12]

2   FUNDAMENTALS

2.1   Thermomechanical material behavior

One of the key properties distinguishing polymers from other common materials, such as metals or ceramics, is their substantial temperature and time dependence of their mechanical properties. Describing a polymer's mechanical response to a certain load or deformation is done with a viscoelastic material model. The main characteristic of viscoelasticity is the delayed material response after loading, resulting in time-dependent material properties. Linear viscoelasticity is a special case of viscoelasticity in which the material's response is no longer dependent on the load level. This behavior is only valid for very small deformation and varies for different polymers. Linear viscoelasticity is most easily determined in a dynamic mechanical analysis by continuously increasing the load amplitude. As long as the measured elastic modulus remains constant, linear-viscoelastic behavior is present. Higher loading decreases elastic modulus and marks the non-linear viscoelastic range. Generally, polymers can be distinguished into amorphous polymers without molecular order and semi-crystalline polymers with amorphous and crystalline phases. Both show a different mechanical response to an increased temperature due to their different relaxation mechanisms. Three properties are usually chosen to evaluate the thermo-mechanical behavior. The storage modulus E', loss modulus E'' and the loss factor tan delta show a significant change over a temperature range.[13]

Physical links between polymer chains cause the structural stability of a polymeric material. The whole variety of molecular interaction forces such as dipole-dipole-bonds, inductive forces, dispersion forces and hydrogen bonds, as well as physical links called entanglements, play a substantial role regarding mechanical properties such as tensile strength and Young's modulus. The entanglements are rarely untangled at low temperatures and therefore act as fixation points in the molecular chain. Several different regions can be defined between certain transition temperatures, as showcased in Figure 1. In the glassy state at low temperatures, the polymer is brittle and elastic. This mechanical behavior is attributed to the low mobility of the polymer chains at this temperature. The β-transition temperature, also called secondary relaxation temperature, marks the

temperature at which small-scale local movement can occur in the polymer chain. Prior to this temperature, the activation energy necessary for those movements is not reached. The next relaxation range is the glass transition region, marked by the glass transition temperature (T_g). Here another activation energy is overcome, allowing for the rotation and rearrangement of chains in the amorphous region. With this increased mobility, the stiffness decreases drastically. The scale at which stiffness is lost depends on the morphology of the polymer. Semi-crystalline polymers contain proportionally less amorphous material and, therefore, react less drastically regarding stiffness loss. Semi-crystalline polymers operating temperature is located either below or above T_g in the rubbery plateau or entropy elastic region. This region increases the toughness of the polymer substantially, allowing for applications related to spontaneous mechanical loads such as impacts. Amorphous polymers should be operated at temperatures below T_g as they lose most of their mechanical properties at T_g. The melting point T_m indicates the beginning of the liquid flow region. Here the crystalline portion of the semi-crystalline polymer melts. Compared to metals, polymers don't possess a well-defined melting point but rather a temperature range at which melting occurs. The temperature range is caused by the different sizes of the molecular lamella packages formed in the crystalline region. Big lamella need more energy and therefore melt at higher temperatures.[13,14]
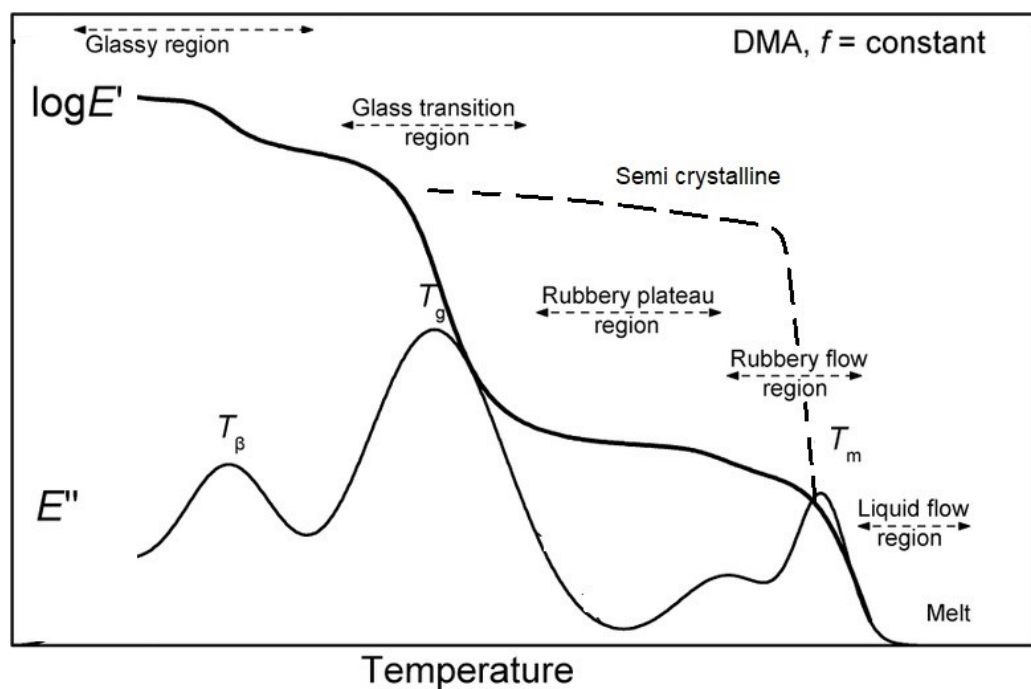
Figure 1:   Thermo-mechanical behavior of an amorphous polymeric material. The dotted line depicts the behavior of a semi-crystalline polymer.[15]

Thermoplastic elastomers (TPE) are special regarding their thermo-mechanical behavior. They consist of two phases, the hard segment and the soft segment, each with a specific reaction to a change in temperature as seen in Figure 2. The T_g of the soft segment is usually located in the negative temperature range. It allows TPE to exhibit elastomer-like properties and marks the beginning of the operating temperature for TPE. Below that temperature, TPE is rigid and brittle. Usually, conventional elastomers cannot be melted due to the crosslinked polymer chains creating a 3D-network. TPE's crosslink points are formed by the hard thermoplastic segment and are therefore temporary. The amount of hard segment linking points has an influence on the overall mechanical behavior in the elastomeric region. A higher hard segment content increases the stiffness at operating temperature. Reaching T_g or T_m of the hard segment allows TPE to flow and be shaped into any form.[16]
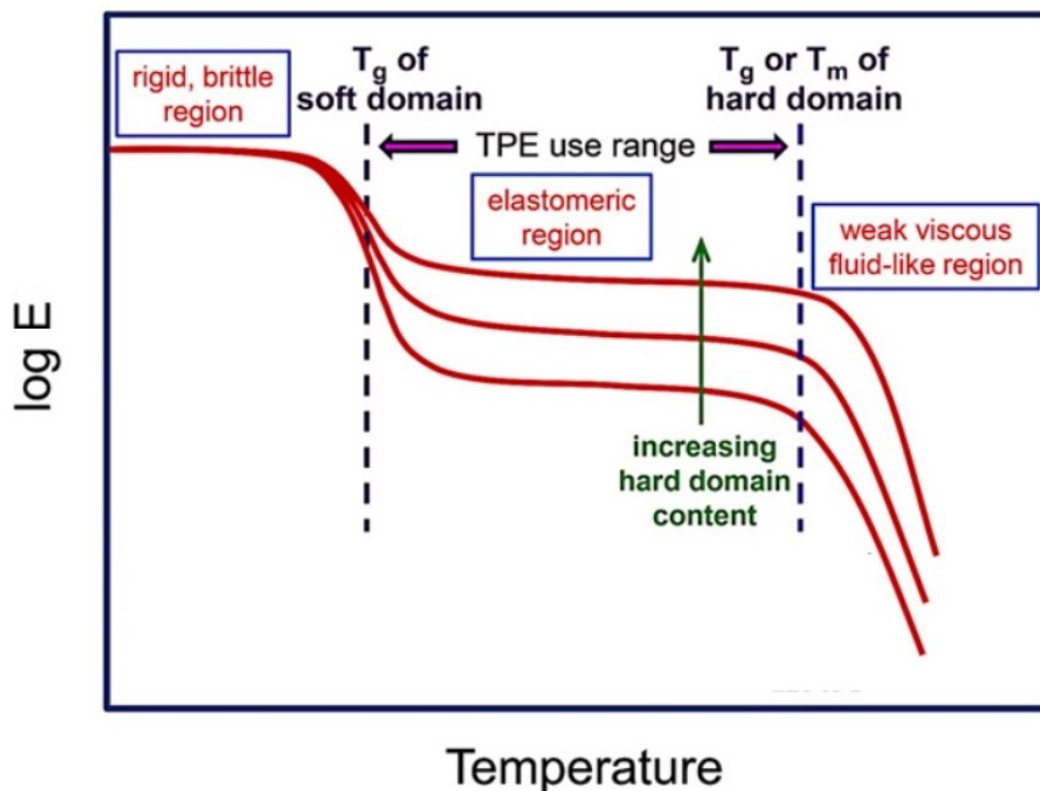
Figure 2:   Thermo mechanical behavior of TPE shows the softening of the soft and hard segments, respectively.[17]

2.2   Powder polymers and their application

Powders are made from a collection of particles with a certain distribution in size and shape. This collection can be split into two phases. The particles themselves represent the solid phase, while the air or gas in between the particles is considered the continuous phase. A particle within a powder possesses different relevant properties, for example, the specific surface, porosity and density, which further influence the properties of the complete powder system. A powder with a higher specific surface allows for better adsorption of other chemical compounds, which is relevant for industrial filters. The surface area is not only calculated from the general shape (such as the diameter of a sphere) but also depends on the porosity as it creates additional surfaces. Regarding powders, there are several different densities which can be defined. The true density ρ_{true} describes the density of the material without any porosity or inclusions, usually depending on the elements within the material. The particle density ρ_{part} considers inclusions and porosity. The most relevant density for powder application is the bulk density ρ_{bulk} which includes the fluid between particles. Especially for logistical problems, the bulk density is of utmost importance as it is essential for calculating the needed space while transporting.[18–20]

The original state of most polymers is a powder form, and it originates from the synthesis process. Basic properties, such as particle size distribution, porosity, and molecular mass, depend on the type of polymerization and the parameters used. In most cases, adding additives and extruding pellets enhances a polymer's properties. Adding additional chemicals to powders is quite different to compounding via extrusion, as the temperatures are not allowed to exceed the melting or flowing point of the material to prevent the particles from fusing and sticking together. Powders modified by additives are called Dryblends and are produced in a two-step process. First, the powder is added to a hot fluid mixer where additives are melted, allowing easier diffusion into the powder. The second step is cooling down the powder in a cool-fluid mixer. Both the hot and the cold fluid mixer need good ventilation to remove unwanted gas components such as moisture. When the powder is fully cooled down, it is sieved to remove any agglomerations that might have formed due to moisture or temperature. Storing the powder for at least a day ensures that the diffusion processes are completed and a steady state is achieved. Overall, the

knowledge of the thermo-mechanical and thermo-rheological behavior is a prime requisite for sufficient processing quality of polymer powders [21]

2.2.1   Polyvinyl chloride (PVC)

PVC currently has the third largest production volume among polymers, only outmatched by PE and PP. That makes PVC the most used polymer powder as most production processes use PVC in powdery form for their products (roughly 80 %). PVC is prone to thermo-oxidative decomposition, making processing at high temperatures a difficult endeavor. Therefore, powder feedstocks are preferred over pellets, removing the need to compound the material at high temperatures and risking degradation. PVC is an amorphous polymer with excellent all-round properties such as low permeability, good resistance to chemicals and low flammability and a T_g of around 90 °C[22]. Its biggest market is the building sector due to its inherent flame-retarding properties caused by the chlorine atom in its monomeric structure, as seen in Figure 3. Nonetheless, PVC has received much backlash from the general public and environmentalists due to its harmful effects on nature. Therefore, a reduction in PVC usage is foreseeable, at least in Europe and North America. [21,23]
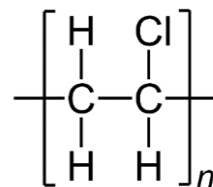
Figure 3: Chemical structure of PVC.[24]

In total, there are four different ways to synthesize PVC, leading to a difference in the finished product's particle size distribution, particle shape, porosity, and bulk density. S-PVC is synthesized in a suspension made from water and polyvinyl alcohol; it is also the most common way of synthesizing PVC. A particle diameter of roughly 50-150 µm can be expected from this process. The porosity is variable by changing the temperature of the reaction to higher temperatures, a decrease in porosity can be observed, resulting in a lower absorption rate of plasticizers. PVC with lower porosity is preferred when a high extrusion throughput must be achieved. E-PVC is synthesized in an emulsion made from

water and an emulsifier, for example, sodium dodecyl sulfate. Once the polymerization is finished, the emulsion is dried via spray drying. Two other less common ways of synthesizing PVC are in bulk or solution. All of those methods lead to different particle shapes and sizes that further influence the mechanical behavior of the powder [21,25,26]

Due to the already mentioned difference in the feedstock to most other polymers, PVC processing is a specialty amongst plastic processing companies due to the special machines needed for a successful and productive process. PVC must be processed with a twin-screw extruder in a counter-rotating setup compared to the commonly used single-screw extruder. This setup allows for excellent homogenization of the material and temperature control. Due to the temperature-sensitive nature of PVC, a hot spot at a specific position in the extruder could decrease the quality of the finished product.[21]

2.2.2 Polytetrafluoroethylene (PTFE)

Polytetrafluoroethylene (PTFE) is the most basic and most common linear fluoropolymer. The polymeric structure, shown in Figure 4, contains only carbon and fluorine. Even though this structure might seem simple at first glance, the corresponding properties that come with those fluorine atoms are complex and unique. PTFEs morphology is semi-crystalline, and due to its linear structure, a high degree of crystallinity is achievable (depending on the processing conditions). Polymers made from monomers that only contain fluorine and carbon are referred to as perfluorinated, while polymers that contain hydrogen in their chain, like polyvinylidene-fluoride (PVDF), are considered partially fluorinated polymers. This categorization is connected to the properties that come with those changes in chemical structure. Generally, when deciding between perfluorinated and partially fluorinated polymers for a specific application, the chemical resistance and mechanical properties are the deciding factor between those two fluoropolymer types.[27]
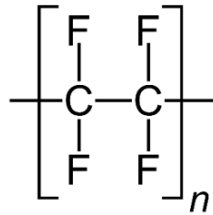
Figure 4: Chemical Structure of PTFE.[28]

Due to the high bonding strength of the C-C and C-F bonds, PTFE can withstand high temperatures. The size of the fluorine atoms in comparison to the carbon atoms allows for a shielding effect against any chemical attacks that might lead to depolymerization of the main molecule chain. Other interesting properties regarding powder rheological behavior are the low coefficient of friction, a low surface energy and electrical properties. [27]

The triboelectric series ranks materials depending on their ability to transmit charge via friction. This transmission depends on the material's electron affinity, electric conductivity, and several other factors. PTFE is placed on the negative end of the triboelectric series, which causes it to receive electrons. This effect can be used to charge particles positively in an electric spray gun to allow for easy application of said particle to a product's grounded surface.[29]

The high thermal stability of PTFE is one of its most unique properties in the spectrum of polymeric materials, but it also causes a significant downside of PTFE, its processability. At 380 °C, well above its melting temperature (327 °C[30]), PTFE still exhibits a very high melt viscosity. Further increase in temperature would lead to decomposition of the material. This makes conventional melt processing that depends on a certain flowability, like injection molding and melt extrusion, impossible. Granulation is not preferred due to the inability to compound the material. The work around for this hindrance is a sintering process. Two processes have been established for processing PTFE, namely Ram Extrusion (continuous process) and compression molding (discontinuous process). For those processes, PTFE powder is used as a feedstock.[31]

PTFE, in comparison to most other polymers, possesses four transition temperatures that are of interest. Two of them are related to the amorphous region. A secondary relaxation

process (T_{gg}) is located at roughly -103 °C[32] and T_g at 116 °C[32]. Both transitions are caused by increased mobility in the amorphous domain, but it is essential to differentiate between the mobile amorphous fraction and the rigid amorphous fraction, the later with reduced molecular mobility due to the proximity of the crystalline regions. The secondary relaxation process is correlated with this rigid amorphous fraction, while Tg is assigned to the undisturbed, mobile amorphous region. Nevertheless, those transitions are still heavily debated concerning their classification. In between those two transition temperatures of the amorphous phase lie two transition temperatures (T_c) at 19 °C[33] and 30 °C[33], which are correlated with changes in the crystalline modification. In most measuring methods, those two temperatures cannot be differentiated from each other due to them overlapping. The first transition at 19 °C demonstrates dominance in regard to measured signals and influence on the material properties. Hence, the present thesis will only refer to the first transition temperature. The phase diagram for the crystalline modifications (phase I to IV) of PTFE is shown in Figure 5. Here Phase II represents a triclinic crystal modification found at low temperatures that transforms at 19 °C to Phase IV, a hexagonal crystal modification. The amount of CF_2 groups needed for a complete 180° turn in the helical molecular chain structure increases from 13 to 15 carbon atoms, and the repeatable distance increases from 0.169 to 0.195 nm. This change in molecular arrangement comes with several changes in mechanical properties, most notably a change in modulus and a powder-specific phenomenon called fibrillation. This fibrillation occurs when PTFE above 19 °C is subjected to shear stress and in contact with other PTFE particles. Due to the stress applied, singular PTFE fibrils are pulled out of the powder particles that cause entanglements in neighboring PTFE particles. These entanglements result in clumping and reduce the flowability of the powder, which can lead to further problems in a production line. Therefore, it is recommended that any transportation or storage of PTFE is done at a temperature below 19 °C. The transition to Phase I increases rotational disordering resulting in a pseudohexagonal modification. Consequently, the mobility increases and a decrease in stiffness occurs. Phase III only occurs at high pressures and is therefore irrelevant for the present thesis.[32,33]
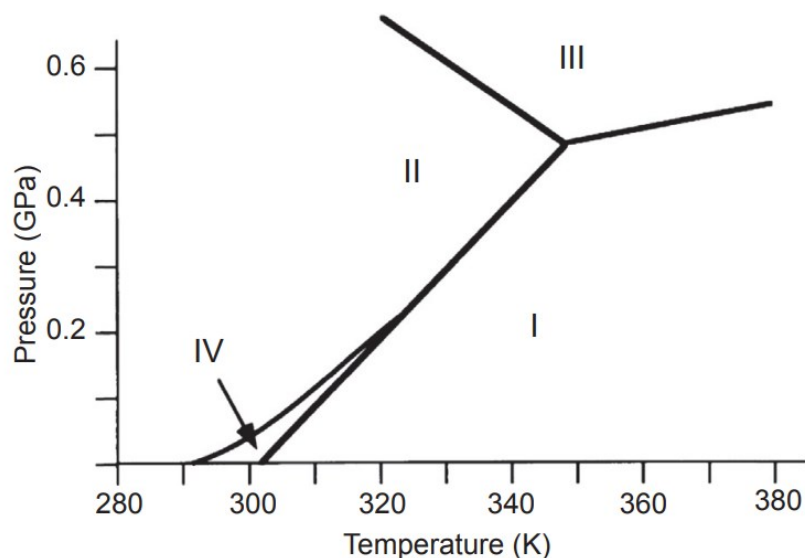
Figure 5:   A Phase diagram showing four different phases of crystalline morphology of PTFE as a function of pressure and temperature. [33]

2.2.3   Polyamide 12 (PA12)

Polyamide is one of the most versatile technical semi-crystalline polymers due to its broad range of mechanical properties. This range is caused by the hygroscopic nature and by the different varieties in molecular structure indicated by the number next to the name. In the case of PA12, there are 11 CH_2 units per amide group which makes 12 carbon atoms in total per repeating unit along the molecular chain, as seen in Figure 6. The frequency at which amide groups occur in the polymer chain determines the thermal and mechanical properties of the polymer. Amide groups can form hydrogen bonds that are generally stronger than Van-der-Waals bonds that occur due to the CH_2 groups.[34]
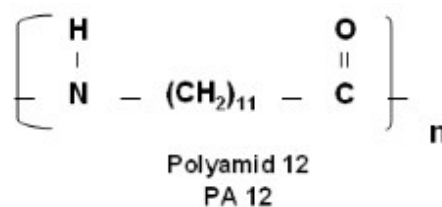
Figure 6: Chemical structure of PA12.[35]

Additionally, moisture absorption is heavily dependent on the number of amide groups due to the polarity of those groups. Powders are prone to moisture absorption due to their high

specific surface. Therefore, drying prior to processing is needed. For PA12, a moisture content of roughly 0.7 % is to be expected at 23 °C / 50 % r.H..[36,37]

PA12 shares its applications with PA11 in the field of coatings and additive manufacturing. Fluidized bed coating can produce thin layers with a thickness of down to 200 µm that can be applied to almost all products and geometries. Electrostatic powder coating is an alternative way of coating products with PA12. The main advantage of electrostatic powder coating is that no preheating step is needed. Pipes and wires can be coated in a continuous process via inductive heating. In recent years PA12 powders found popularity in an additive manufacturing process called selective laser sintering (SLS). In a few instances, PA12 is added to paints as an additive, increasing hardness, flexibility and wear resistance.[38,39]

PA12 is a semi-crystalline polymer. It can form several different types of crystal modification. The two most common ones are the α and γ-modification, which refer to the triclinic and monoclinic crystal modification. Most thermal processes usually result in a γ-modification while polymers obtained from solutions lead to an α-modification. PA12 Powders provided for SLS processes are produced from a solution. Typical processes are either spray drying or precipitation. Spray drying operates via the evaporation of the solvent in a furnace. Precipitation, on the other hand, is a much broader term for serval different approaches that yield polymeric microspheres directly from the polymerization process. Some examples are distillation precipitation, reflux precipitation, photo-induced precipitation, and self-stabilizing precipitation. The big difference to other polymerization methods is the lack of surfactant or stabilizers, which results in a much purer and therefore more controllable particle distribution. The α-modification present in those SLS-powders possesses a higher degree of crystallinity, which also influences the glass transition temperature.[39–42]

Three transition temperatures, γ-transition, β-transition and α-transition, can be found in PA12 and are located at roughly -135, -65 and 50 °C[43], respectively. They all relate to relaxation processes due to molecular motion within the amorphous phase of the semi-crystalline polymer. The γ-transition at -135 °C is not exclusive to PA12 but rather any material with a chemical structure that contains four methylene groups in succession, as the relaxation is caused by the movement of those methylene groups. The cause of the β-

transition is still heavily debated in the polymer science community. A study conducted by Le Huy et al.[44] reveals that the β-transition is not invariant to the solvent type as a change in the number of solvent molecules absorbed only influences the β-transition if the solvent is water. One explanation for the existence of this transition is the motion of water located between two amid groups. On the other hand, the α-transition or glass transition is influenced by any solvent that blocks or weakens the hydrogen bonding of the amid groups. A reduction in hydrogen bonds, by increased moisture content, the T_g shifts to lower temperatures as less energy is needed for molecular motion.[43,44]

2.2.4 Thermoplastic Elastomer (TPE)

Due to their unique processing and property profile, TPEs occupy a very special place in polymer engineering. Conventional elastomers such as butadiene rubber can only be shaped before curing. In comparison, TPEs can be processed like thermoplastic materials via injection molding or extrusion while keeping properties such as low Young's Modulus, high flexibility at low temperatures, high elasticity, and softness. This unique behavior is achieved by phase separation into a hard and soft segment. The hard segments create strong and rigid physical linking points comparable to the cross-linking points of an elastomer. As those linking points are not of chemical nature (no covalent bonds), the creation is reversible by heating the material to a specific temperature (melting point).[45]

Polyurethane elastomers are made from three basic chemicals, a polyether/polyester diol that will form the soft segment and determine the low-temperature behavior, a rigid diisocyanate primarily responsible for the hard segment and a chain extender that reacts with a diisocyanate to form the urethane groups and therefore also influencing the hard segment. The hard segment is the deciding factor for the TPE's upper operating temperature and melting point. As those three components are not limited to only one chemical structure, much variety can be achieved by combining the different components. That way, the properties can be tailored to the requirements.[46]

As already mentioned, TPE's properties are caused by the phase separation of a soft and hard segment. This phase separation is influenced by the compatibility of the chemicals used for each segment, the molecular weight, and additional thermal treatment such as annealing. The resulting morphology is detrimental to the properties of the material. TPEs

can be categorized into several types depending on the chemical group in the hard segment. The most common types are the urethane types (TPE-U or TPU) other types are the TPE-S (styrene type) and TPE-O (olefine-type). [46]

Some common chemicals used for TPE-U are:

- Soft segment: polyoxyproyplene diol, polyoxytetramethylene diol[46]
- Hard segment: 4,4'-diphenylmethane diisocyanate MDI, Hexamethylene diisocyanate (HDI)[46]
- Chain Extender: hydroquinone bis(2-hydroxyethyl) ether, 1,4 butanediol and ethylene glycol (for low hard segment content)[46]

Other common types of TPE are:

- TPS: Styrenic thermoplastic elastomers triblock copolymer structures (Styrene-Butadien-Styrene, Styrene-Isoprene-Styrene) used as an additive to optimize the tack in compounding processes. [46]
- TPO: Polyolefin-based thermoplastic elastomers used in automotive and wire/cables. Good resistance to weather and low density. Used in interior and exterior parts such as bumper covers and air dams and in electrical applications such as flexible cords.[46]
- MPR (Melt processible rubber): physical PVC/Nitril-Butaien blends with excellent resistance to oil and soft touch.[46]

The feedstock used for injection molded products is usually granulate-shaped. This allows for a high throughput when mass-producing items of relatively simple geometry. For more complex geometries, TPE-U powders are processed via SLS. The combination of structural freedom (e.g. lattice structures) and highly elastomeric properties allow TPE-U printed products to be highly resistant to shock and impact forces. [47]

2.3   Characterization methods for polymer powders

2.3.1   Dynamic Mechanical Analysis (DMA)

DMA is one of the most important testing methods in polymer science due to the large amount of information gained from a single measurement. It allows for thermo-mechanical characterization of viscoelastic materials by applying an oscillating (usually a sinusoidal waveform) force or displacement at a specific frequency. Depending on which parameter (force or displacement) is chosen, the other value is measured by the system. There are two measuring system types: stress controlled (preset force) and strain controlled (preset displacement) analyzers. Stress-controlled measuring systems are preferred over strain-controlled due to their higher accuracy and the option to measure in an indirect strain-controlled way. This is achieved by creating a feedback loop of the measured displacement/strain and adjusting the applied force accordingly. [48]

Prior to choosing the preset parameter, an amplitude sweep is required. An amplitude sweep is a measurement at constant temperature and a ramping force or displacement. A constant value for the modulus indicates the linear-viscoelastic range in which the measured values are independent of the applied load. A force or displacement value is chosen for the measurement within this range. Due to the polymer's viscoelastic behavior, the material response (strain ε) to a certain stress σ is delayed by a phase angle δ as demonstrated in Figure 7. This delay or phase angle is indicative of the material's storage modulus E´ and the loss modulus E´´. While E' represents the mechanically reversible part of the complex modulus E* and corresponds to the Young´s modulus at a similar loading time, E'' refers to the loss of mechanical energy converted into heat. The limits of the phase angle are 0 for an ideal elastic material and $\frac{\pi}{2}$ for an ideal viscous material, polymers exhibit both behaviors and therefore have a phase angle between 0 and $\frac{\pi}{2}$. Usually, the damping under dynamic load is determined from the phase angle δ as mechanic loss factor d = tan δ It is also the ratio of the loss to the storage modulus tan δ =E´´/E´. For thermomechanical characterization, the DMA experiment is carried out in a specific temperature range with a constant heating rate of usually 2 K/min. [48,49]
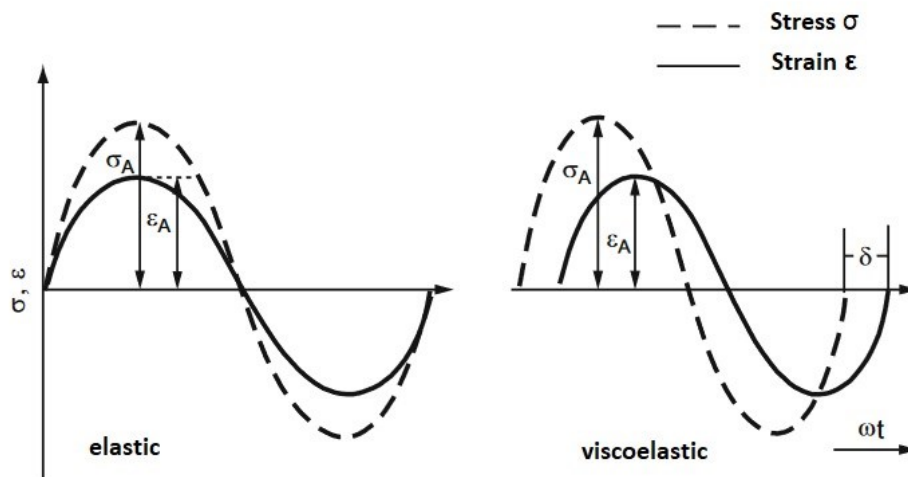
Figure 7 :   Comparison of the response of an elastic and a viscoelastic material to a dynamic stress.[13]

A significant influence on the measurement is the fixation of the sample in the analyzer and the sample dimension, more specifically, the accuracy that the sample dimensions can be measured. The latter mostly influences the measured modulus, while certain points of interest, such as transition temperatures, are less affected by it. Fixations are classified into axial and torsional fixations and are showcased in Figure 8. Torsional fixations in a parallel plate setup are mostly used for materials with very low stiffness, for example foams. Bending fixtures, such as the three-point bending fixture, are also included in the axial category and are mainly used for materials with high stiffness. The three-point bending fixture has no restraint in the horizontal direction. Due to the degree of freedom in the horizontal direction, the sample usually needs to be longer than the fixation to prevent sample slippage. The four points bending has the same requirements regarding the degree of freedom but applies the force with two edges instead of one, which results in a constant bending torque between those two edges. The cantilever fixation system expands the load case by an additional shear stress induced by the clamping on either two (single cantilever) or three (double cantilever) positions on the sample. The clamps prevent the sample's movement in the horizontal direction, resulting in a generally stiffer system and therefore, higher moduli. Commercially available DMA software includes a shear correction to counteract the higher values. [48]
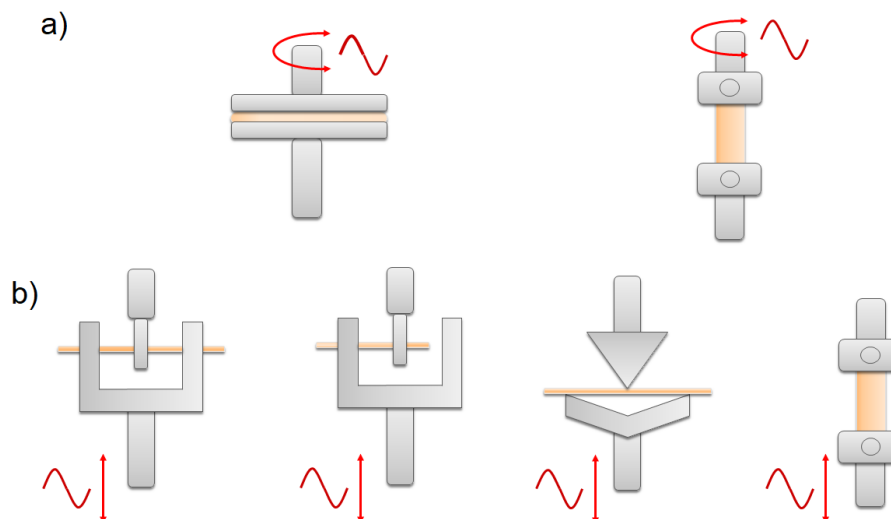
Figure 8:   Different types of fixtures used in DMA grouped by classification a) torsional fixtures from left to right: parallel plate (can also be used as an axial fixture), torsion fixture) b) axial fixtures from left to right: dual cantilever, single cantilever, 3points bending, tension fixture.

Measuring powders in DMA comes with a few difficulties in handling the sample. Free-flowing powders do not offer mechanical stability and can therefore not sustain their shape under load. Even cohesive powders have very low tensile strength. Consequently, a support material is needed to contain the powder. Different systems have been developed for powder characterization via DMA. Material Pocket by Perkin Elmer, Inc. (Waltham, US) consists of two metal sheets connected by a thin hinge mechanism which sandwiches the powder between the metal sheets. The Powder Clamp by TA Instruments, Inc. (US, New Castle) and the Powder Pocket by Anton Paar (Graz, AT) consist of two parts. Currently powder containers are only produced in stainless steel. The upcoming Powder Pocket by Anton Paar will also include aluminum containers. The lower part holds the powder, while the upper part closes the containment and allows for clamping at three different points. The corners of the Powder Pocket are open to enable humidity exchange with the environment. Figure 9 shows the Powder pocket system clamped in a double cantilever system. The yellow part of the Powder Pocket is the containment, while the blue part closes the container. The blue part (lid) has three ridges which allow for proper fixation. In the Anton Paar system, the bottom fixation is moveable, while the upper fixation is stationary. Due to the composite of metal and sample, the measured moduli will be much higher, therefore this assembly is not valid for any quantitative assessment regarding the

determination of the absolute value of the modulus. Nonetheless, changes in the modulus are still visible and can be used to assess the transition temperatures of polymer powders. [48,50–52]
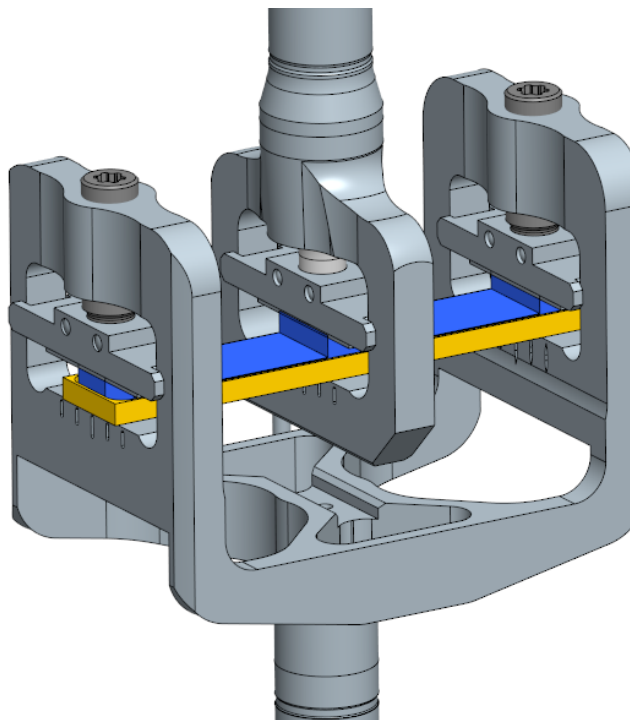
Figure 9:   A standard testing setup for the Powder Pocket clamped in the double cantilever system: the containment (yellow part), lid (blue part).

2.3.2   Differential Scanning Calorimetry (DSC)

A well-known thermal analysis method is the Differential scanning calorimetry (DSC). It allows for an easy and quick characterization of the sample by determining the melting temperature, transition temperatures and morphological properties such as degree of crystallinity. There are two different measuring principles used in DSC, the "Heat Flux DSC" and the "Power Compensation DSC". One measures the difference in heat flux between two crucibles in the same heating chamber by measuring the temperature difference between the sample and the reference crucible. The second method uses two isolated chambers and a control unit that compensates the temperature difference by feeding the one chamber with more power. Figure 10 depicts the measuring principle of the Heat Flux DSC, one crucible is empty and acts as a reference the other crucible contains the sample. The crucible material should not influence the heat flux for the temperature range used in the test. Additionally, the crucible should allow for good thermal conductivity between the

chamber and the sample therefore, aluminum crucibles are the preferred material for testing polymers. Both crucibles undergo a certain temperature program and due to the material's heat capacity and possible exo- or endothermic processes, the temperature of the sample and reference will differ.
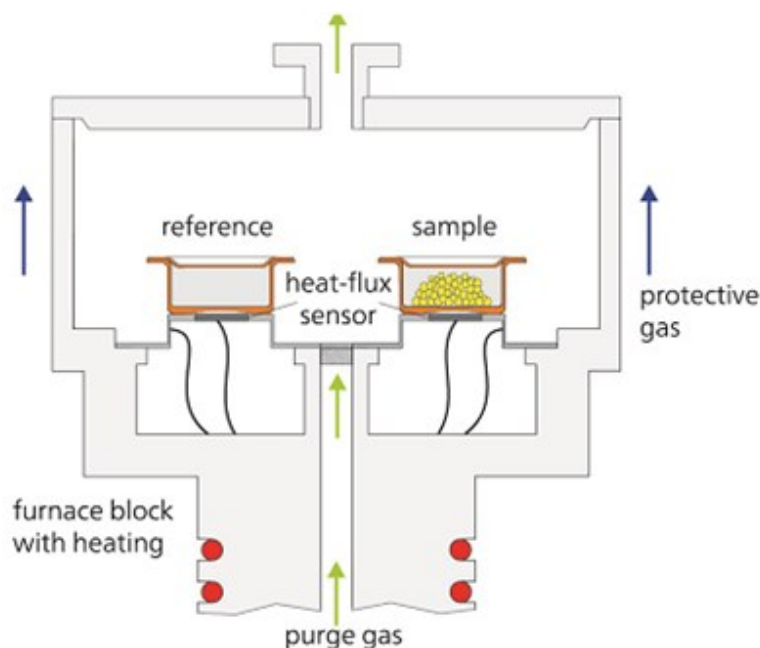
Figure 10: A schematic for a DSC measuring system. [53]

Figure 11 exemplifies several different exo- and endothermic processes such as the glass transition and melting. The already mentioned exo- and endothermic processes can be seen as steps and peaks in the heat flux over temperature diagram. Processes like crystallization or crosslinking release heat when they occur and are, therefore exothermic. On the other hand, endothermic processes absorb heat, such as the process of melting and the glass transition. A standard DSC measurement only needs 5-10 mg of sample and is therefore less prone to thermal inhomogeneity. With a better thermal homogeneity, a high heating rate of 10 K/min is possible (compared to 2 K/min for DMA).[54]

The downside of DSC is its lack of sensitivity concerning the determination of thermal transition regions in comparison to DMA. In a white Paper released by J.Foremann et al.[55], evaluating the T_g of Polycarbonate with DSC was estimated to be half as sensitive as with DMA Wetton, R. E.[56] mentions that specifically for α-relaxations such as the T_g, DMA sensitivity is 1000 times higher than DSC.
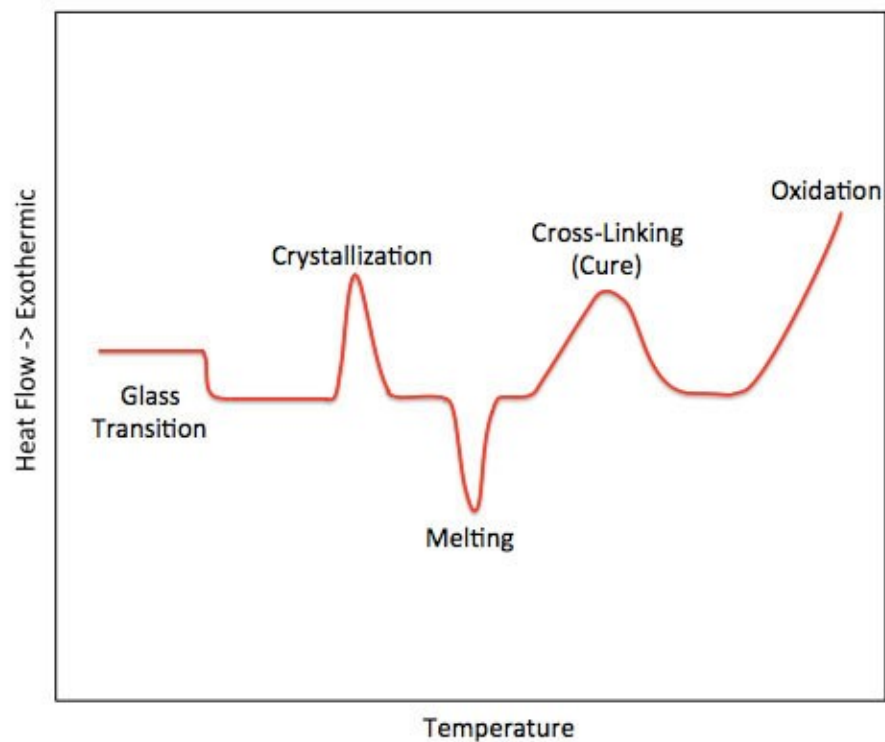
Figure 11: An exemplary diagram of a DSC measurement, including typical thermal processes such as melting and glass transition. [57]

2.3.3   Powder Rheology

Powder rheological properties are of utmost importance in storing and transporting powdery goods. To evaluate those properties, special mechanical tests have been developed. The properties obtained from those mechanical tests are called powder rheological properties. Despite the name rheology, the methods used have nothing in common with conventional melt rheology.

One potential use of those powder rheological properties is the estimation of transition temperatures that influence said properties. One potential advantage of those methods would be the direct connection to the application and the consequences that might occur when those powder rheological properties change. For example, a change in the internal friction angle could be used as a design criterion for storage applications. The main downside of those measurements is the fact that they are isothermal. That means only one data point is obtained per measurement. This fact makes a precise determination of T_g quite tedious. Nonetheless, the information gained from just two data points (one above

T_g and one below T_g) could already be enough to indicate a morphological change in the material.[58]

Powders exhibit a vastly different behavior compared to solid materials, especially in terms of mechanical, thermal or electrical properties. Powder rheological measurements provide insight into the flow properties of the powder. Those properties include cohesion, compressibility, wall friction angle, internal friction angle and flow function. Those properties can be measured in a shear cell. There are two different types of shear cells currently available. The direct Jenike shear tester (seen in Figure 12) uses the translatory movement of a ring to apply shear stress on the powder. This shear cell has the disadvantage of a limited shear length determined by the length of the powder bed and is, therefore, less automated than the ring shear cell. In comparison, the ring or annular shear cell is a rotational apparatus with infinite shear length, which was used for the investigation of the present thesis. The ring shear cell is depicted in Figure 13. The lid containing fins is pressed onto the bottom container holding the powder. The lid applies a predetermined normal stress. The lid has fins spread along its circumference that enters the powder vertically. The fins apply shear stress via rotational movement of the lid.[59,60]
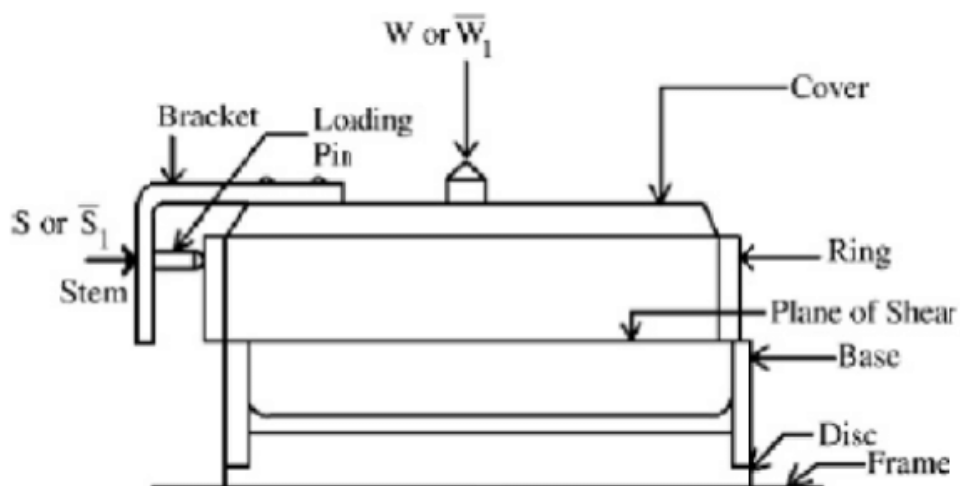
Figure 12: Schematic of a Jenike shear cell; the upper ring is moving relative to the base and therefore creates a shear plane.[61]
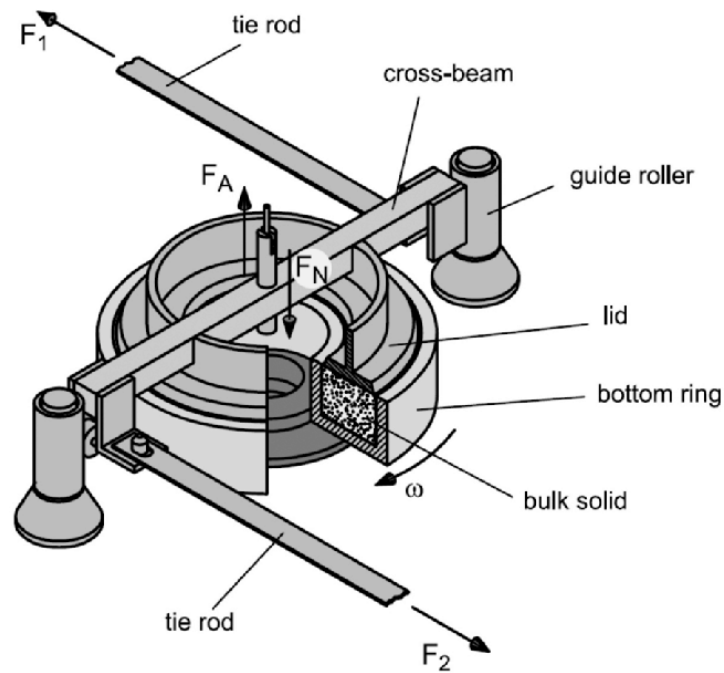
Figure 13: Schematic of a ring shear cell: the lid presses onto the top surface of the powder (described as "bulk solid" in the figure), applying normal stress.[62]

An evaluation of the flow properties of powder might be very intuitive in first approach, but quantifying those properties takes a deep understanding of the mechanical and physical circumstances of the powder. Flow properties depend on several factors, such as particle size distribution, temperature, and load/stress history. The physical and chemical structure also influence the flow behavior due to possible interaction forces. The terms good or bad flow properties are very subjective as those ratings depend on the application. The flow-factor *ff* gives a quantitative assessment of a powder's ability to flow A powder achieves the state of flow when stresses exceed the powder's unconfined yield strength (σ_c). σ_c is the maximum normal stress that can be applied to a pre-consolidated powder volume until a break occurs (Figure 14). The powder is pre-consolidated with certain stresses σ_1 (Major Principle Stress) in a confined volume. σ_2 is the Minor Principle Stress that occurs perpendicular to σ_1. This pre-compression plays a vital role in the resulting σ_c value as it is not a material constant but changes with prior stress states.[59]
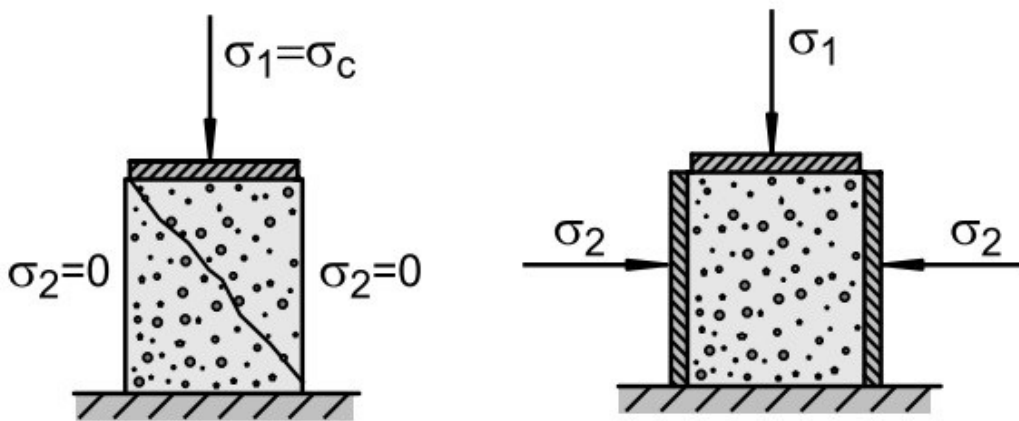
Figure 14: Depiction of the load cases to determine σ_c, σ_1 and σ_2. [59]

Equation 1 shows how ff is calculated. Figure 15 gives context for the classification of different powders that change from very cohesive (1 > ff > 2) to free flowing (ff > 10). A Powder with a high ff value needs much higher pre-compression stress to reach the same σ_c as a powder with a low ff. Therefore, a free-flowing powder will have a high ff value, while cohesive or non-flowing powders have low ff values. [59,60]

$$ff = \frac{\sigma_1}{\sigma_c}$$ (1)
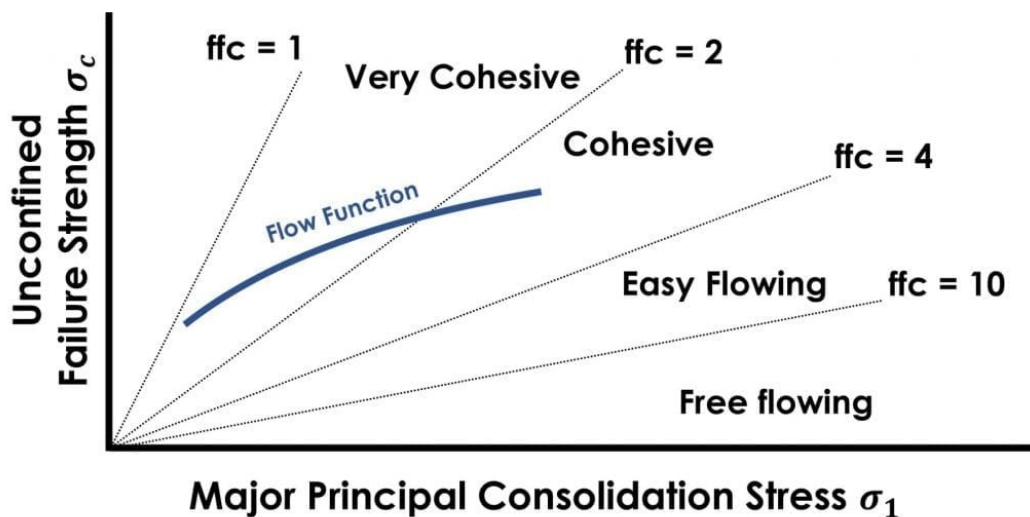
Figure 15: Classification of powders regarding their flowability. [63]

As mentioned, the prior stress state is a deciding factor for the results measured in a shear cell. This is why a shear measurement is split into two phases, the pre-shear and the shear-to-failure step. The pre-shear step is usually done at a high normal stress level of 3, 6 or 9 kPa. The normal stress is held at a constant value, while the shear stress increases over time due to the rotation of the upper measuring system. The pre-shear step is completed when the shear-stress has reached a constant value (=steady state). This steady state is assessed by an event control setting that compares the last n points of the shear stress. When those points are within a certain range of each other, the steady state is achieved and the next step starts. Sometimes, this assessment does not yield consistent results, especially for free-flowing powders. In this case, the time for the pre-shear is increased and the event control is turned off. This increase in pre-shear time leads to a plateau of the shear stress and, therefore, to a steady state. A comparison of those two pre-shear evaluation methods can be seen in Figure 16. The diagram shows the raw data obtained from a shear measurement performed on PVC at 100 °C with a normal stress of 6 kPa. The measurement was repeated three times, with one run containing three pre-shear steps and three shear-to-failure steps. The shear cell used had a volume of 18.9 mL and the upper measuring system's rotational speed was 0.005 min^{-1}. The pre-shear values obtained from the standard method are marked by a dot, while the alternative method is marked by the triangles. The conventional method leads to higher deviation in the measured pre-shear and can't guarantee a repeatable steady state of the powder.[64]
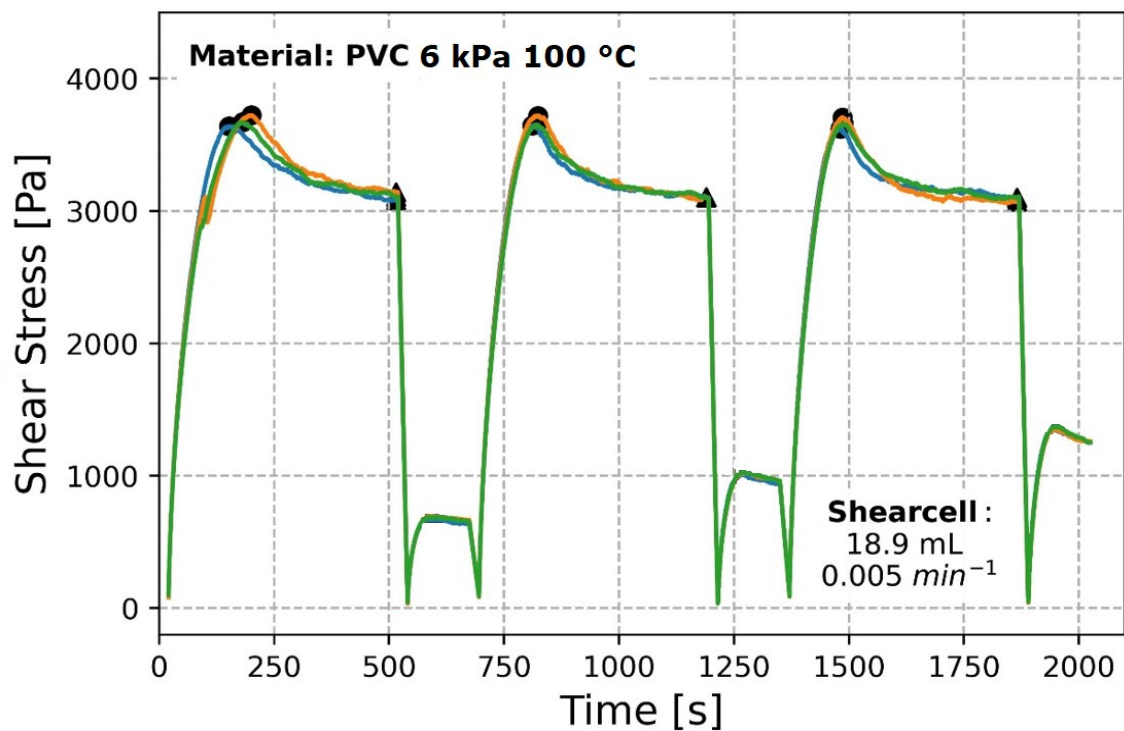
Figure 16: Comparison of two methods performed on PVC at 100°C with a normal stress of 6 kPa: the usual method used to determine the pre-shear point is marked by the dots (●); the alternative method used for free-flowing powders is marked by a triangle (▲).

The second phase of the shear measurement is the shear-to-failure step. In this step, the normal stress is decreased to a certain percentage of the normal stress applied in the pre-shear step. The measurement is carried out until the shear stress reaches a maximum. This maximum indicates a powder break. If the shear stress exceeds the yield stress of the compacted powder a break occurs, and the shear stress decreases (similar to the behavior of a ductile polymer in a tensile test). This two-step process is repeated three times while increasing the normal stress level for the shear to failure step (e.g. 40 / 60 / 80 % of the pre-shear normal stress). A linear regression can be fitted by plotting the shear-to-failure points for the different normal stresses. This linear regression line represents the yield locus curve. Any Mohr's circle that leads to a failure (powder break) must be tangent to the yield locus curve. The theoretical yield locus curve does not follow a linear behavior (especially for low normal stresses) therefore, it is not recommended to choose a normal stress of 10 % or lower of the pre-shear normal stress. The yield locus curve must have a positive slope k, as higher normal stresses will result in a more compact powder bed which can withstand higher shear stresses. Therefore, the intercept on the y-axis d is the shear

stress a powder can withstand without any supporting normal stresses. This value is equal to the cohesion C of a powder.[59,60]

The yield locus curve allows for the construction of two specific Mohr circles. The small Mohr circle represents the unconfined powder with a σ_2 of 0. The other two criteria for the circle are the symmetry along the x-axis and the tangent yield locus. This leads to Equation 2 for calculating the small Mohr circle's center position $(x_0|0)$ and radius r. The determination of σ_c is now equal to the major stress of the small Mohr circle as seen in Equation 3.[59,60]

$$x_0 = r = kd + \sqrt{k^2 d^2 + d^2} \qquad (\ 2\ )$$

$$\sigma_c = x_0 + r \qquad (\ 3\ )$$

x_0... Center position of the small Mohr's circle

r... Radius of the small Mohr's circle

k... Slope of the linearized yield locus

d... Intercept on the y-axis of the linearized yield locus

σ_c... Unconfined yield strength

The construction of the second Mohr circle/big Mohr circle is more complex. This time σ_2 is not predefined instead the pre-shear point is used as the third criterion. This pre-shear point is located at the shear stress at the steady state τ_P and the applied normal stress σ_P for the pre-shear. This point must be located on the Mohr circle because it is the state of the powder at the beginning of the shear-to-failure curve. Through trigonometric operations, Equation 4 and 5 can be used to calculate the center σ_M and the radius R, respectively. Figure 17 depicts the completed construction of both Mohr's Circle and the yield locus. All points of interest are labeled, the black colored points are obtained from the measurement, while the red points are trigonomically calculated. [59,60]

$$\sigma_M = (\sigma_P(1+ k^2) + kd) - \sqrt{(\sigma_P(1+ k^2) + kd)^2 - ((\sigma_P{}^2 \cdot \tau_P{}^2)(1+ k^2) - d^2)} \qquad (4)$$

$$R = \frac{k(\sigma_M + \frac{d}{k})}{\sqrt{1 + k^2}} \qquad (5)$$

σ_M... Center position of the big Mohr's circle

σ_P... Normal stress at pre-shear point

τ_P... Shear stress at pre-shear point

R... Radius of the big Mohr's circle
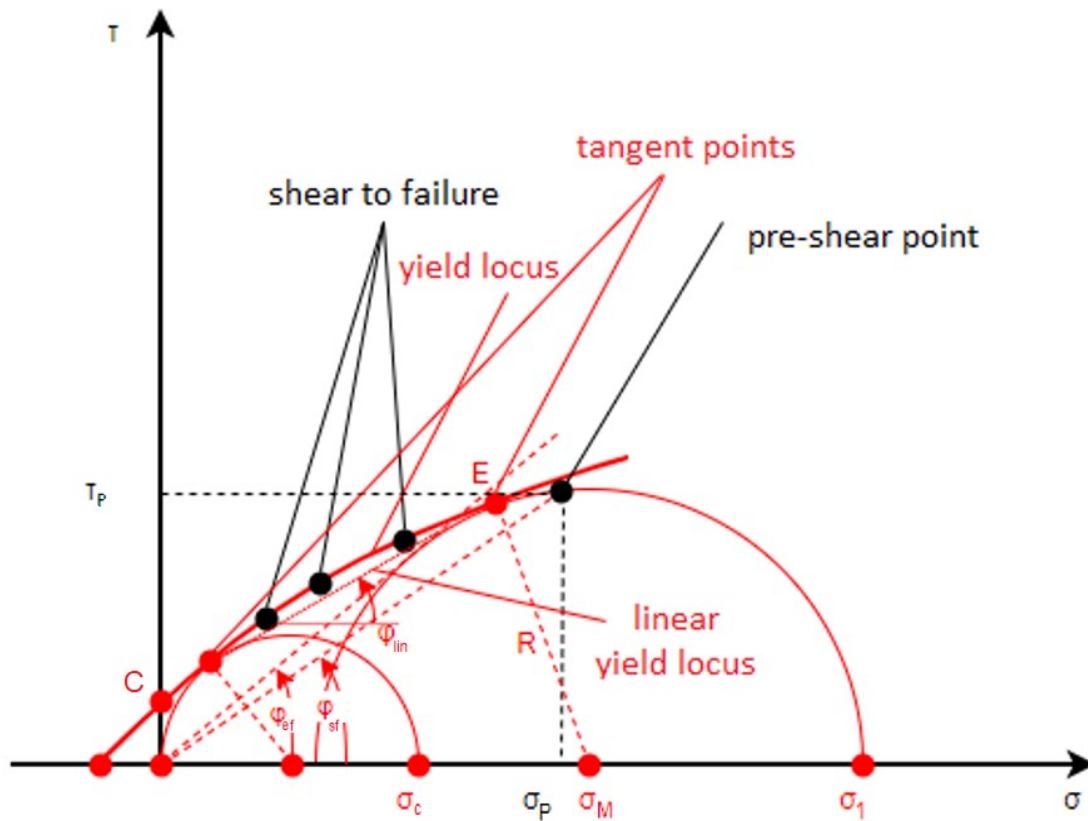
Figure 17: Schematic of the yield locus curve and Mohr circle construction. The black points are measured values. The red lines and points are calculated/constructed from the black points and boundary conditions.

Two important values, the angle of linearized yield locus φ_{lin} and the effect angle of internal friction φ_{ef} can be obtained from this diagram are calculated according to Equation 6 and 7

$$\varphi_{lin} = \tan^{-1} k \qquad\qquad\qquad (\ 6\ )$$

$$\varphi_{ef} = \sin^{-1} \frac{R}{\sigma_M} \qquad\qquad\qquad (\ 7\ )$$

φ_{lin}… Angle of linearized yield locus

φ_{ef}… Effective angle of internal friction

Following paragraph will list the powder rheological properties used for further thermo mechanical characterization in the present thesis. It should be noted that all of those properties are to some extend connected due to the way they are obtained from the Mohr's circles.

Major Principle Stress σ_1 describes the highest occurring compressive stresses in a powder for the given load case. This value is strongly dependent on the circumstances given by the measurement, for example the pre-set normal stresses. σ_1 is correlated with the bulk density of the powder, generally a higher σ_1 will result in a higher bulk density[59]

The unconfined yield strength σ_c gives the maximum compressive stress that the powder can withstand without any supporting stresses from the outside. It can be interpreted as the yield strength of the powder. The yield point, in the case of powders, is not the undesired failure point usually associated with plastic deformation in solids but rather the beginning of flow, which is the desired state in most powder applications. This value plays a vital role in the design of silo outlet diameters.[59]

The flow function ff is a purely mathematical expression of the quotient of σ_1 and σ_c. It is often used to categorize the flow ability of a powder. Ruggi et al.[65] state that optimizing part quality in the SLS process using PA12 is achieved by maximizing ff, while minimizing other powder rheological values like cohesion and the effective internal friction angle [59,65]

Cohesion C reflects the interaction forces between the particles. These interaction forces are usually related to Van der Waals forces. Other forces that can influence the cohesion are electro static forces, mechanical interlocking and moisture. In special circumstances, for example wet powders surface tension forces can influence the cohesion drastically.[59]

The angle of linearized yield locus φ_{lin} is not directly connected to a physical phenomenon, but it is often used as an approximation for internal friction angle. The internal friction angle describes the friction between powder particles at the beginning of flow.

The effective angle of internal friction φ_{ef} plays a vital role in the designing process of silos and bunkers. It is a representative value for the friction occurring between the powder particles in stationary flow. Knowing this value is necessary in order to prevent dead zones in silos. Wieleba[66] also states that φ_{ef} is related to the dissipated energy due to cyclic deformation in PTFE silos. The dissipated energy is converted into heat, therefore increasing the temperature of the powder.[59]

3 EXPERIMENTAL

3.1 Material grades and sample preparation

In total, four different materials have been tested in this thesis. All four materials, PVC, TPE, PA12 and PTFE, were provided in powder form by Anton Paar (Graz, AT) and its partners.

The PVC material (trade name is confidential) is filled with 5-10 w% Titanium dioxide and 1-5 w% Calcium carbonate. Additionally, 1-5 w% Poly(methyl methacrylate/butyl acrylate) is contained in the compound. Both, the TPE material (trade name DuraForm® Flex) and the PA12 material (trade name Duraform®) were produced by 3DSystems (US, Rock Hill). The PTFE material used for this thesis was provided by Anton Paar directly, as they use it internally to produce certain components. The trade name is TFM1600, and is distributed by HazeFlon (NL, Breda).

Solid samples were manufactured via vacuum compression molding in cooperation with Meltprep (AT, Graz). PVC PA12 and TPE were manufactured via vacuum compression molding but due to the technological restriction of temperature and pressure PTFE samples were not manufactured with this method but instead milled from a semi-finished product. The specimen geometry was 40x10x2 mm, this geometry was achieved with both methods, but the vacuum compression molding led to a higher variance in thickness as it is determined by the amount and type of powder used. The measured thicknesses can be seen in Table 1. Samples produced from milling (PTFE) had the smallest deviation in their

thickness. The compression step was set at 7 minutes for all specimens. For PVC, in particular, several different times and temperatures were tested with restricted quality of the resulting specimens. At lower temperatures, the powder particles were only slightly sintered without complete melting and homogenous solidification, while at higher temperatures, decomposition of the samples occurred, as seen in Figure 18. Since the quantitative values from DMA are of minor interest, the DMA measurements were done on the more brittle samples manufactured at 180 °C temperatures for 7 minutes with no apparent thermal decomposition. For all other materials, a sufficiently good specimen quality could be achieved by this procedure of compression molding. A full display of the processing parameters for each material can be seen in Table 2

Figure 18: Discoloration due to decomposition of the PVC samples produced at different temperatures:265 °C for 3,5 min (right), 220 °C for 5 min (center) and no obvious decomposition at 180 °C for 7 min (left).

Table 1: Thickness of the solid samples used for DMA.

Thickness [mm]	PVC	PA12	TPE	PTFE
Sample 1	1.96	2.08	1.85	2.03
Sample 2	2.04	2.02	1.83	2.02
Sample 3	2.05	2.04	1.61	2.04
Mean	2.02	2.05	1.76	2.03
Std. Deviation	0.05	0.03	0.13	0.01

Table 2:   Parameters used to produce samples via vacuum compression molding.

Material	Temperature [°C]	Time [min]
PVC	180	7
PA12	225	7
TPE	220	7
PTFE	-	-

For PA12, storage and drying play an important role when determining the properties of said material. Due to its hydrophilic nature, PA12 tends to absorb moisture from the air, especially in powder form. This effect is even more critical due to the high specific surface. Hence, PA12 was dried at 70 °C in a CTS C-40/200 climate chamber (Clima Temperatur Systeme GmbH, Hechingen, DE). This temperature allows the moisture to leave the polymer without degradation (according to the data sheet of the material, the maximum operating temperature is set at 105 °C). Pretests were conducted to determine the duration of the necessary drying process. Those pretests were done directly in the Powder Pocket as well as drying in two separate glass bowls. The weight of PA12 powder was measured on a Denver Analytical Balance SI-234 scale (Denver, Colorado, USA). The device has a precision of 0.1 mg which caused uncertainty when measuring the mass of PA12 in the Powder Pocket due to the low total powder mass of about 100 mg and the change of mass during the drying process (1 mg total change). The moisture content was calculated according to Equation 8 (ISO 62:2008:Plastics — Determination of water absorption). The calculated moisture content for all the different containers can be seen in Table 3. Figure 19 displays the loss of moisture over the drying period. The initial 10 minutes remove a lot of the moisture. The moisture loss of the Powder Pocket matches the moisture loss of the glass bowls well.

$$c = \frac{m1 - m2}{m2} \cdot 100\%$$
(8)

c… moisture content [%]

m1… current mass of the powder [g]

m2…mass of the dry powder [g]

Table 3: Measured masses of three PA12 powder samples (two in glass bowls and one in Powder
Pocket) and corresponding moisture contents for various drying times at 70 °C.

Drying time	Glas Bowl 1		Glas Bowl 2		Power Pocket	
	Weight	Moisture Content	Weight	Moisture Content	Weight	Moisture Content
[min]	[g]	[%]	[g]	[%]	[g]	[%]
0	14.4173	0.70%	15.7021	0.68%	0.1279	0.79%
10	14.3293	0.08%	15.6050	0.06%		
40	14.3213	0.03%	15.6014	0.03%		
60	14.3193	0.01%	15.5994	0.02%	0.1270	0.08%
90	14.3186	0.01%	15.5988	0.02%		
130	14.3188	0.01%	15.5972	0.01%	0.1269	0.00%
200	14.3178	0.00%	15.5965	0.00%		
240	14.3176	0.00%	15.5963	0.00%	0.1270	0.08%
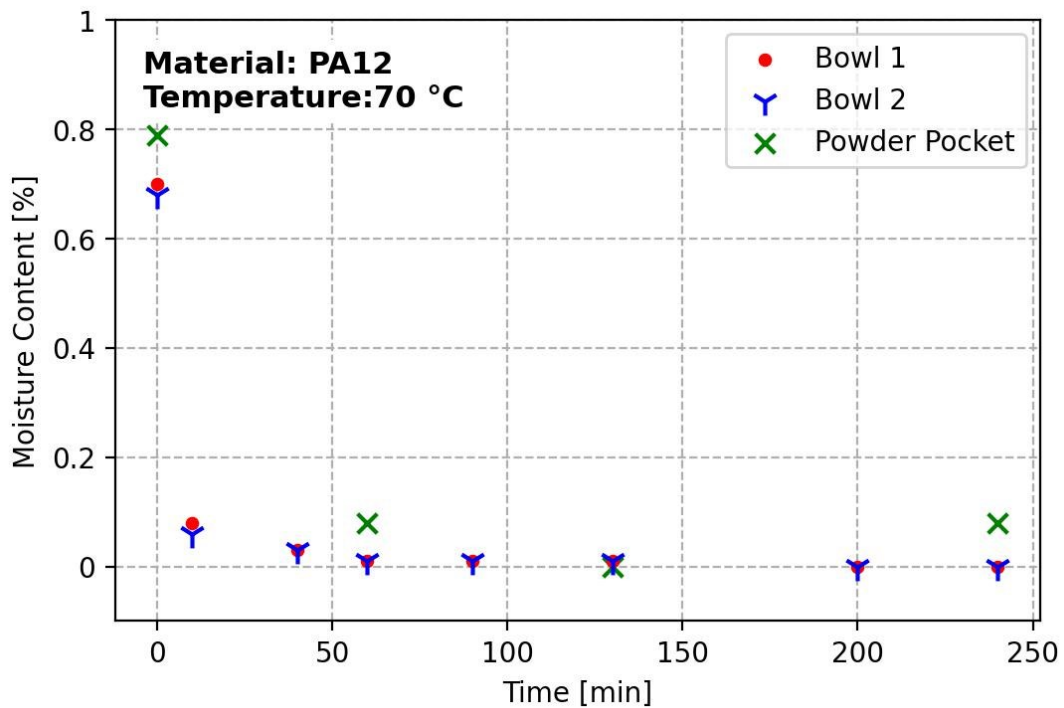
Figure 19: Depiction of the moisture content in the PA12 powder over progressive drying time at
70 °C.

Based on the results of this pretest, any PA12 powder used for measurements was dried
for at least four hours before testing. Due to exposure to atmospheric humidity while
transporting the sample from the climate chamber to the measuring setup, an additional
drying step of 30-60 minutes directly in the convection oven was integrated into the test
definition.

3.2 Test Parameters for DMA

DMA measurements were conducted on the Modular Compact Rheometer (MCR) 702 by Anton Paar. The dual cantilever (CTL) system was used for all tests (Powder Pocket and solid samples). The CTL-40 with a fixation distance of 40 mm was used for the Powder Pocket measurements, while for the solid samples, a shorter distance of 20 mm (CTL-20) had to be used. The testing setup for the solid samples can be seen in Figure 20. The solid samples were a little bit shorter in length than the Powder Pocket due to the limitations set by the vacuum compression molding tool. This caused them to slip through the CTL-40. To prevent slippage, the CTL-20 was chosen. The sample was heated via convection heat of the Convection Temperature Device (CTD) 600. Reaching temperatures below room temperature requires one of two accessories for the MCR, the EVU (evaporation unit), which uses liquid nitrogen to achieve a minimum temperature of -160 °C or the GCU 20 (Gas Chiller Unit), which uses compressed gas for temperatures down to -90 °C.

Figure 20: PVC-sample fixated in the CTL-20.

For all tests, a 2 K/min heating rate was chosen with a 2 points/min sample rate. The dynamic strain amplitude was set according to a previous amplitude sweep to ensure stable measuring conditions within the linear-viscoelastic range. The strain referred to here is the flexural strain on the surface of the sample located in the middle fixation point. The measuring system automatically transfers information like the distance between the

fixations and geometry to the RheoCompass software. This procedure was conducted and evaluated for every material (powder and solid). A summary of all the parameters used can be seen in Table 4. It should be noted that the dynamic strain amplitude for powder DMA was generally lower due to the higher stiffness of the total system caused by the Powder Pocket. The force amplitude resulted in a range of 0.5-8 N, depending on the polymer and other preparation parameters, for example, the difference between stainless steel and aluminum Powder Pocket. All resulting forces are within the allowable force range of the MCR 702 (0.0005 N-40 N).

It should also be noted that due to the fixation in the cantilever, a constant force was applied to the specimen, which was set to 0 N at the beginning of the measurement.

Table 4: Parameters used for DMA measurements.

Material	Form	Starting Temperature	End Temperature	Dynamic strain Amplitude
Unit		[°C]	[°C]	[%]
PVC	Powder	-60	120	0.005
PVC	Solid	-60	140	0.006
TPE	Powder	-90	0	0.004
TPE	Solid	-90	150	0.02
PA12	Powder	0	120	0.007
PA12	Solid	0	120	0.01
PTFE	Powder	-130	160	0.002
PTFE	Solid	-130	160	0.01

3.3   Test Parameters for DSC

Measurements were conducted on two different devices, depending on their availability. Three materials (PVC, TPE, PTFE) were tested with the Discovery DSC 250 by TA Instruments (US, New Castle). PA12 was measured on Mettler Toledo DSC1 (US, Columbus). All tests were conducted at a heating rate of 10 K/min with a sample mass of about 5 mg. The scales used were manufactured by Satorious AG (DE , Götting). The model SECURA26-1S was used for PVC, TPE and PTFE, while the model R200D was used for PA12. The used temperature settings can be seen in Table 5. All measurements were performed in an inert atmosphere (N_2 gas flow) without specific preconditioning of the powder materials except PA12. The PA12 powder was dried for three hours at 70 °C in a typical open container. Afterwards,

the aluminum pan was filled and prepared for the DSC measurement. This fully prepared pan was dried for one more hour. The sample was directly transferred from the oven to the DSC and immediately tested. This method reduced the time the powder was exposed to the humidity to a minimum.

Table 5:   Parameters used for the DSC measurements on the polymer powders.

	Heating Rate	Gas Flow	Starting Temperature	End Temperature
Unit	[K/min]	[ml/min]	[°C]	[°C]
PVC	10	30	30	110
TPE	10	30	-80	220
PTFE	10	30	-80	360
PA12	10	30	0	210

3.4   Test parameters for powder rheological measurements

The powder rheological measurements were done on a rheometer type MCR 502 by Anton Paar (AT, Graz). The shear measurements are performed in the 18.9 mL shear cell by Anton Paar. This shear cell is a shear ring type with the measuring system containing fins that apply the shear stress to the powder. When filling the shear cell, the powder was sieved by a standard metal sieve to break up possible agglomerations in the powder. The sample was prepared in a specialized tool, allowing for easy and exact volumetric filling. Figure 21 shows this tool; it has a base that allows for secure placement of the shear cell and two rods used to guide a scraping tool. The following steps were performed before every measurement:

- Overfilling the shear cell with sieved powder
- Push down 100 times with the thin side of the scraping tool to compress the powder while changing the position and angle of the scraping tool.
- Push down another 100 times while keeping the scraping tool at the same position and rotating the shear cell.
- Scrape off any excess material.
- Verify the compacted state by weighing the sample.

Figure 21: Preparation tool for the volumetric filling of the shear cell.

For the shear measurements, specific temperatures were selected based on the results of the DMA measurements. The temperatures were chosen above and below the glass transition temperature of the various materials. One additional measurement was performed either above or below the glass transition temperature but at a different temperature than the original two to test for a temperature-dependent behavior of the measured properties without thermal transition. The temperature was set via the Convection Temperature Device (CTD) 600. Due to the low heat conductivity of the powder, a long preheating cycle was set before measuring the material to ensure a homogenous temperature distribution in the powder. This preheating step was set to 45 minutes after reaching the desired temperature with a tolerance of ± 0.2 °C. The upper measuring system was positioned 0.1mm above the shear cell to prevent air turbulences from altering the sample. Another measure was taken to protect the sample from air swirls. A protective plate was placed on the upper measuring system, as seen in Figure 22. The upper measuring system's rotational speed for all measurements was set to 0.005 min^{-1}. The material ring was placed on the shear cell to catch overflowing material.
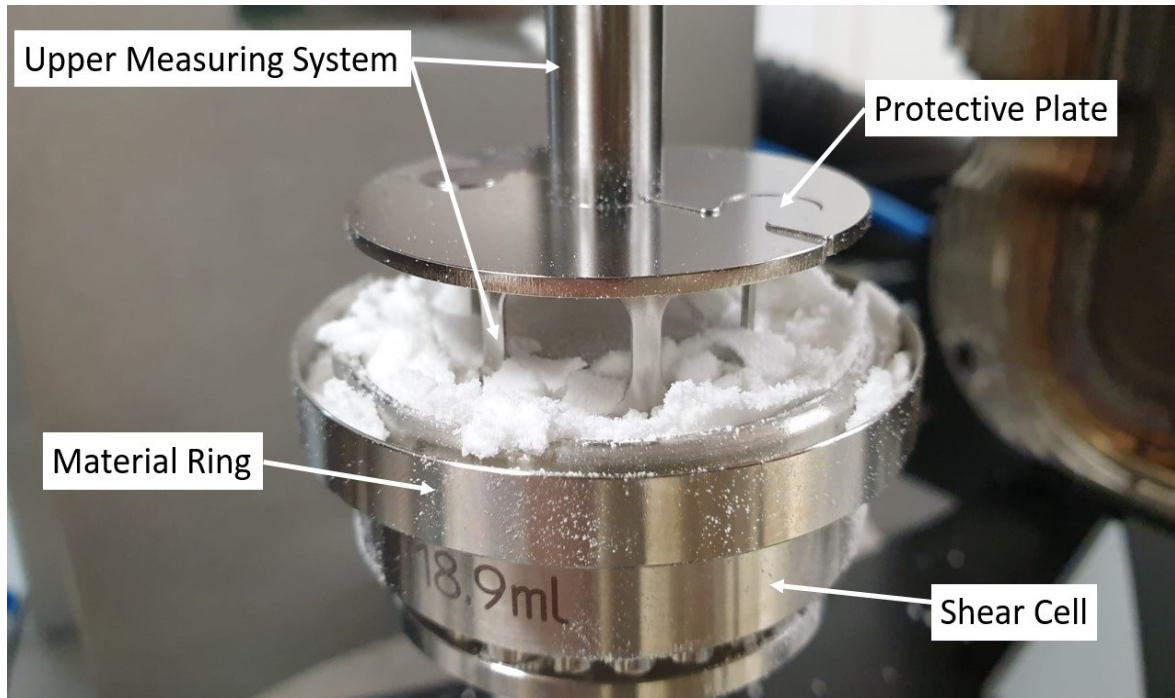
Figure 22: Shear cell measuring setup after the test has been conducted.

The measurements were conducted in two consecutive phases: the pre-shearing phase and the shear-to-failure phase. Pre-shearing was done at three different normal stress levels in axial direction:3, 6 and 9 kPa (if possible), with three shear-to-failure cycles per pre-shear level. The normal stress for the shear-to-failure curves was selected differently for every polymer, depending on the general flowability of the powder. The value of the normal stress is chosen as a percentage of the pre-shear normal stress applied beforehand. For example, 40 / 50 / 60% of a 3 kPa pre-shear would lead to 1.2/1.5/1.8 kPa for the normal stress applied in the shear-to-failure step. Sometimes even for the same polymer different normal stresses were chosen due to their changing behavior at different temperatures. A summary of the selected temperatures and the parameters used for every temperature can be seen in Table 6

Table 6:   Temperatures and corresponding stress levels chosen for the shear measurements.

Material	Temperature	Pre-shear normal stress	shear to failure normal stress
Unit	[°C]	[kPa]	[%]
PVC	30	3/6/9	20/30/40
	70	3/6/9	20/30/40
	100	3/6/9	30/40/50
TPE	-90	3/6/9	30/40/50
	0	3/6/9	30/40/50
	80	3/6/9	30/40/50
PA12	30	3/6/9	40/60/80
	80	3/6/9	40/50/60
	100	3/6/9	40/50/60
PTFE	-130	3/6/9	40/50/60
	-60	3/6/9	40/50/60
	-20	3/6/9	40/50/60
	30	3	10/20/30
	80	3	10/20/30
	160	3	10/20/30

The event control setting for the pre-shear was turned off to reach an over-consolidated state in the powder. This allows for more consistent measurements of free-flowing powders. Conventionally only the shear-to-failure curve maxima are used to determine the linear locus line. With this method, additional points are generated from the pre-shear maxima. It should be noted that those values are generally lower than the linear fit from just the shear to failure maxima due to the nonlinear behavior of the curve. This method will lead to higher values for σ_1, σ_c and τ_c while reducing the angle of the linearized locus. Fitting a nonlinear function instead of doing a linear regression leads to less consistent measurements due to the occurring deviation of the measurement.

4   RESULTS

4.1   Optimization of DMA test parameters for powder characterization

In order to receive meaningful results out of the DMA measurements, determining the optimal test parameters and test preparation is necessary for each polymer type. The mechanical measurement of powder naturally brings a lot of problems, for example, temperature inhomogeneity and unexpected movements of singular particles. The latter can lead to an abrupt increase/decrease in a deformation of the total system, which could be falsely interpreted as a loss/increase in modulus. The ambivalence is caused by the fact that a particle can be pushed into a position allowing for more or less deformation. This phenomenon causes the resulting curve from a powder DMA to be less smooth and continuous than the measurements from solid samples.

Prior to any tests, an amplitude sweep was conducted for all materials in solid DMA and with the Powder Pocket. The determination of the linear viscoelastic range was done according to ISO6721-10 (decrease of 5% in E'). This standard only applies to solid polymeric materials and therefore excludes the measurements done with the Powder Pocket. When choosing a strain amplitude for the Powder Pocket measurements the visco elastic range was not the main concern. The conditions that influenced the choice of the strain amplitude were the maximum force limit (due to the much higher stiffness the maximum force limit was easily reached) and the consistency in the recorded data. In some strain ranges the measured values would fluctuate less, allowing for more accurate measurements. Figure 23 shows an amplitude sweep of solid PVC, while Figure 24 displays the amplitude sweep of PVC in the Powder Pocket. Notably, the Stiffness level is completely different and the decrease in stiffness seems to not be well pronounced for the Powder Pocket measurements. The red line indicates the strain chosen for further measurements, while the blue line indicates the upper limit of the viscoelastic range according to ISO 6721-10. The remaining amplitude sweeps can be found in the appendix 1.
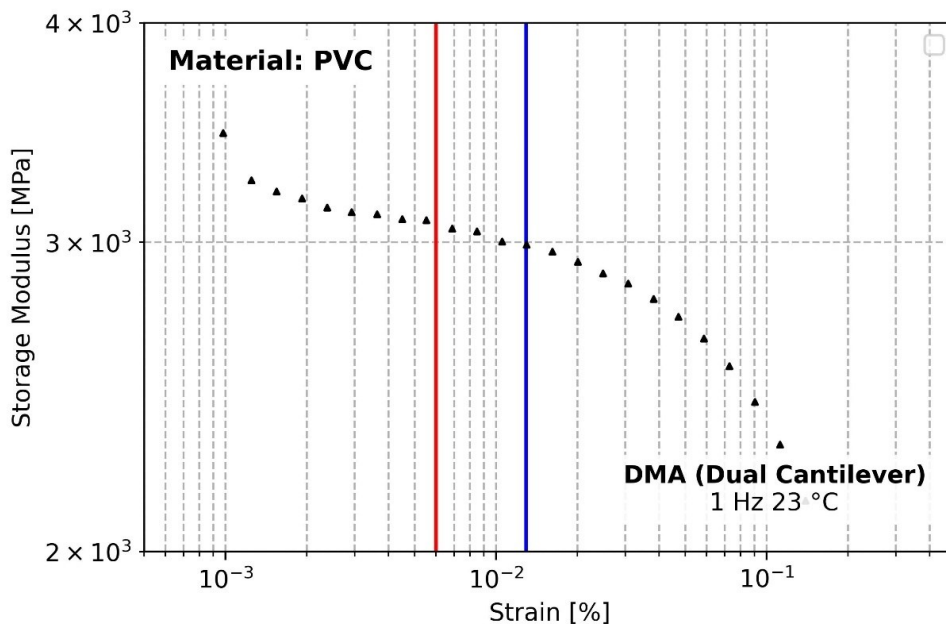
Figure 23: Amplitude sweep of PVC (solid) conducted at 23 °C and 1 Hz. The red line indicates the chosen strain, while the blue line indicates the upper limit of the viscoelastic range.
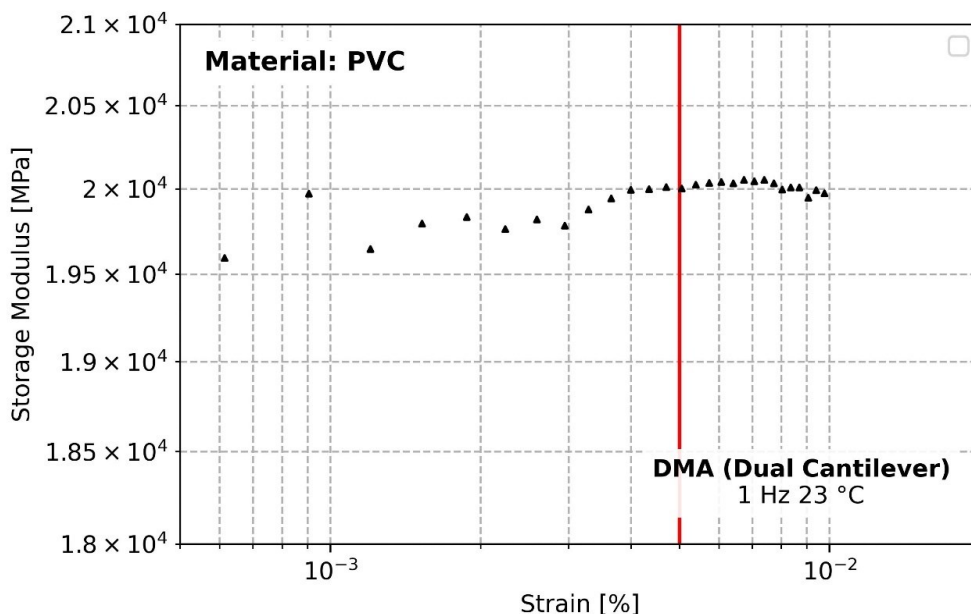
Figure 24: Amplitude sweep of PVC (powder) conducted at 23 °C and 1 Hz. The red line indicates the chosen strain, while the blue line indicates the upper limit of the viscoelastic range.

Therefore, the assumption was made that a more compacted state of the powder would result in a DMA curve that more closely resembles the DMA curve of a solid sample, allowing for a more accurate measurement. This assumption was tested before any other

testing parameters due to the simplicity and high expectations for success. The compacted state was achieved by the clamping force of the CTL. The maximum allowed torque on the screws is set at 80 cNm. The torque used for the measurements was capped at 60 cNm as this torque already shows a visible elastic deformation of the whole measuring system. This pretest was also only conducted on PVC and PTFE due to the similarity in powder characteristics between PVC, TPE and PA12.

 The result of the different clamping torque on the DMA curves can be seen in Figure 25. When changing the clamping torque from 30 cNm to 60 cNm, a gradual qualitative improvement in the signal's smoothness can be seen. Another notable change caused by the different clamping torques is the peak shape. When evaluating the tan delta curve for 60 cNm the peak is well-defined and can be easily assessed at roughly 88 °C. In comparison, the peak measured at 20 cNm results in a broad peak with an undefined maximum between 87 °C and 94 °C. This second peak could be related to the rearrangement of particles in the Powder Pocket. This rearrangement could be caused by the oscillating deformation of the sample or by the difference in thermal expansion of the polymer and the Powder Pocket. Close to the T_g, a polymer's thermal expansion changes drastically, which supports the validity of this assumption. [67] Further optimizations primarily focus on the sample preparation before the actual measurement.
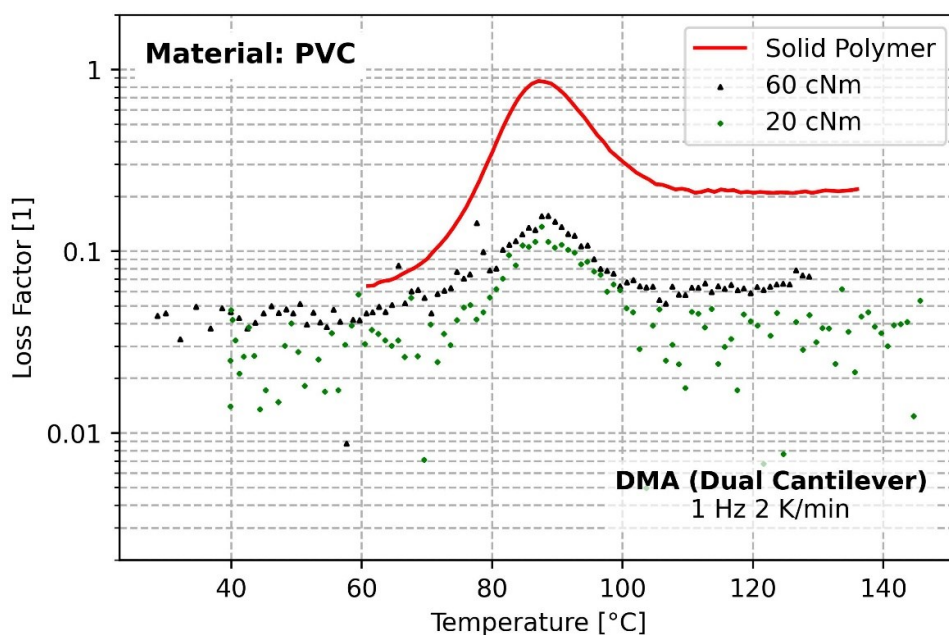
Figure 25: Improvement in the measured signal due to the higher clamping torque.

The following parameters were investigated: powder pocket material, sample volume, sample distribution and pre-compression step. For a deeper understanding of the influence of those parameters, the isolated influence of each parameter and the interaction of several parameters was tested simultaneously. A particular combination of preparation steps might have a bigger impact than the sum of its parts (non-linear interaction).

The Powder Pocket was manufactured in both aluminum and stainless steel. Currently, the most common material used for powder containers in DMA is stainless steel. The aluminum container allows for better heat transfer due to the higher thermal conductivity ($239 \ W \ m^{-1} K^{-1}$) compared to stainless steel ($25 \ W \ m^{-1} K^{-1}$). Another suspected positive effect would be the higher thermal expansion of aluminum, which would be closer to the coefficient of thermal expansion of polymers. The similar thermal expansion of the Powder Pocket and the sample reduces the thermal stresses when the sample is heated. Another notable difference between those two options is the stiffness. An overall higher stiffness level could decrease the visibility of characteristic changes in the DMA curves. Figure 26 shows the different stiffness levels due to different Powder Pocket materials. Noticeably, the changes in E' are not well pronounced for the Powder Pocket systems compared to the solid polymer sample.
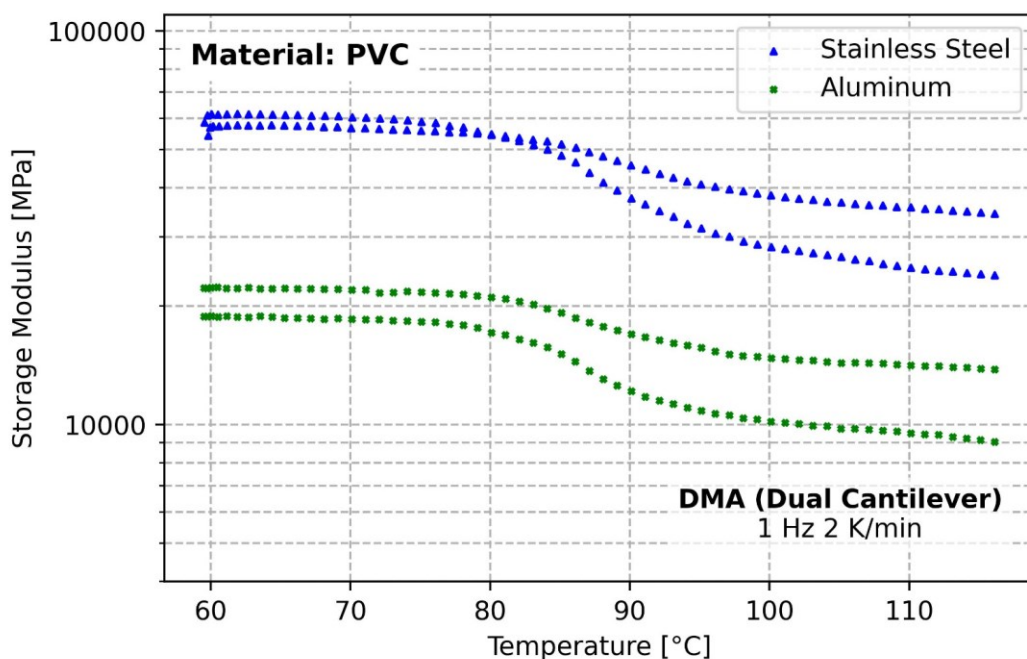
Figure 26: Storage Modulus over temperature for different Powder Pocket materials in comparison to the solid polymer.

When looking at the corresponding curves for E'' and tan δ seen in Figure 27 and

Figure 28, the positive effect of the aluminum Powder Pocket on the measured signal with a more pronounced peak at T_g is apparent. Table 7 displays quantitative values for this positive effect. The visibility of curve characteristics such as peaks or slopes is represented by the multiplication factor that gives the quotient of either two baseline values (below and above transition) or a baseline (below transition) and a peak value. A higher multiplication factor means that there is better visibility of said characteristic. The baseline value was calculated by the mean of ten data points in that area. Overall, the aluminum Powder Pocket resulted in a higher multiplication factor and therefore better visibility. Reproducibility is limited due to the unpredictable nature of powders. This uncertainty is caused by user-specific deviations in the preparation of the samples. But other factors, such as sample volume and distribution, could also influence the results from a quantitative standpoint. Therefore, further investigation of those other factors is needed.
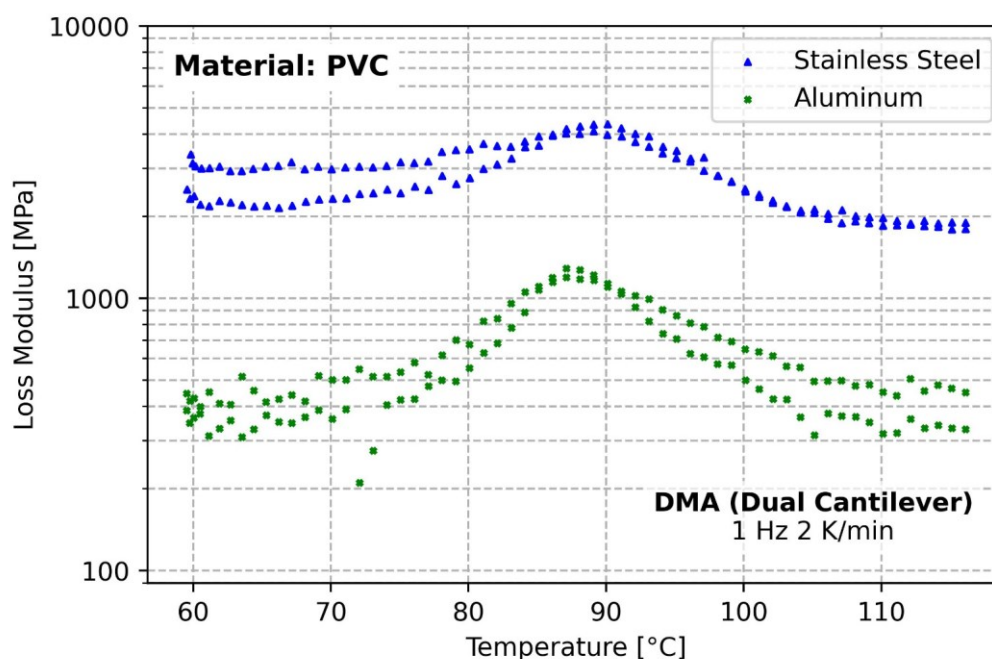
Figure 27: Loss Modulus over temperature for different Powder Pocket materials in comparison to the solid polymer.
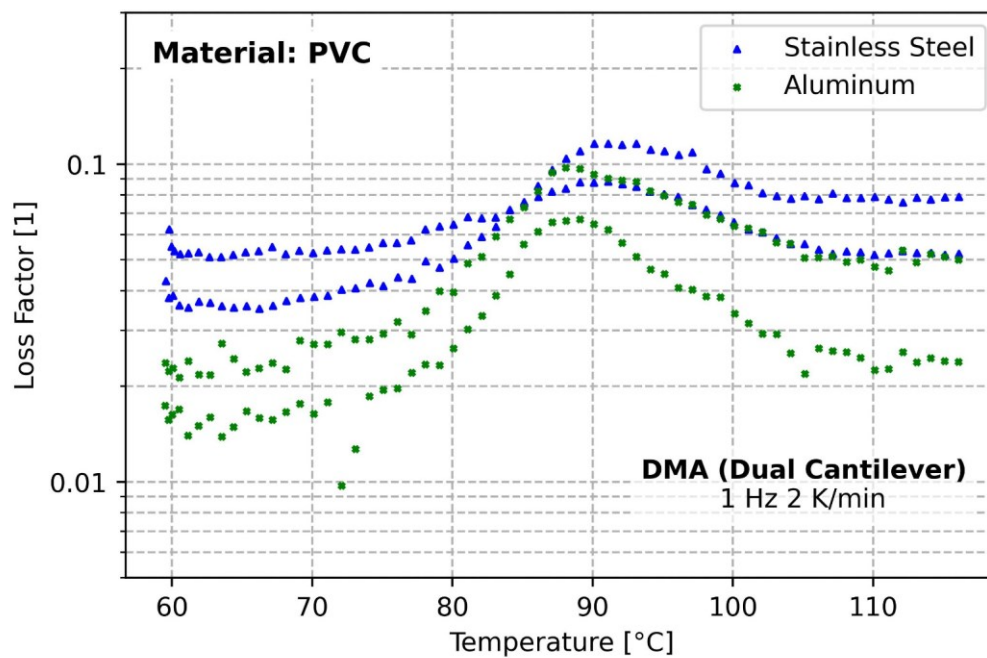
Figure 28: Loss Factor over temperature for different Powder Pocket materials compared to the solid polymer.

Table 7:   Change in characteristic values for different DMA curves

Storage Modulus	Upper Baseline [MPa]	Lower Baseline [MPa]	Multiplication Factor
Stainless Steel	57400	35300	1.6
	61300	24800	2.5
Aluminum	22200	14000	1.6
	18800	9400	2.0
Loss Modulus	Peak Value [MPa]	Baseline [MPa]	Multiplication Factor
Stainless Steel	4100	1860	2.2
	4360	1950	2.2
Aluminum	1200	210	5.7
	1290	430	3.0
Loss Factor	Peak Value [1]	Baseline [1]	Multiplication Factor
Stainless Steel	0.088	0.052	1.7
	0.116	0.036	3.2
Aluminum	0,067	0.016	4.3
	0.098	0.023	4.2

The mass of the sample influences the temperature profile within the sample. For example, DSC samples only weigh 5-10 mg to prevent thermal lag. Similar reasoning could be applied to the powder pocket system. On the other hand, using more powder could be favorable regarding the mechanical aspect of the measurement. The more sample material is put into

the Powder Pocket, the more polymeric and viscoelastic character the whole compound has. In the case of a DSC, the amount of sample is not influencing the actual measured data much due to the normalization of the data. Choosing a certain mass for the Powder Pocket system proved to be difficult due to the generally bigger sample size and the different densities of the powders. Even the same material could end up with a different bulk density due to particle shape and size and therefore behave differently in the powder pocket. Therefore, a volumetric approach is preferred over a gravimetrical.

To achieve consistent and repeatable volumetric filling of the powder pocket, a specialized tool was to be designed similar to the shear cell sample preparation tool. Due to time constraints, an improvised method was used to achieve consistent filling of the power pocket. This method contains four steps which are illustrated in Figure 29. Step 1 begins with a complete filling (or overfilling) of the power pocket. A standard teaspoon, drawn in blue, is used to scrape off some of the material (step 2). The spoon is supported on the sides by the Powder Pocket. The volume can be adjusted by changing the angle at which the spoon is held. Due to the shape of the spoon the powder is left with an indent which can be seen in step 3. To achieve a filling, as seen in step 4 the powder pocket is lightly shaken while laying on a flat surface to ensure a horizontal alignment and therefore obtain a flat surface.
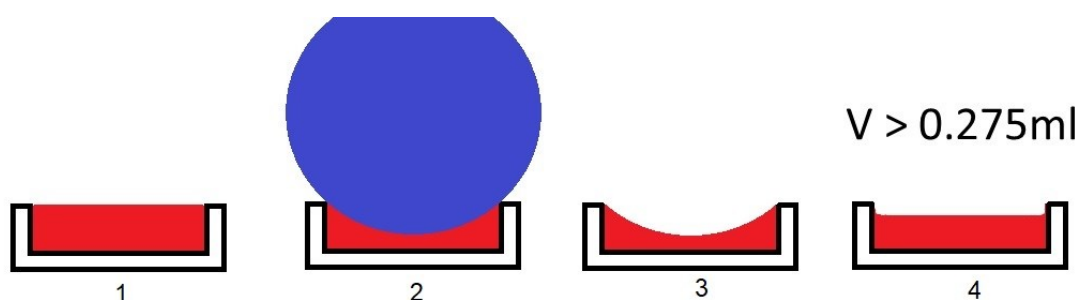
Figure 29: Volumetric filling method of the power pocket.

Spreading the powder evenly before closing the Powder Pocket ensures a flat surface and maximum contact area. A heaped pile of powder would only contact the lid at the peak, reducing the heat transfer from the Powder Pocket to the powder. In a demonstrational video by TA instruments the powder was not spread evenly, suggesting that the effect of spreading the powder might be negligible. To determine the effect of and evenly spread powder a heaped sample preparation was tested in comparison. Here the steps shown in

Figure 29 do not apply and the powder was simply filled into the Powder Pocket as seen in Figure 30.

Figure 30: Heaped TPE powder in the Powder Pocket.

The arrangement of particles is temporary and can be altered by applying forces on the particles. Similarly, how the bulk density changes to tapped density when objected to vibration or tapping motion, a cyclic pre-compression step could lead to a more stable and well-ordered particle arrangement. This preparation step could further improve the measurement quality by decreasing the noise caused by particle movement.

A Design of Experiment (DoE) was chosen for statistical analysis of those preparation methods. A DoE is a systematic approach for optimizing a process usually used in the chemical industry[68] or manufacturing of plastic products[69]. A DoE shows the effect of a certain parameter on a chosen response. The parameter can be of quantitative nature, like time or temperature or of qualitative nature, like a material or specific handling. The response can be again of qualitative or quantitative nature and is generally the point of interest. For powder DMA, three responses were defined:

- The similarity of powder DMA curve and solid DMA curve
- Noise in the powder DMA curve
- Position of T_g

Every parameter must be defined by two stages (usually high/low or -1/1). The definition of "low" or "high" is irrelevant to the statistical evaluation. It is only used to match the results after the analysis. In case of the sample volume, a high and a low value can be easily defined. In comparison, for the Powder Pocket material, each material was arbitrarily assigned to -1 (stainless steel) and 1 (aluminum). Table 8 shows the list of all parameters and the designated stages.

Table 8:   The assignment of the different parameters and their value in the DoE.

Parameter	"low" / -1	"high" / +1
Powder Pocket Material	Stainless Steel	Aluminum
Sample Volume	< 0.275ml	> 0.275mL
Sample Distribution	Heaped	Spread
Pre-Compression	No pre-compression	3 x 10 N for 30 s

Verifying whether the volume was below or above 0.275 ml was done by a geometrical check. Figure 31 shows the two different sample volumes and the geometrical check for each type. Picture a) shows a low sample volume configuration. Here the upper side of the lid should be below the outer edge of the lower Powder Pocket piece. In comparison picture b) shows a schematic for a high sample volume. Here the upper side of the lid is located above the edge. The red lines on the left side of the sketch mark both requirements.
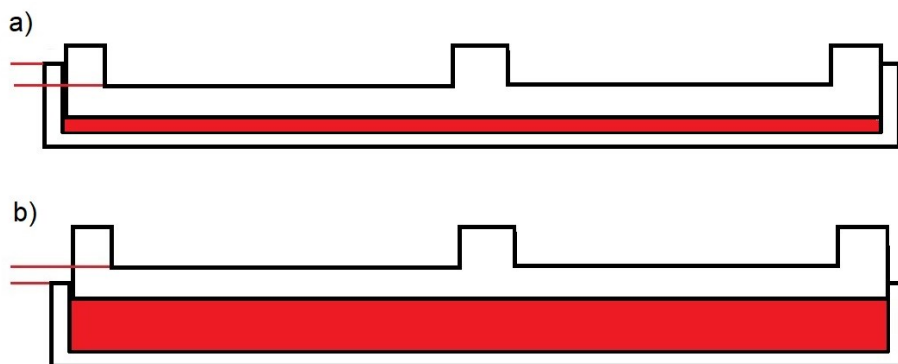
Figure 31 : a) Geometrical check for a low sample volume, b) Geometrical check for a high sample volume.

Another important aspect of the high-volume sample is the fixation in the CTL. With high sample volumes, the Powder Pocket lid tends to tilt when being fixated in the CTL as seen in Figure 32. This tilt can push some of the material to the side resulting in an uneven distribution of the sample. Therefore, tightening the screws must be done with care. In all measurements the right screw was tightened until the first contact with the Powder Pocket was made. Then the left screw was tightened in the same way. This way, the tilting effect was prevented, and the middle screw could be tightened fully with 60 cNm. Afterwards, the outer screws were tightened with 60 cNm as well.
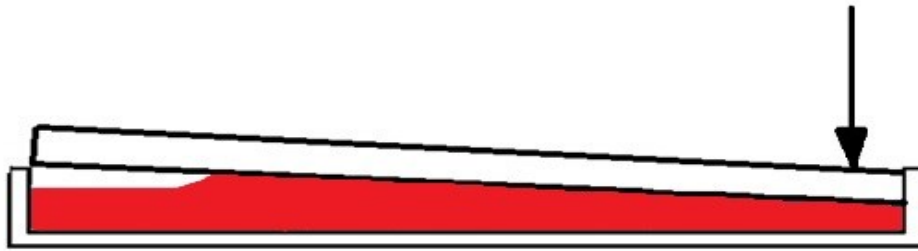
Figure 32: Visualization of the tilt caused by the one-sided fixation of the Powder Pocket at high sample volume.

As part of the DoE, Equation 9 is used to calculate the influence of a parameter on a chosen response. [70]

$$A = \bar{y}_{A\,high} - \bar{y}_{A\,low}$$ (9)

A… Influence of a parameter A on a response value

$\bar{y}_{A\,high}$… Average of all response values with a "high"/+1 parameter setting

$\bar{y}_{A\,low}$… Average of all response values with a "low"/-1 parameter setting

All possible combinations of parameters are tested for a full factorial test, which results in a total of 2^4 tests. Each variation was tested twice, which resulted in 32 tests per material. The procedure of the experiments can be seen in Table 19 with all four parameters.

With the test procedure defined, quantifying the response values is the only thing left for a DoE analysis. The similarity of curves and noise are very subjective terms that need to be quantified to achieve a meaningful result from the DoE. One way to compare two curves with each other and evaluate their similarity is the so-called cross-correlation. A cross-correlation is originally a tool used in signal processing[71] to calculate the time difference between two identical signals. This is done by correlating two curves at one specific time and then shifting them by one increment. This increment can be a certain time span or for DMA a certain temperature jump. In case of the powder DMA, two tests will never lead to the exact same curve. Nonetheless, the correlation value that can be extracted from that method could be used to indicate how well those two curves correlate with each other while also checking for any temperature shifts that might occur due to the different measuring setups. This correlation value is normalized and ranges from -1 to 1, with 1 being a perfect correlation of both curves. Figure 33 illustrates the cross-correlation of a sine

(F curve) and a cosine (G curve) function. A time shift of $\frac{\pi}{2}$ is required for a perfect correlation of 1. This is indicated by the red dot on the cross-correlation function in Figure 33 a). In contrast, the worst possible correlation of -1 is seen at a shift of $-\frac{\pi}{2}$ in Figure 33 b). For a periodic function like sine and cosine the cross-correlation function shows several peaks (with a period of 2π). An arbitrary curve such as a DMA curve usually only yields one peak.
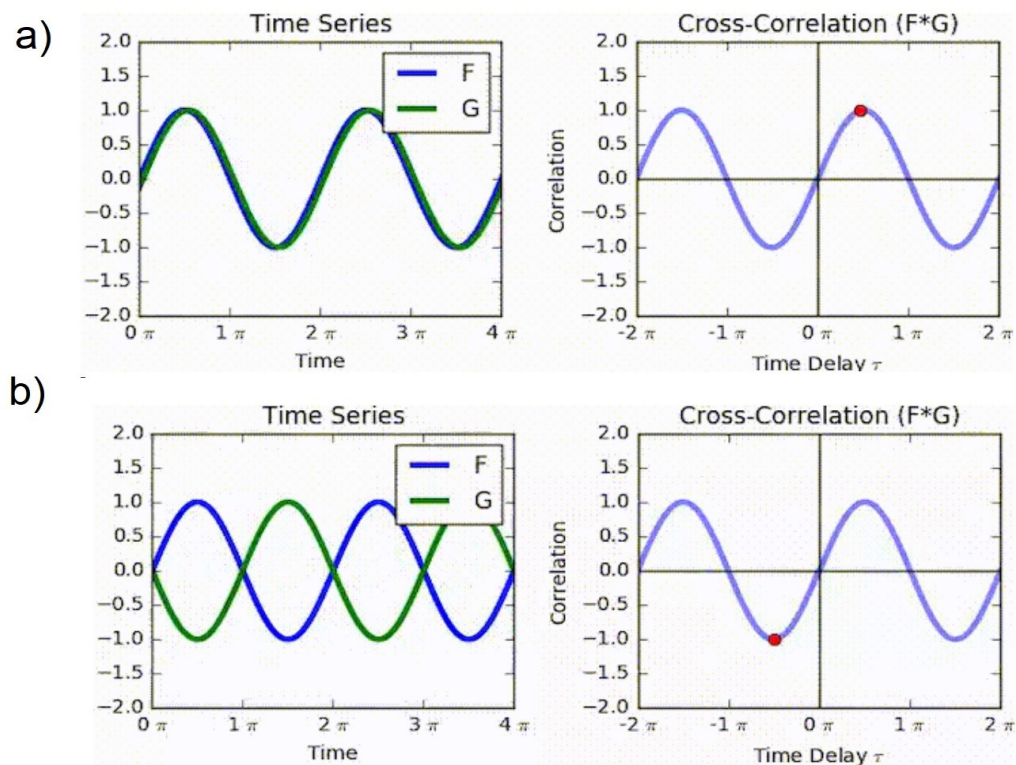
Figure 33: Cross-correlation of two sinus waves with a lag of $\frac{\pi}{2}$. a) Perfect correlation of curve F and G. b) Worst possible correlation of curve F and G. [72]

The cross-correlation of the DMA curves was done via Python Script, which was adapted with consent from a Matlab script made by Ao.Univ.-Prof. Mag.rer.nat. Dr.rer.nat. Liu Qian. The script has two lists for input a shorter list (usually time or temperature-dependent data points of the powder curve) and a longer list (usually time or temperature-dependent data points of the solid curve). The correlation is calculated with Equation 10. Here the variable y is a placeholder for any data point representing a mechanical value in the DMA curves. More specifically, the analysis was done for E'' and tan δ as those were the most promising

values for the Powder Pocket system evaluation. Both sums in the formula contain all data points that overlap between the long list and the short list.

$$r_x = \frac{\sum(y_{short} - \bar{y}_{short}) \cdot (y_{long} - \bar{y}_{long})}{\sqrt{\sum(y_{short} - \bar{y}_{short})^2 \cdot (y_{long} - \bar{y}_{long})^2}}$$

$$(\quad 10 \quad)$$

r_x... correlation coefficient of both curves at a given shift x

y_{short}... Data point from the short list

y_{long}... Data point from the long list

$\bar{y}_{short}$... Arithmetic mean of the short list values

$\bar{y}_{long}$... Arithmetic mean of the long list values

Once the correlation value has been calculated, the short list is shifted by one increment. A sampling rate of 2 Pts./min and a heating rate of 2 K/min would result in 1 K per increment. Due to fluctuations in the sampling rate, the recorded data wasn't always precisely 1 K apart, which would result in faulty analysis of the cross-correlation. The data was linearly interpolated to circumvent this problem and increase the cross-correlation's resolution. In the end, the increments were 0.1 K and consistent throughout the measurement.

Another critical aspect of the cross-correlation is the admissible lag in which the correlation is still valid. The less the two curves overlap, the less the correlation value holds any significance. Unusually high or low correlation might occur when only the side end of both curves overlap, which contain no considerable changes in their value (like peaks or steps). Figure 34 illustrates such a case, the red rectangle marks the overlapping area. Both curves stay relatively constant, resulting in a high similarity and, therefore, a high correlation coefficient. Thus, the requirement is set that at least half of all points must overlap for a valid correlation coefficient. This limit is visualized in the cross-correlogram in Figure 35. showcases the problem mentioned when the lag reaches a high number, both ends of the correlogram show strong oscillation of the correlation value, indicating insufficient overlapping data points.
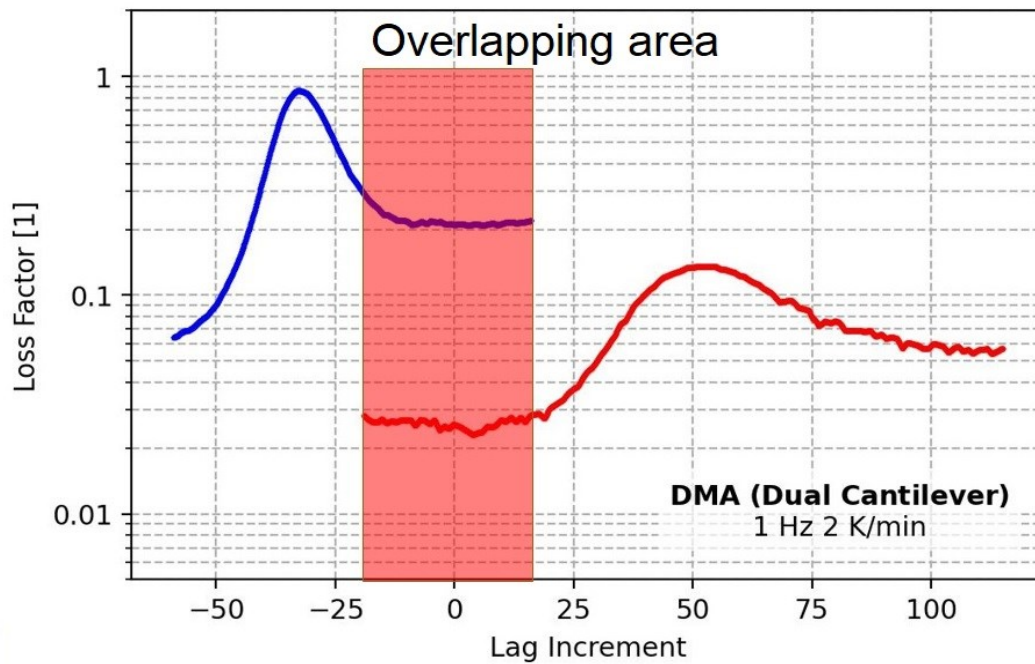
Figure 34: Schematic of a hardly overlapping loss factor curves for a cross correlation which is excluded in the present evaluations.
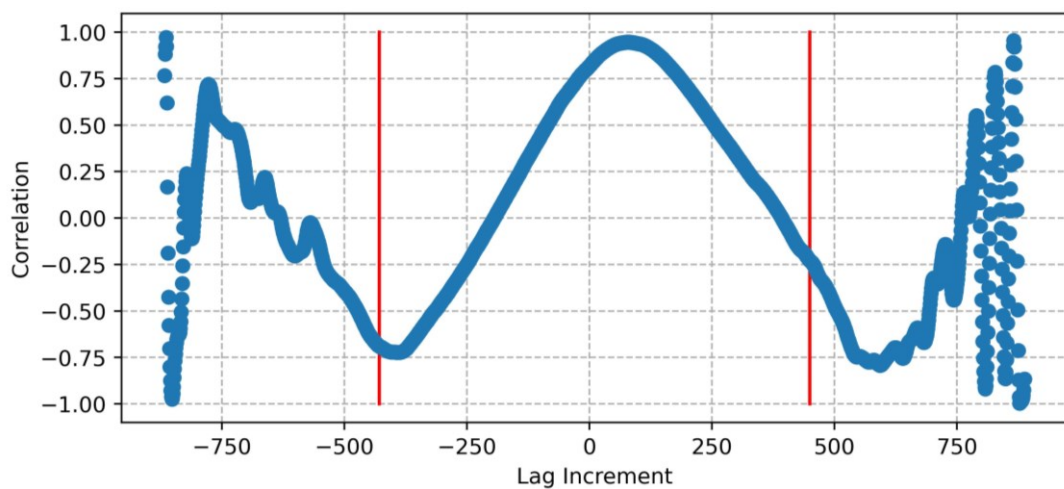
Figure 35: Exemplary cross-correlogram of the Loss Factor of PTFE. The red lines indicate the limits of the valid evaluation area.

Figure 36 shows three different powder DMA curves with different sample preparation. In the legend, the corresponding correlation value is given. The green curve is most similar to the solid curve and shows a correlation value of 0,99. The second best is the black curve with a similar curve shape but a less pronounced peak here, the correlation value decreased to 0.95. Sample preparation method 10 should be avoided here, the curve shows almost no similarity with the solid curve and the correlation value indicates this by

decreasing further to 0.80. It should be noted that the value of the correlation coefficient is not universally comparable but should only be used for comparison relative to the same material.
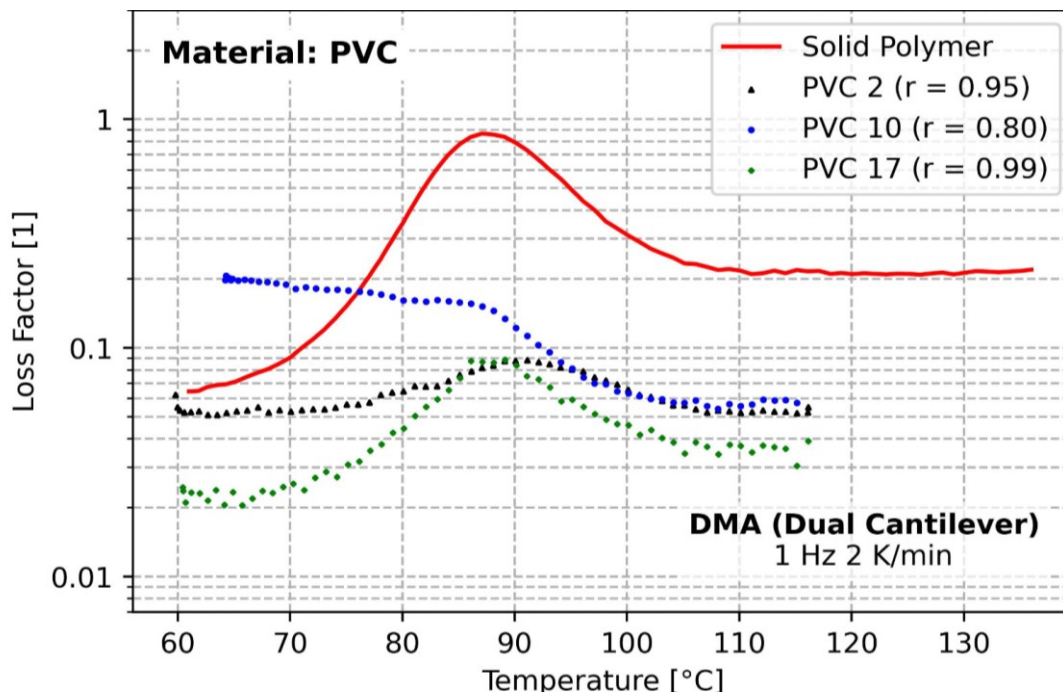
Figure 36: Demonstration of different correlation values for a PVC measurement. PVC 17 (green) is the best in correlation, followed by PVC 2 (black) and PVC 10 (blue).

The second response value is the noise of the DMA curve. The noise of a signal is crucial for interpretation, especially if the interpretation requires precision. Smoothing a curve is a common way of making curves more presentable and easier to evaluate. Too much noise makes smoothing a curve impossible and complicates the evaluation. Figure 37 portraits the difference in noise in two different powder DMA measurements and one solid DMA curve for comparison. The aluminum powder pocket was used for the green curve, resulting in a subjectively higher noise in the measured signal compared to the stainless steel pocket and solid polymer measurement. To quantify this noise, the smooth function was used in the software RheoCompass to create a reference curve. Then the percentage from which the signal deviates from the smoothed curve was calculated according to Equation 11. Calculating the noise for the curves shown in Figure 37 results in a noise value of 9.7% for the green curve and 3.1% for the blue curve. The red curve (solid sample) resulted in the lowest noise of 2.1%, as expected.
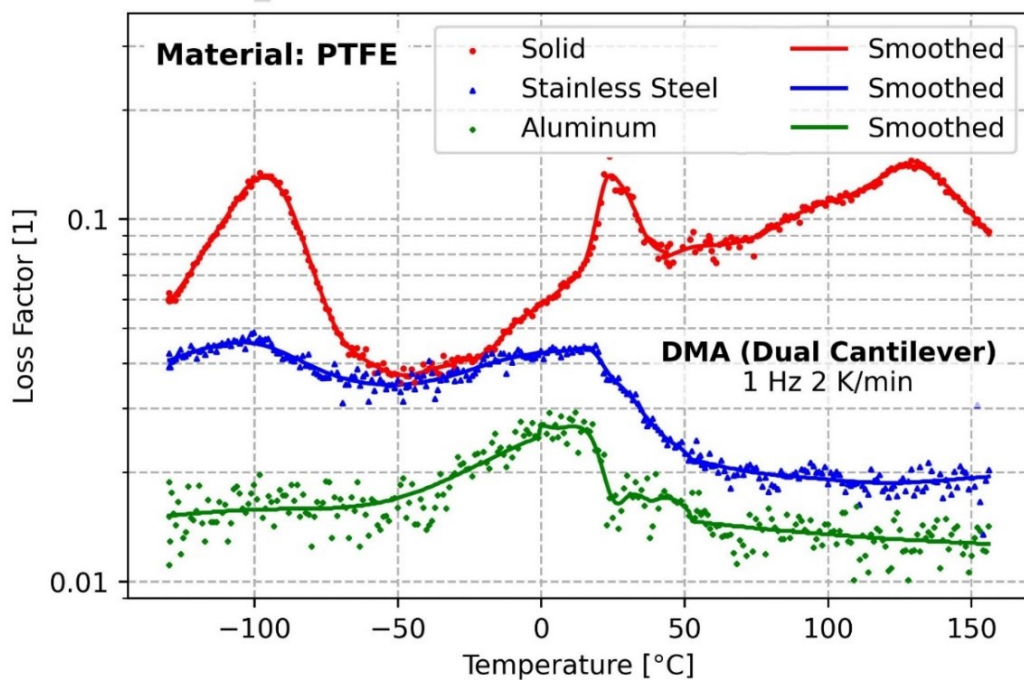
Figure 37: Comparison of two powder measurements and one solid measurement with different noise.

$$n = \frac{\sum \dfrac{(y - y_s)}{y_s} \cdot 100\%}{N}$$

(11)

n... Quantified noise of a DMA curve

y... Data point from an unsmoothed curve

y_s... Data point from a smoothed curve

N... Total amount of data points

The last response value that will be evaluated in the DoE is the position of the glass transition temperature. Several different approaches can be chosen for this response value. For all DMA methods, the T_g of the polymer powder will be compared to the T_g of the solid polymer. Two methods were tried that didn't yield any reproducible results. Determination via lag at maximum correlation could not represent the Tg appropriately but seems to be useful in identifying low-quality measurements. The second failed method used several different functions in a curve fitting method with no success.

The final method simply uses the smoothed curve that was already used for the calculation of the noise. The X-positon (= temperature) of the maximum value of either loss modulus

or loss factor was taken from this smoothed curve. A range of interest was set beforehand to prevent any artifacts from influencing the resulting T_g. The ranges were selected according to T_g values found in literature. The value from literature should be within that range, with the limits set in accordance with the spread of the data (roughly 10-30 °C above and below literature value). After manual inspection of the measured data of PA12, the upper temperature limit was increased from 70 to 100 °C to include the peaks occurring at roughly 80 °C. The list of those ranges is summarized in Table 9. After determining the T_g values of the polymer powders, the T_g obtained from the solid DMA is subtracted. A temperature difference is generally easier to interpret in a DoE analysis, but the actual T_g values are also given for reference. If the evaluated T_g is close to the temperature limit, there is likely no peak in that range and overall no valid peak in the measurement.

Table 9: Range of interest for four materials

Material	Literature Values	Lower Temperature Limit	Higher Temperature Limit
Unit	[°C]	[°C]	[°C]
PVC[22]	90	80	100
TPE[73]	-70	-80	-50
PA12[74]	50	40	100
PTFE T_{gg} [32]	-100	-110	-70
PTFE T_c [33]	20	-20	40
PTFE T_g [32]	120	100	150

All three response values were calculated for all four materials. They can be found in Table 20 to Table 31 in the appendix 2. The tests with grey letters are marked as "unusable". All tests were evaluated manually and marked as unusable if no clear T_g was observable. As seen in those tables, all test runs with unusually high lag values failed the manual evaluation.

The response values are then used to conduct the DoE analysis. The result of this analysis shows the influence of those four parameters on the response value. Some noticeable trends can be taken from the DoE. The representative main effect plot shown in Figure 38 depicts the effect of the different preparation methods on tan δ for PVC. The effects were calculated according to Equation 9. The first sub-diagram shows the influence of the Powder Pocket Material, with -1 being stainless steel and +1 the aluminum, on the correlation between the curve obtained from powder DMA and solid DMA. Choosing the

aluminum Powder Pocket increases the correlation coefficient drastically, as indicated by the values 0.93 and 0.83. The second sub-diagram gives an insight into the sample volume and its influence on the correlation coefficient. Here a higher sample volume (+1) decreases the correlation coefficient. The third effect plot shows the slight increase in correlation coefficient when spreading (+1) the powder in comparison to the heaped powder (-1). The last sub-diagram shows a similarly weak positive influence of the pre-compression step (+1) on the correlation coefficient.
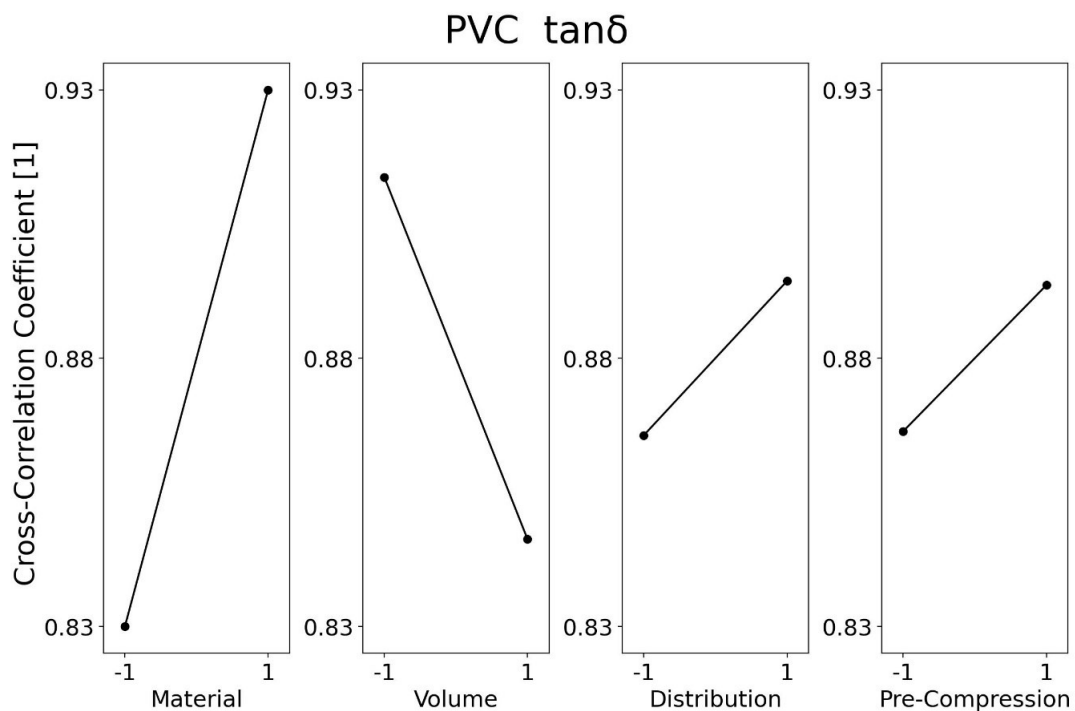
Figure 38: Main effect plot for PVC evaluating tan δ.

The remaining effect plots are found in the appendix 3 (Figure 61 to Figure 89). Tan δ shows an improvement in correlation with the solid curve with the usage of an aluminum Powder Pocket over the stainless steel for PVC, TPE and PA12. Using a small sample volume also seems to positively affect the correlation coefficient, at least for PVC, TPE and PA12. Distribution and Compression don't seem to follow a trend in their influence on the correlation among the four materials tested.

PTFE seems to behave entirely differently in its response to the sample preparation. It should also be noted that the different transition temperatures of PTFE react differently to the sample preparation as well. This is especially noticeable in the correlation coefficient of the low temperature transition. Here the value of the correlation ranges from 0.16 to

0.93. When comparing the parameters, the Powder Pocket material dominates the influence on the correlation drastically. The average for all measurements using the stainless steel Powder Pocket amounts to 0.85, while the aluminum Powder Pocket only results in a correlation coefficient of 0.29. This difference in similarity can be primarily attributed to the fact that the measurements using the aluminum Powder Pocket had no visible or only barely visible peak at low temperatures while the stainless steel option results in a clearly visible peak. Figure 39 displays this difference caused by the Powder Pocket material. The test numbers refer to the number set by the DoE in Table 19 in the appendix. At roughly -100 °C, a peak can be observed for the stainless steel curve (blue curve), while the peak is missing for the aluminum curve (red curve). The only preparation that seems to improve all three areas of interest in PTFE is a high sample volume. One hypothesis for this behavior could be made when looking at the sample after the test. PTFE seems to form a quasi-solid sheet similar to the solid sample made from compression molding. When using a low sample volume, the material wasn't fully covering the Powder Pocket and therefore the quasi-solid sheet was filled with holes, as shown in Figure 40. Those holes could have had a negative influence on the DMA measurements.
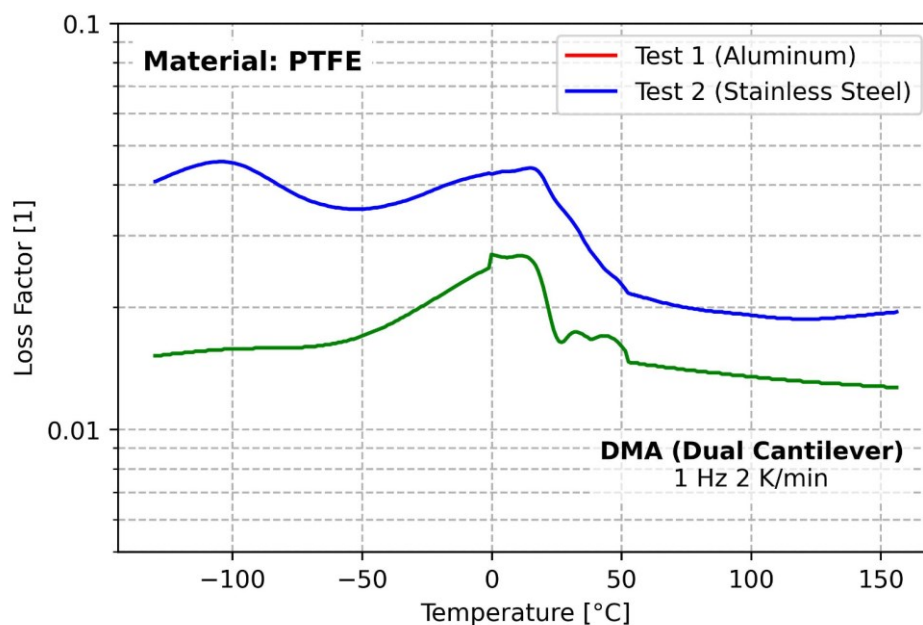
Figure 39: Influence of the different Powder Pockets on the detection of the low temperature transition via tan δ. Test 1 (red) and representative of a measurement using the aluminum Powder Pocket while test 2 (blue) displaying the peak at low temperatures measureable via stainless steel Powder Pocket.

Figure 40: PTFE sample with too low sample volume after completing the DMA.

The effect plots regarding the noise of the DMA curves show clear trends for all materials. Another thing that should be noted is that compared to the correlation effect plots, a lower value is now the desirable outcome (as it indicates less noise and therefore easier evaluation of the data). With the exception of TPE, using a stainless steel Powder Pocket seems to reduce the noise of the signal. In the case of TPE, the Powder Pocket only slightly influences the noise (almost neutral). A high sample volume reduces the overall the noise in the signal for all materials and seems to have, together with the Powder Pocket material, the highest influence on the noise. Heaping the material and no pre-compression slightly improve the noise of the DMA curve.

The evaluation of the position of the thermo-mechanical transition with this method must be reviewed critically. Evaluating the general trend depends on whether or not the shift in temperature is negative or positive. In comparison, the correlation and noise only lead to positive values. The measured T_g could be higher or lower depending on the sample. Therefore, looking at the y-axis scaling is important when arguing for the effect on the position of T_g. Additionally, evaluation is only logical if a peak is even present in the curve. This criterion excludes the PTFE$_{Tg}$ and to some extend PTFE$_{Tgg}$ and PA12, as the latter only yielded a peak for certain preparation methods. The remaining materials (PVC, TPE and PTFE$_{Tc}$) again seem to be influenced mainly by the Powder Pocket material and the sample volume. PVC generally yields excellent results regarding the position of T_g the choice of the power pocket only influences the results by 0.4 °C while the sample volume had a much bigger influence of roughly 2.5 °C. TPE, on the other hand was much more influenced by the Powder Pocket material, with a change of 6 °C on average. The shift caused by the sample volume is only 1.2 °C. The aluminum Powder Pocket and a higher sample volume

resulted in a ΔT_g closer to zero for both materials. The crystalline transition temperature of PTFE was also more accurately determined by a higher sample volume but in regard to the Powder Pocket the stainless steel version is preferred as it seems to be the case for all response values.

The following tables summarize the results from the DoE analysis for the evaluation of tan δ. Table 10 displays the optimal preparation parameters for each material regarding the correlation to the corresponding solid curve. Table 11 gives an insight into the preparation parameters that result in the least noise in the powder DMA curve for each material. The most accurate determination of T_g in powder DMA, in reference to the T_g obtained from solid DMA, is achieved by the parameters shown in Table 12.

Table 10: Summary of the best possible preparation for the evaluation of tan δ according to the main effect plot to maximize the correlation coefficient. The = symbol indicates that both choices are equal.

Correlation	Powder Pocket	Volume	Distribution	Compression
PVC	Aluminum	< 0.275ml	spread	3x10N
TPE	Aluminum	< 0.275ml	spread	-
PA12	Aluminum	< 0.275ml	heaped	3x10N
$PTFE_{Tg}$	Stainless Steel	> 0.275ml	spread	=
$PTFE_{Tc}$	Aluminum	> 0.275mL	heaped	0
$PTFE_{Tgg}$	Stainless Steel	> 0.275mL	spread	3x10N

Table 11: Summary of the best possible preparation for the evaluation of tan δ according to the main effect plot to minimize the noise.

Noise	Powder Pocket	Volume	Distribution	Compression
PVC	Stainless Steel	> 0.275mL	heaped	3x10N
TPE	Aluminum	> 0.275mL	heaped	0
PA12	Stainless Steel	> 0.275mL	heaped	0
$PTFE_{Tg}$	Stainless Steel	> 0.275mL	spread	3x10N
$PTFE_{Tc}$	Stainless Steel	> 0.275mL	spread	3x10N
$PTFE_{Tgg}$	Stainless Steel	> 0.275mL	spread	3x10N

Table 12: Summary of the best possible preparation for the evaluation of tan δ according to the main effect plot to minimize the ΔTg. The x symbol indicates that no valid DoE analysis could be done for that material/transition.

ΔT_g	Powder Pocket	Volume	Distribution	Compression
PVC	Stainless Steel	> 0.275mL	heaped	3x10N
TPE	Aluminum	> 0.275mL	spread	3x10N
PA12	x	x	x	x
PTFE$_{Tg}$	x	x	x	x
PTFE$_{Tc}$	Stainless Steel	> 0.275mL	spread	0
PTFE$_{Tgg}$	x	x	x	x

Some parameters are more significant than others and in some cases the choice showcased only changes the result slightly. Therefore, it is advised to look at the full main effect plots in the appendix 3. The final recommendation gives the all-around best possible combination with the highest value placed on an accurate and reproducible determination of T_g via tan δ across all materials. An aluminum Powder Pocket with high sample volume are highly recommended, while spreading the powder and pre-compression is an optional step that can improve the results slightly.

4.2   Thermomechanical behavior of powders compared to the solid state

Many differences between powders and solids exist regarding their thermo-mechanical behavior. These differences can be of physical, metrological, and applicable nature. Powders are due to their lack of continuity and cohesion ever-changing in their response. There is always the risk that the same material, even with the same powder-specific properties, acts differently when exposed to a certain test. Therefore, the sample preparation must be conducted with utmost care and as consistently as possible.

When looking at the results obtained from powder DMA, some differences to conventional measurements of solid-state specimens stand out. One noticeable fact is that the difference between T_g measured from E'' and tan δ don't seem to differ much when using the Powder Pocket system. The T_g shift occurring in conventional DMA is of mathematical nature as tan δ is the quotient of E'' an E'. In a hypothetical DMA curve in which E' stays constant, E'' and tan δ would experience the exact same change over temperature and the T_g shift would be 0. DMA measurements, using the Powder Pocket create a similar scenario. The metal from the Powder Pocket dominates the E' and only slight changes happen at T_g.

This causes the maxima of E'' and tan δ to move closer to each other. In case of PVC the solid samples resulted in an average T_g of 80.08 °C obtained from E'' and 87.47 °C obtained from tan δ as seen in Figure 41. Delides[75] even estimates the shift of Tg between those two methods to be 10-15 °C. Measurements on polymeric composites from Adekunle et al.[76] coincide with this estimation. DMA measurements by Jansen[77] indicate a shift between 5 and 10 °C for amorphous polymers. For the results of the powder DMA this shift is reduced to 2 °C.

The second observation when comparing the results from powder to solid DMA is the temperature lag of T_g. The shift is apparent when looking at the ΔT_g for T_g obtained from E''. This value is directly obtained from the measurement (not through calculation) and is, therefore, directly connected to the changes in the measurement. The average of all T_g values obtained from E'' for PVC in the Powder Pocket is 86.63 °C, resulting in a difference of 6.55 °C to the solid curve.
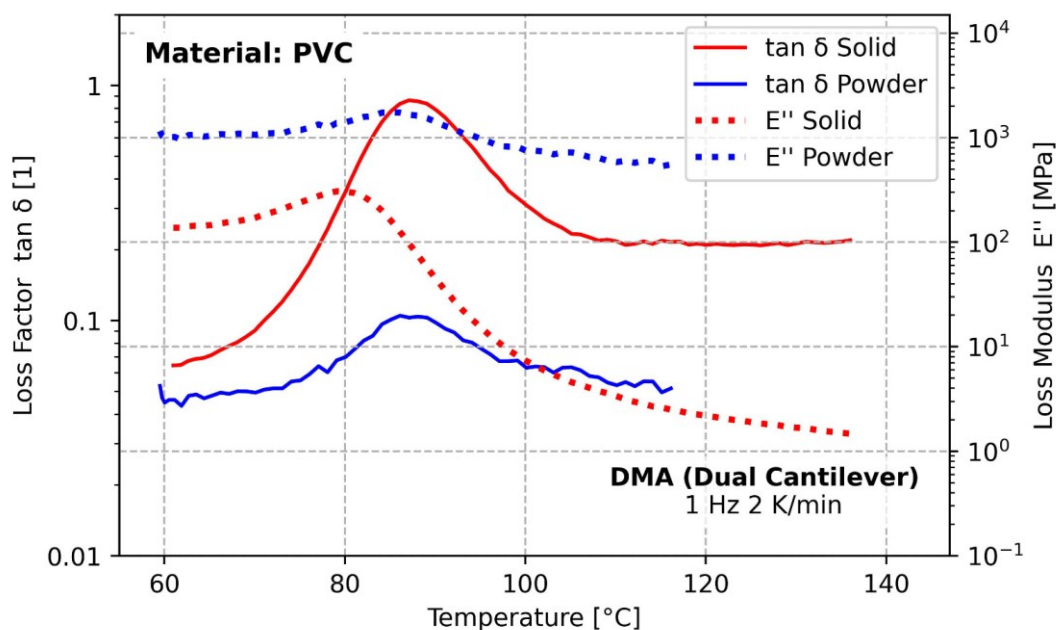
Figure 41: Representative comparison measurements for PVC, using the recommended preparation method for Powder DMA (test 5) and the solid DMA curve, showing both tan δ and E'' .

When combining both phenomena observed in powder DMA their effect on the T_g obtained from tan δ almost cancels each other out. The lag possibly caused by lower thermal conductivity is counteracted by the fact that the maxima of E'' and tan δ converge. This

leads to very accurate results for T_g when using the maximum of tan δ (ΔT_g is on average only 1 °C). Similar tendencies are shown for TPE in Figure 42. The T_g values obtained are summarized in Table 13.

Table 13:   Comparison of Tg values obtained from solid DMA and powder DMA for PVC and TPE.

DMA Type	Solid		Powder		Powder - Solid	
	T_g (E'')	T_g (tan δ)	T_g (E'')	T_g (tan δ)	ΔT_g (E'')	ΔT_g (tan δ)
Unit	°C	°C	°C	°C	°C	°C
PVC	80.1	87.4	86.6	88.4	6.5	0.9
TPE	-68.3	-60.9	-66.5	-63.8	1.8	-2.8

Figure 42: Representative comparison measurements for TPE, using the recommended preparation method for Powder DMA (test 5) and the solid DMA curve, showing both tan δ and E''.

The crystalline transition temperature found in PTFE behaves differently in solid and powder DMA. This difference is displayed in Figure 43. Regarding this transition temperature in solids, E'' and tan δ result almost in the same temperature. For powders the results fluctuate strongly but on average, the crystalline transition temperature is roughly 10 °C lower than when observed in solids (Table 14). This observation is surprising as the testing method should result in delayed responses. A strong decrease in crystallinity was measured via DSC but showed no significant influence on the crystalline transition temperature in the second run. Nonetheless, a change in crystalline morphology could still

influence the mechanical behavior. This change would not be visible by DSC as it relies only on thermal characterization of the polymer. Tg could not be detected in any powder DMA measurement. In comparison, T_{gg} could be observed under certain conditions. The average value of T_{gg} (ignoring the test runs marked from Table 28 and Table 29) resulted in -100.24 °C for T_{gg} obtained from E'' and -96.19 °C from tan δ. This results in a deviation from the solid state specimen of 4 °C and 2 °C, respectively.

Table 14: Comparison of Tc obtained from solid DMA and powder DMA for PTFE.

DMA Type	Solid		Powder		Powder - Solid	
	T_c (E'')	T_c (tan δ)	T_c (E'')	T_c (tan δ)	ΔT_c (E'')	ΔT_c (tan δ)
Unit	°C	°C	°C	°C	°C	°C
PTFE	22.8	22.8	8.4	13.8	-14.3	-9.0

Table 15: Comparison of Tgg (secondary relaxation in the amorphous phase) obtained from solid DMA and powder DMA for PTFE.

DMA Type	Solid		Powder		Powder - Solid	
	T_{gg} (E'')	T_{gg} (tan δ)	T_{gg} (E'')	T_{gg} (tan δ)	ΔT_{gg} (E'')	ΔT_{gg} (tan δ)
Unit	°C	°C	°C	°C	°C	°C
PTFE	-104.2	-98.2	-100.2	-96.2	4.0	2.0
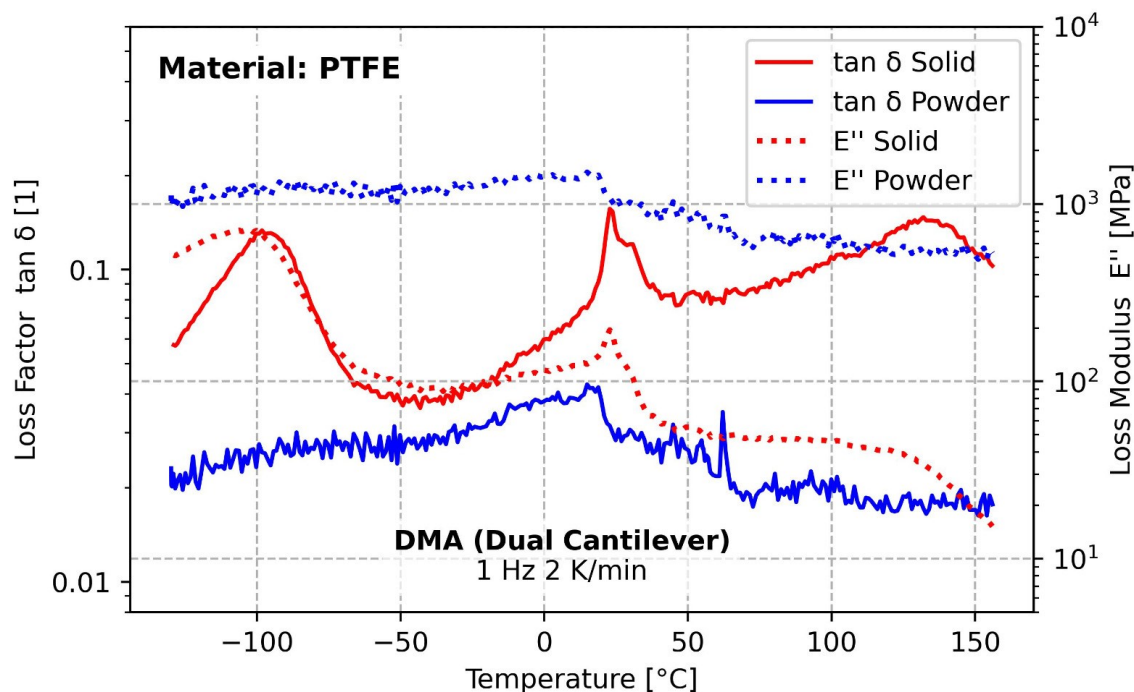
Figure 43: Representative comparison measurements for PTFE, using the recommended preparation method for Powder DMA (test 5) and the solid DMA curve, showing both tan δ and E''.

PA12 shows a similar behavior as PTFE in that a transition is only detectable under certain conditions for the following analysis only viable measurements were used. Another interesting fact about the measured T_g values is their substantial shift to higher temperatures. The mean of T_g obtained from tan δ via powder DMA is 84.18 °C while the T_g obtained from E'' result in a value of 79.24 °C. That's roughly a shift of 35 °C for both methods and can hardly be correlated with the T_g measured in the solid samples. The shift is displayed in Figure 44. This behavior could be related to changes in the degree of crystallinity and crystal modification when the powder is melted. A study conducted by Askadski et al.[78] suggests that a higher degree of crystallinity shifts T_g to a higher value. The model provided in the study is based on Polyethylene. A change from 30 % to 65 % in degree of crystallinity causes the T_g to shift by roughly 50 °C. The model used for this prediction is based on the activation energy of the polymer. The shift of 35 °C obtained from the measurements could be potentially predicted by the same model upon changing the activation energy accordingly.

Table 16: Comparison of T_g obtained from solid DMA and powder DMA for PA12.

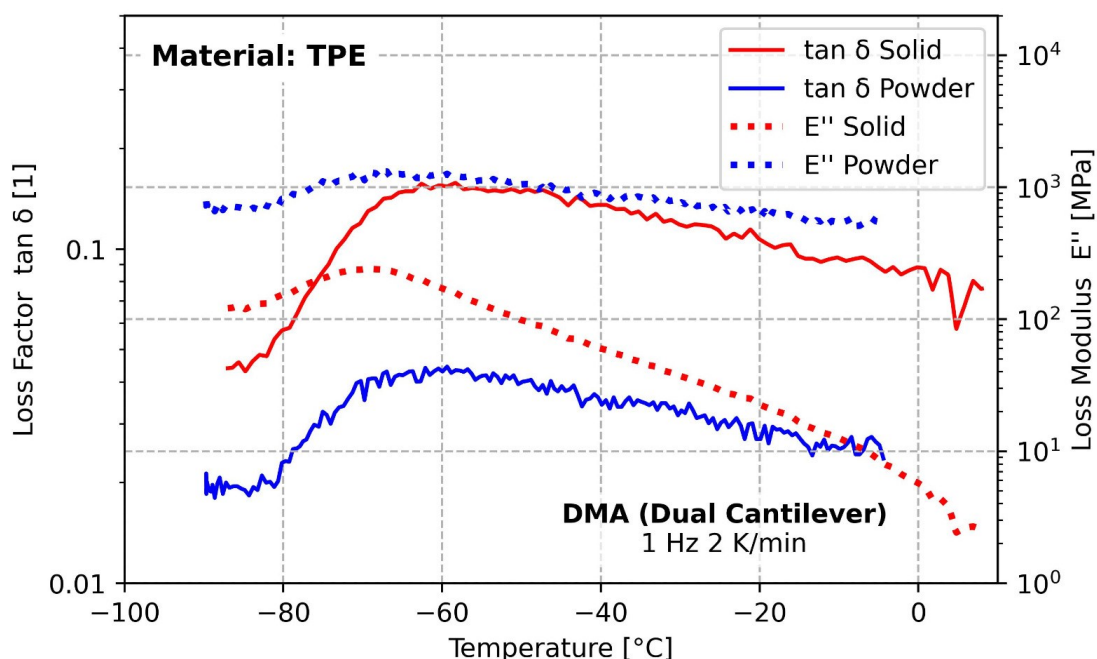| DMA Type	Solid		Powder		Powder - Solid	
	T_g (E'')	T_g (tan δ)	T_g (E'')	T_g (tan δ)	ΔT_g (E'')	ΔT_g (tan δ)
Unit	°C	°C	°C	°C	°C	°C
PA12	43.8	52.5	79.2	84.2	33.6	35.4
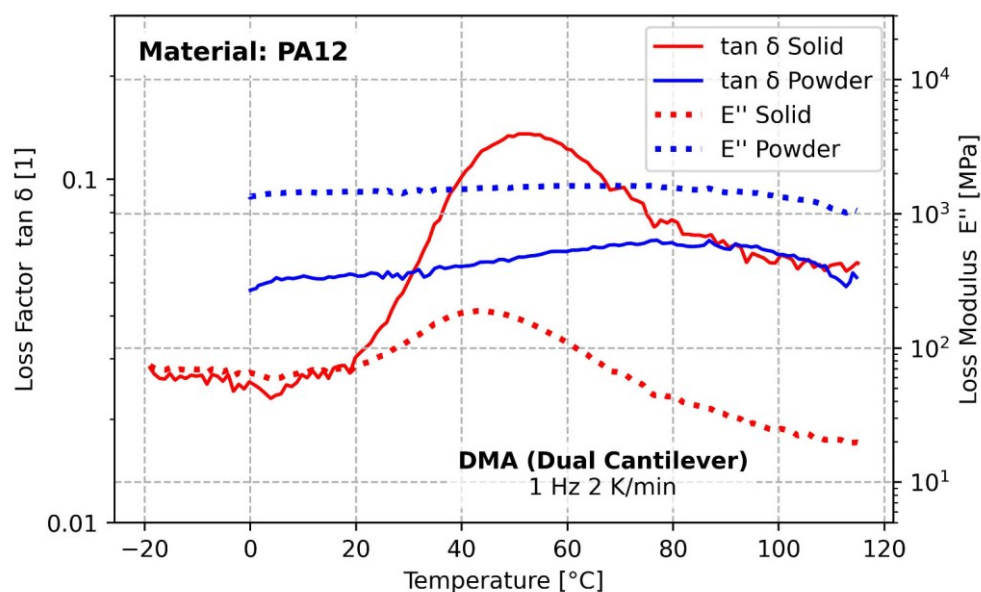
Figure 44: Representative comparison measurements for PA12, using the recommended preparation method for Powder DMA (test 5) and the solid DMA curve, showing both tan δ and E''.

4.3   Thermo-calorimetric properties

This chapter covers the results of the experiments regarding the thermo-calorimetric properties of polymer powders. These properties allow for the determination of T_g and give an insight into the degree of crystallinity for semi-crystalline polymers. For each material, three tests were conducted with the same testing parameters. Two runs were conducted per material to see if any differences may occur when deleting the thermal history. To determine the degree of crystallinity of PA12, PTFE and TPU, the melting enthalpy ΔH_m was obtained via integration of the curve at the melting peak. Another value needed to determine the degree of crystallinity is the melting enthalpy, $\Delta H_m{}^0$, of a theoretically 100% crystalline polymer which is taken from literature. Table 3 shows the $\Delta H_m{}^0$ obtained from literature. The value for TPE only references the melting enthalpy of the hard segment.

Table 17:   Values of melting enthalpies for 100% crystalline TPE, PA12 and PTFE obtained from literature.

Material	$\Delta H_m{}^0$ [J/g]
TPE[79]	209
PA12[80]	155
PTFE[81]	82

The glass transition, if possible, was determined via the inflection point of the heat flux curve. The inflection point was easily obtained through an evaluation tool in the DSC software TRIOS by TA Instruments (New Castle, US,). In case of PTFE, T_C was determined at the crystalline transition peak maximum. Due to being experimentally limited by the lowest possible temperature of the DSC device, which was at -90 °C, the T_{gg} of PTFE could not be analyzed. This temperature limitation also made the inflection point analysis of TPE difficult. A recommendation by TA Instruments set the minimum temperature for a heating rate of 10 K/min even lower at -50 °C. The summary of all the results obtained from the DSC can be found in Table 32 to Table 35 (in the appendix). Any exothermic mechanisms are in positive y-direction, while endothermic mechanisms are in negative y-direction.

The PVC measurements have a noteworthy oddity in the DSC curve, as seen in Figure 45. Right before the T_g at roughly 84 °C, an endothermic phenomenon between 60 and 70 °C can be observed. This peak should not be attributed to the PVC but rather an additive in the dry blend. The components of the PVC powder are listed in the datasheet and notable

is the 1-5w% content of Poly (methyl methacrylate/butylacrylate), which is a copolymer of PMMA and PBA. A similar DSC curve was measured in a study by Nasr et al.[82], here the mixture contained 75 w% PVC and 25 w% PMMA and a small endothermic peak can be seen before T_g as well. Another interesting aspect is that the endothermic peak shifts to lower temperatures and reduces in size for the second run, as displayed in Table 32 (in the appendix), probably due to morphological changes of the PVC/PMMA/PBA-blend after the first heating phase. One possible explanation could lie in the crosslinking abilities of PVC and PMMA, which might decrease when being melted and forming agglomerates.
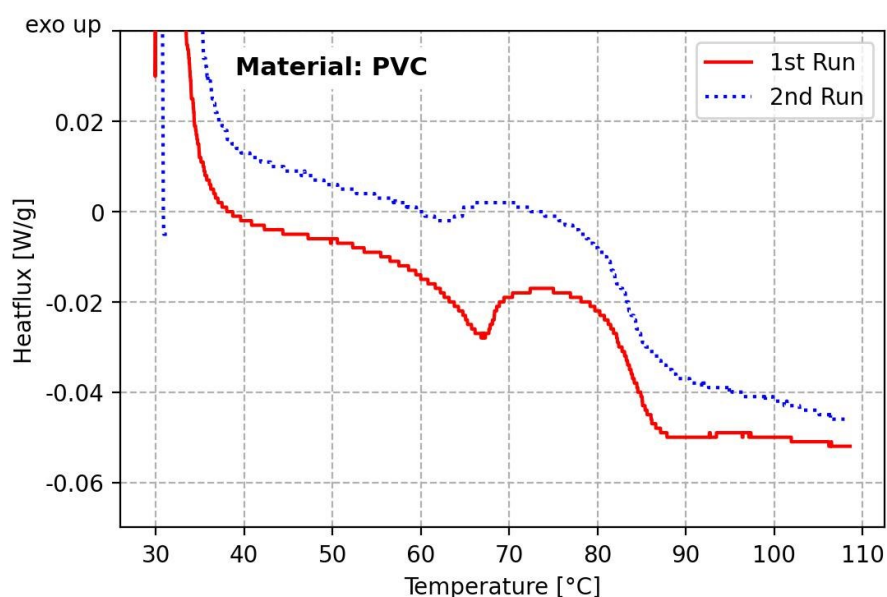
Figure 45: DSC curves measured for PVC powder showing two runs in a temperature range from 30 to 110 °C.

As mentioned, the temperature limitation at the lower end caused the evaluation of T_g of the soft phase to be difficult and uncertain for TPE. A study conducted by Kojio et al.[73] found the T_g of the soft segment at -70 °C. They also suggest that a transition related to a mixture of the hard and soft segment could occur at 50 °C. A T_g for the pure hard segment could not be detected in this present thesis, as seen in Figure 46. On the other hand, two melting peaks were observed with a peak at roughly 0 °C belonging to the soft segment while the melting peak at high temperatures (~186 °C) refers to the hard segment of the TPE, coinciding well with the values found by Kojio et al.[73]. The degree of crystallinity refers to the hard segment and is displayed in Table 33 (in the appendix), here a slight decrease from 8% to 6% occurred in the second run.
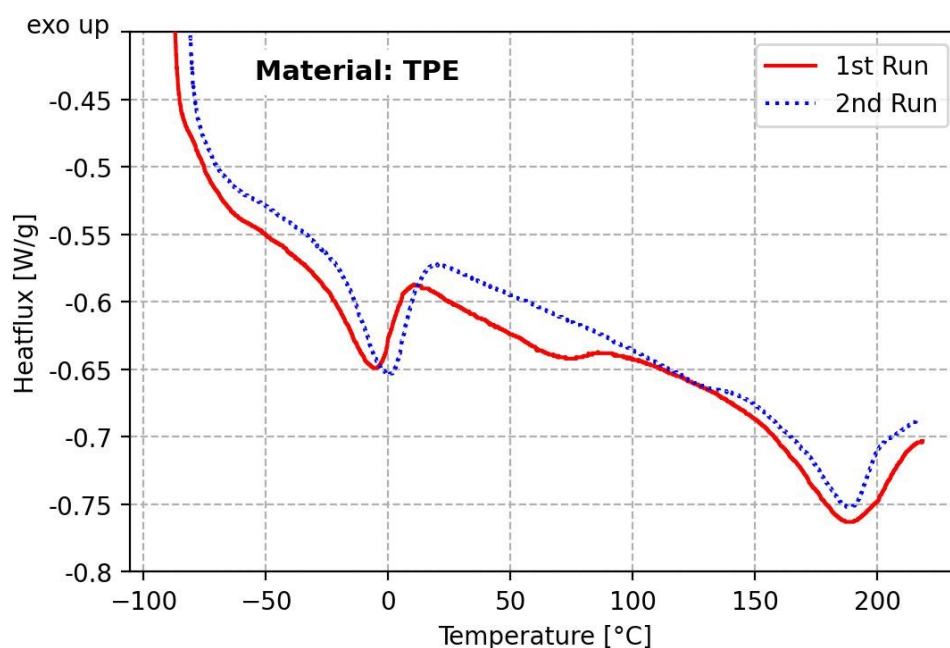
Figure 46: DSC curves measured for TPE powder showing two runs in a temperature range from -80 to 220 °C.

The T_g of PA12 could not be determined via DSC as seen in Figure 47. The signal obtained at T_g for semi-crystalline polymers is generally weak, especially for polymers with a high degree of crystallinity. Due to the low proportion in amorphous phase present in the polymer the change in heat flow caused by T_g is not visible. Studies regarding the T_g of PA12 vary a lot in their results. A study by Olejarczyk et al[83]. tested a PA12 type used specifically for SLS. No T_g could be detected from their DSC measurement either. Other studies could detect a T_g at 53 °C (Shirinbayan et al.[74]). Another interesting result from the DSC measurements is the change in the degree of crystallinity X_c and Tm between the first and the second heating run. This clearly indicates a thermal history of the material. For the original sate, the crystalline domains had enough time to rearrange themselves to bigger and thicker lamella packets, increasing the temperature needed to melt those crystalline regions with higher degree of crystallinity. For the second run, the degree of crystallinity changes from 66% to 27% with a shift of the Tm from 185 °C to 177 °C, as displayed in Table 34. This change could also be due to an altered crystalline morphology caused by the cooling phase before the second run. Another theory could be that the polymer powder had a different crystalline modification. α-Modification is obtained directly from solution

and generally tends to have a higher degree of crystallinity than the more common γ-modification obtained from the melt.[83–86]
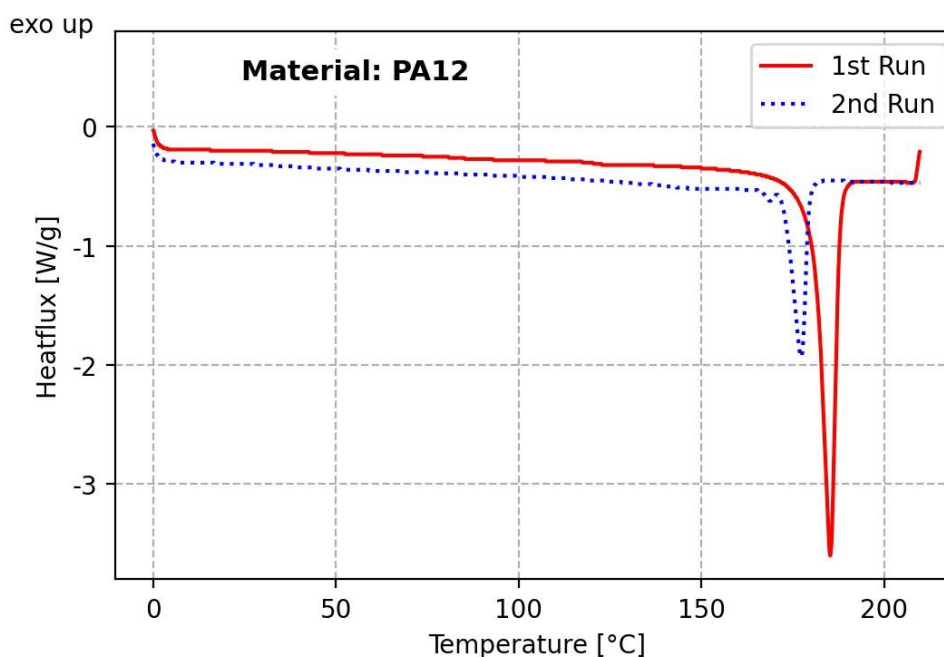
Figure 47: DSC curves measured for PA12 powder showing two runs in a temperature range from 0 to 210 °C.

Due to the temperature limitation of the DSC device with a possible start temperature of -90 °C, only the crystalline transition peak around room temperature and the T_g at roughly 130°C of PTFE could be analyzed. The crystalline transition temperature was measured at 17 °C as seen in Figure 48, resulting in a slightly lower value than the 19 °C found mentioned by Ebnesajjad et al.[33]. In the first run, an overlapping peak could also be found at roughly 29 °C, which marks the second crystalline transition temperature. The T_g at approximately 130 °C could not be found due to high degree of crystallinity of 72% (displayed in Table 35) and the therefore low amount of amorphous phase. These results coincide with an application note conducted by Strasser and Schmölzer[87]. Due to ageing and rearrangement of the crystalline structure, the degree of crystallinity and T_m were higher in the original state of the material, this effect is removed in the second run and a morphological state according to the cooling rate of the DSC is achieved.
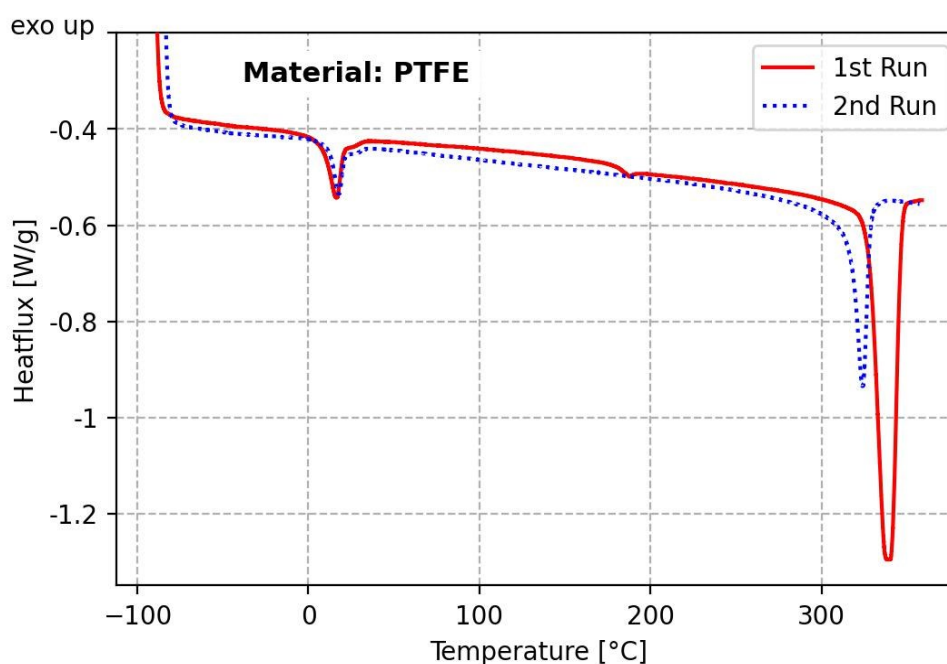
Figure 48: DSC curves measured for PTFE powder showing two runs in a temperature range from -80 to 360 °C.

A full comparison of the determined thermal transitions of PVC, TPE, PA12 and PTFE via powder DMA and DSC can be found in Table 18. Transition temperatures obtained from DSC tend to be lower than the ones obtained from powder DMA with the exception of the crystalline transition. Powder DMA could be a suitable substitution for DSC when analyzing thermal transitions in polymer powders. The main advantage of DSC over powder DMA is the determination of melting temperatures. Removing molten polymer from the Powder Pocket proved to be difficult, therefore it is not recommended to use the Powder Pocket for the determination of the melting temperature. In comparison, the single-use crucibles used for DSC circumvent this problem by removing the need to clean the crucibles.

Table 18: Comparison of values for thermal transitions measured by DSC and powder DMA.

Method	Powder DMA tan δ	DSC
Unit	[°C]	[°C]
T_g PVC	88.4	83.7
T_g TPE	-63.8	-78.4
T_g PA12	84.2	x
T_{gg} PTFE	-96.2	x
T_c PTFE	13.8	17.3
T_g PTFE	x	x

4.4   Comparison of powder rheological properties to the DMA results

In this chapter, several powder rheological properties were measured at different load levels and temperatures to determine the best way to detect morphological changes. The properties chosen for evaluation were:

- Major Stress σ_1
- Unconfined Yield Strength σ_c
- Cohesion c
- Flow Function ff
- Angle of linearized yield locus φ_{lin}
- Effective angle of internal friction φ_{ef}

Another aspect that needs to be clarified is reproducibility. Since the polymer powders showed a strong free flowing powder behavior, the standard evaluation method included in the RheoCompass software was not a valid option as it led to strong deviation in the results obtained. A different evaluation inspired by a round-robin test by Berry et al[64]. was chosen. A visual guide can be found in Figure 49 to show the connection between the raw data obtained from the shear measurement and the yield locus curve. This method excluded the first pre-shear and shear-to-failure step from the evaluation. Instead, the second and third pre-shear maxima are used as additional shear-to-failure points. The pre-shear stress is calculated as the mean value of the last 20 data points of the second and third pre-shear curve. The shear-to-failure points are then used to plot the linearized yield locus to determine the necessary points to draw the Mohr circles.
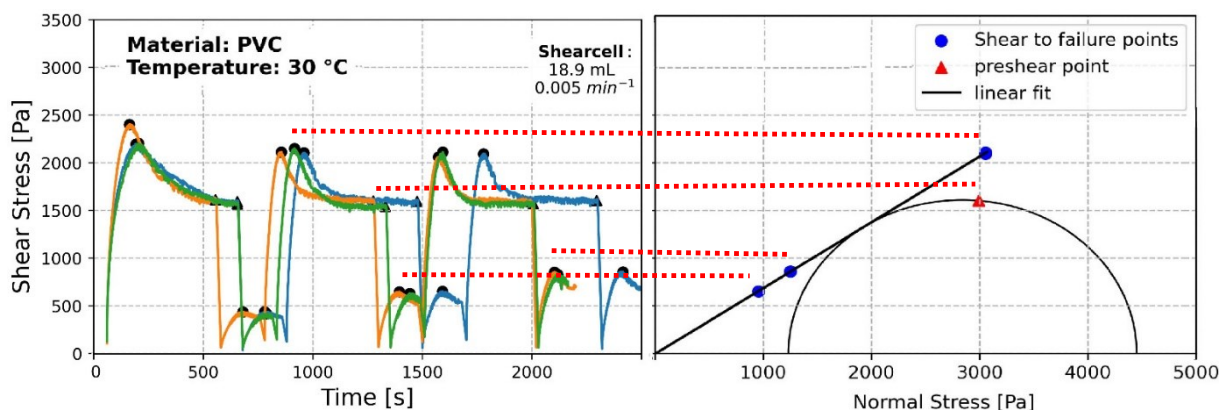
Figure 49: Side by Side view of the raw data obtained from the shear measurement (left) and the yield locus curve (right). The exemplary material used is PVC at 30 °C and a normal stress of 3 kPa.

Figure 50 to Figure 52 display the Mohr's circle for different normal stress levels. The smaller Mohr circle is not visible due to the highly free flowing properties of the polymer powder, which results in very small values for c and σ_c. The linear regression fits well through the shear to failure points, justifying the use of a linear model for the yield locus curve. From those curves, all the powder rheological properties were calculated according to the Equations mentioned in chapter 2.3.3. [64]
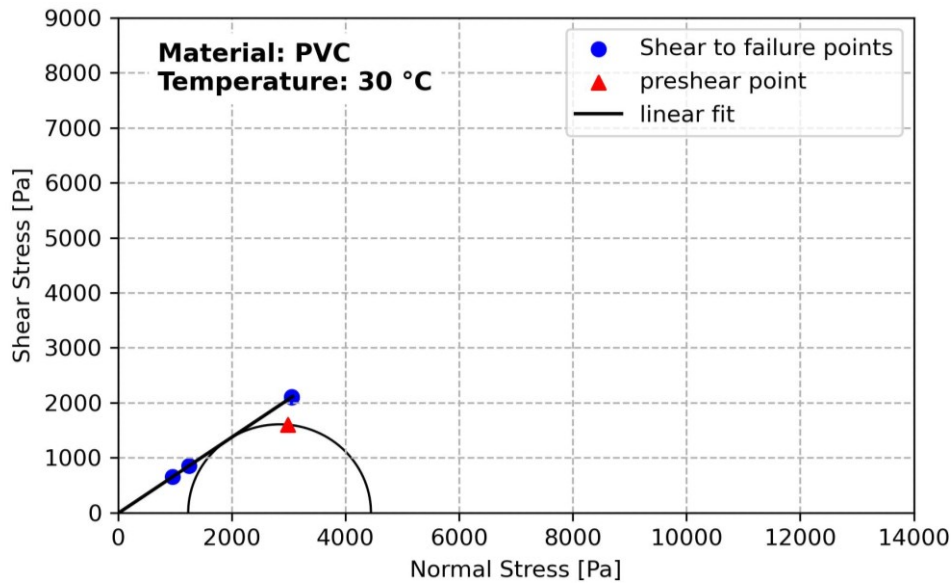
Figure 50: A depiction of the Mohr's circle obtained from the pre-shear and shear to failure points, for a normal stress level of 3 kPa.
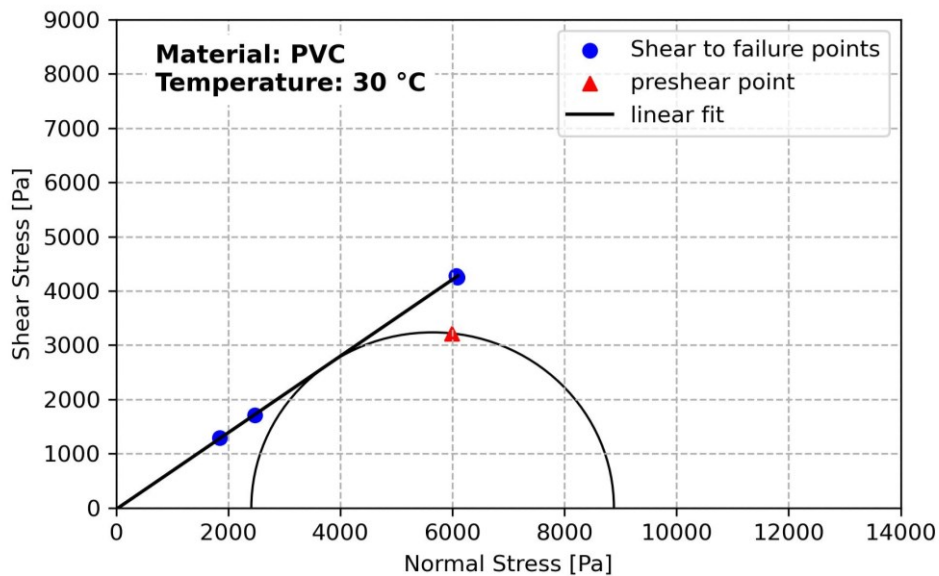
Figure 51: A depiction of the Mohr's circle obtained from the pre-shear and shear to failure points, for a normal stress level of 6 kPa.
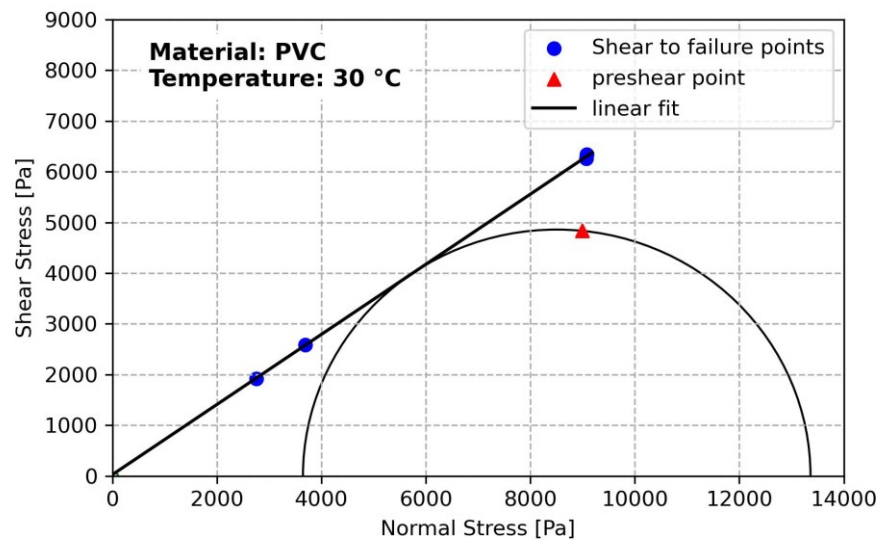
Figure 52: A depiction of the Mohr's circle obtained from the pre-shear and shear to failure points, for a normal stress level of 9 kPa.

The following paragraph discusses the viability of different powder rheological properties to be used as an indicator for T_g. PVC will be used as an example in the graphs, but every material seems to follow similar tendencies. Figure 54 a) displays σ_1 measured at three temperatures 30 ,70 and 100 °C. The two lower temperatures (30 and 70 °C) represent the region below T_g, while the measurement at 100 °C is well above T_g. The changes in this value are not significant enough to detect any change caused by T_g. A slight indication for T_g can be observed when evaluating σ_c. In Figure 54 b) a higher normal stress level seems to improve the detection of T_g. The data points for 6 and 9 kPa show a significant change between 70 and 100 °C, which is not the case for 3 kPa. The flow function appears to be impractical when detecting changes due to its high deviation and the scale at which flow functions can occur as seen in Figure 54 c). The flow function ff is obtained from the division of σ_1 and σ_c (Equation 1). Especially in free flowing materials σ_c approaches zero, which could lead to excessively high numbers when dividing. The flow function ff is also prone to big deviation as it is obtained through the division of two other measured values, therefore, combining the error of σ_1 and σ_c. It should also be noted that those stresses are prone to error themselves due to the trigonometrical way they are obtained. A slight change in angle from the linearized yield locus could already lead to vastly different Mohr Circles and, therefore, vastly different values for σ_1 and especially σ_c. Cohesion c suffers from the same

problem as it is strongly dependent on the angle the linearized locus has. Nonetheless, a significant change close to T_g can be observed in Figure 54 d). As seen in Figure 54 e) and Figure 54 f), both φ_{lin} and φ_{ef} show excellent repeatability. Additionally, the angles display a noticeable change in their value above and below T_g. A higher normal stresses lead to generally better visibility and less deviation. These two powder rheological properties are most suitable for detecting a thermos mechanical change in the powder. Those angles also worked best for TPE, PA12 and PTFE (diagrams in the appendix 4). For PTFE, other powder rheological properties such as σ_1 or σ_c also seemed promising when determining the crystalline transition at room temperature, as seen in Figure 102 and Figure 103 in appendix 4. This transition influences the material in such an extreme way that even the handling of the sample differs from the other powders. Due to the fibrillation caused by the transition of the crystal modification, the powder particles agglomerate and act similarly to a solid. This phenomenon is especially noticeable when removing the powder from the shear cell. Figure 53 shows a picture of the PTFE powder after shear testing at 30 °C. At this temperature, no sintering process occurred and the "pseudo solid" is only held together by the fibrillation effect. The effect was more prominent when higher normal stresses were applied in the shear test. Due to the strong cohesion between the particles, no powder break occurred, therefore, no shear-to-failure point could be measured at 30 °C and above. Therefore, the experiment could not be conducted at normal stress of 6 and 9 kPa at and above 30 °C. The measurements at higher temperatures were only done for 3 kPa.

Figure 53: PTFE Powder keeping its shape after testing at 30 °C due to strong interaction forces caused by fibrillation.
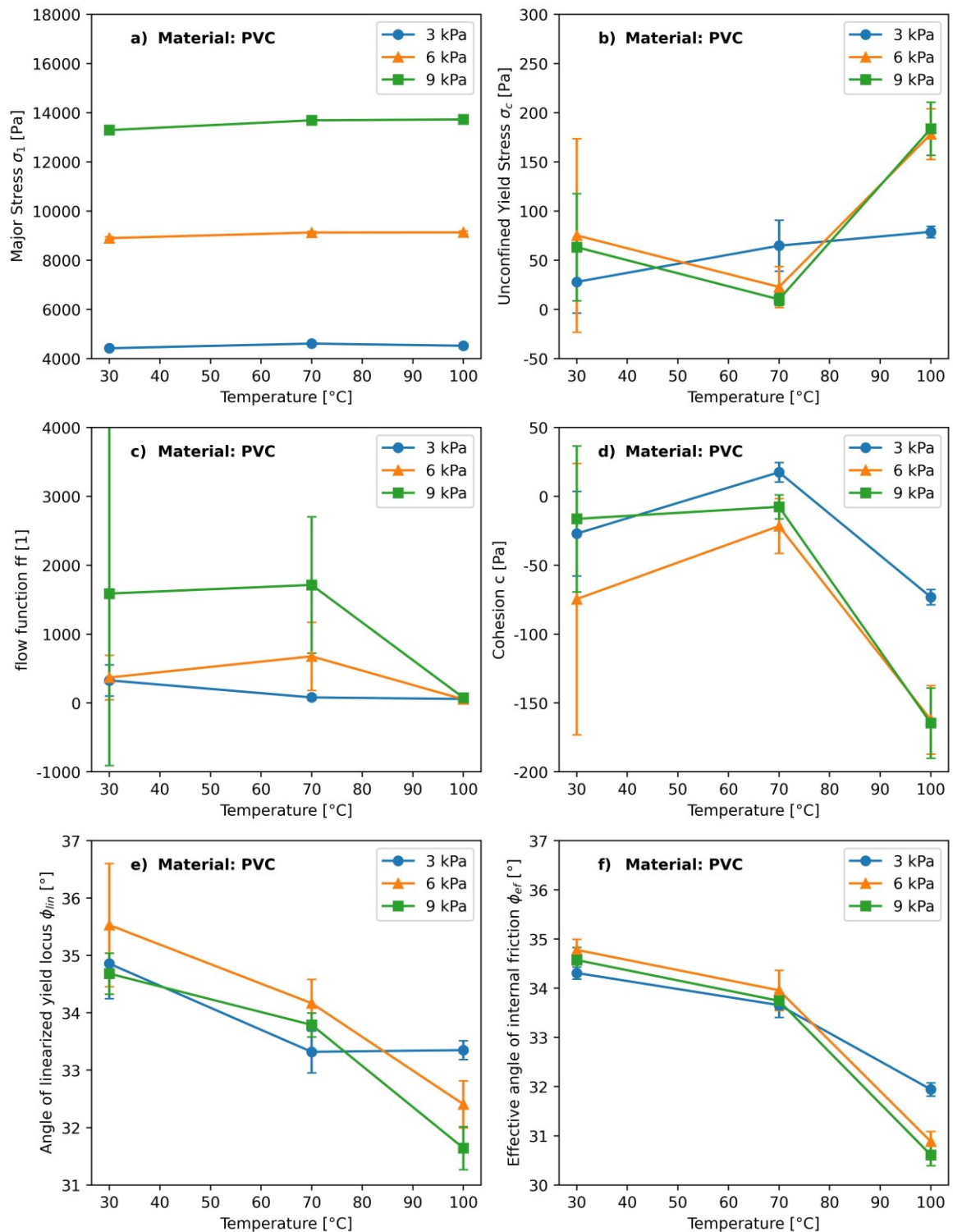
Figure 54: Comparison of six powder rheological properties of PVC for three normal stress levels at test temperatures of 30, 70 and 100 °C.

The usage of rheological properties as an indicator for thermo-mechanical transitions in comparison to the conventional methods has proven to be rather unsuccessful. Due to the isothermal nature of the measurement exact determination of a transition temperature is not possible. Additionally, the time investment needed to accurately determine a transition temperature is not feasible when other methods such as DMA or DSC can give quicker and more accurate results. Rough estimations can be done nonetheless as seen for PVC in Figure 54 f) a transition happens between 70 and 100 °C which coincides with the results of the powder DMA , solid DMA and DSC of roughly 87 °C. Similar results can be seen for TPE in the appendix. Here the range at which the transition was measured is even less precise (between -90 and 0 °C) but still coincides with a transition temperature of -65 °C measured with other conventional methods.

5   CONCLUSION AND OUTLOOK

In this thesis conventional characterization methods used to determine thermo-mechanical transitions were compared to new methods for polymer powders using PVC, TPE, PA12 and PTFE as model materials. Dynamic mechanical analysis DMA and Differential scanning calorimetry DSC are currently preferred for thermo-mechanical and thermo-calorimetric analysis, respectively. The usage of a Powder Pocket as an extension of the classical DMA allows for the testing of polymer powders filled in a metal container. The second method that was evaluated in the present thesis is the use of powder rheological properties as a broad screening method for thermal transitions. Both methods have the main advantage of mechanically measuring the powder directly without any additional preparations that could alter the morphology of said powder.

Regarding the choice of the most suitable thermomechanical property function for the determination of the thermal transitions of powders, the hypothesis of two opposing influences was made. The Powder Pocket causes thermal transitions such as the T_g determined by $E''(T)$ and $\tan \delta (T)$ to converge, which generally lowers the T_g obtained from the $\tan \delta(T)$ curve. On the other hand, the reduction of thermal conductivity due to the powder sample causes a delay of the measured T_g. Those two phenomena counteract each other resulting in good values of T_g obtained on powders from the $\tan \delta(T)$ curve.

Therefore, tan δ(T) proved to be the best fitting property function compared to the behavior in the solid state.

The main focus of this work was on improving the Powder Pocket system. For this task, a DoE was performed to evaluate the influence of different sample preparation parameters such as Powder Pocket material, sample volume, sample distribution and pre-compression of the powder. Four different preparation parameters, the Powder Pocket material, sample volume, sample distribution and a pre-compression step, were tested regarding their improvement of the quality of the measured DMA curve. The Powder Pocket material influenced the results in the most significant way, followed by the sample volume. The results from the DoE showed that for PVC, TPE and PA12 an aluminum Powder Pocket with higher thermal conductivity will result in a curve more closely resembling the measurement of a solid DMA. Using the stainless steel Powder Pocket allowed for more precise detection of a secondary relaxation peak in PTFE. Also a reduction in noise was clearly observed with the usage of the stainless steel Powder Pocket for all materials except TPE (here the choice of Powder Pocket was the least impactful parameter). The choice of sample volume solely depends on the goal of the measurement. A lower sample volume allows for more visible peaks, while a higher sample volume allows for a more accurate determination of the T_g and a lower noise in the signal. One hypothesis for the improvement caused by higher sample volume could be that a bigger volume also contains an overall wider distribution in particle size. This could lead to a denser packing of the powder particles resulting in less powder movement (reducing noise) and better thermal conductivity (more accurate T_G). The improvement in correlation caused by the lower sample could be explained by the decrease in inner friction. Due to the lower volume fewer layers of particles are present in the powder bed which results in less interaction between particles and more direct transfer of the deformation. The distribution of the powder in the Powder Pocket and the pre-compression step show inconsistent results. The tendencies were also less pronounced compared to the other two preparation parameters.

The sensitivity of Powder DMA using the Powder Pocket is comparable to DSC. All thermal transitions that can be detected by DSC can also be determined by the powder DMA. It should still be noted that the results obtained from powder DMA deviate more than the results from DSC, due to the lack of a consistent sample preparation and the exorbitant

amount of possibilities for particle arrangement within the sample. However, the Powder Pocket enables direct DMA measurements on polymer powders at the MCR and thus further increases the possible range of measurable materials.

The second method investigated for its suitability for thermo-mechanical characterization was rheological shear measurements of powder. The determination of powder rheological values is usually done at a constant temperature. Therefore, no temperature sweeps were possible. Nonetheless, the angle of linearized yield locus φ_{lin} and the angle of internal friction φ_{ef} seem to be promising properties suitable for thermo-mechanical characterization. Both showed a stronger decline in the temperature range close to T_g and the deviation of the obtained values was quite low, verifying the quality of the measurement.

Improving the reproducibility in sample preparation should be the goal for the future development of the Powder Pocket system. A consistent volumetric filling of the Powder Pocket could lead to an overall improvement in the deviation of the data. A tool to achieve such a consistent sample preparation could be included in the geometry of the Powder Pocket, eliminating the need for additional tools.

The Powder Pocket was only tested for free flowing powders. The interaction forces between the particles drastically change the mechanics of powders and are therefore of great importance in thermo-mechanical tests. Further investigations should be conducted on powders with overall higher cohesion to confirm the validity of the Powder Pocket for this type of powders. Other powder specific characteristics, such as particle size distribution could also be a limiting factor for a successful measurement. A high average particle diameter could significantly change the mechanical behavior and lead to problems regarding the thermal conductivity of the powder.

Other investigations should be done more specifically focused on PA12. The Powder Pocket allows for the detection of T_g directly of the powder. In the process of producing the solid specimen the material loses its characteristic morphology. A study analyzing different degrees of crystallinity of the same material could show off the unique characterization method enabled by the Powder Pocket. This could position the Powder Pocket as a one-of-a-kind testing method in the field of material science.

6 REFERENCES

1. H. Senff , C. Gaboriau, inventor. Method for preparing polyamide powder by anionic polymerisation. US20100113661A1

2. Su D, et al. *e-Polymers*. 2022;22:553-565

3. Winslow FH, et al. *Ind. Eng. Chem.* 1951;43:1108-1112

4. J. R. Griffin , M.E Muhle , G. T. Renola , D.L Litteer , P.Brant, inventor. Aufschlämmungs- oder Gasphasenpolymerisationsverfahren. DE69534108T2

5. James Edward Beuerle. *A Study of ElectrostaticallyApplied Powder Paint in the Automotive Industry*. Massachusetts: Massachusetts Institute of Technology; 1992. Available at: https://dspace.mit.edu/handle/1721.1/40191?show=full. Accessed April 1, 2023

6. Ayrilmis N. *International Journal of Adhesion and Adhesives*. 2022;113:103062

7. Francis LF. In: Stadler BJH, et al., eds. *Materials processing: A unified approach to processing of metals, ceramics and polymers*. Amsterdam: Academic Press is an Elsevier; 2016:343-414. *Science Direct e-books*

8. Rey-Vinolas S, et al. In: Planell JA, et al., eds. *Bone repair biomaterials: Regeneration and clinical applications*. Second edition. United Kingdom: Elsevier Ltd; Woodhead Publishing; 2019:179-197. *Woodhead Publishing in materials*

9. Lee B-L. *Powder Technology*. 1990;63:97-101

10. microtrac. Available at: https://www.microtrac.com/applications/knowledge-base/different-particle-analysis-techniques-compared/. Accessed April 2, 2023

11. Naderi M. In: Tarleton ES, ed. *Progress in Filtration and Separation: Fundamentals and Core Principles*. Oxford: Academic Press; 2014:585-608

12. Teunou E, et al. *Journal of Food Engineering*. 1999;42:109-116

13. Ehrenstein GW. *Polymer Werkstoffe: Struktur Eigenschaften Anwendung.* 3. Auflage. München: Hanser Verlag; 2011. Onleihe. http://www.hanser-elibrary.com/doi/book/10.3139/9783446429673

14. Perkin Elmer. Available at: https://resources.perkinelmer.com/lab-solutions/resources/docs/app_thermaldynmechanalybasicspart2.pdf. Accessed April 24, 2023

15. Kalogeras IM. In: Isayev AI, ed. *Structure*. Weinheim, Hoboken, New Jersey: Wiley-VCH; John Wiley & Sons; 2016:1-134. *Encyclopedia of polymer blends*; Volume 3

16. Crawford DM, et al. *Thermochimica Acta*. 1998;323:53-63

17. Grady BP, et al. In: Mark JE, et al., eds. *The science and technology of rubber*. Fourth edition. Amsterdam, Boston: Elsevier Academic Press; 2013:591-652

18. Alengaram UJ. In: Colangelo F, et al., eds. *Handbook of sustainable concrete and industrial waste management: Recycled and artificial aggregate, innovative eco-friendly binders, and life cycle assessment*. Duxford, United Kingdom: Woodhead Publishing; 2022:23-43. *Woodhead Publishing series in civil and structural engineering*

19. Lin R, et al. In: McSweeney PLH, et al., eds. *Encyclopedia of Dairy Sciences*. 3rd ed. San Diego: Elsevier Science & Technology; 2021:504-520

20. Bansal RC, et al. *Activated carbon adsorption*. Boca Raton: Taylor & Francis; 2005

21. Röhrl E. *PVC-Taschenbuch*. München: Hanser Verlag; 2007. Hanser eLibrary. http://www.hanser-elibrary.com/doi/book/10.3139/9783446411777

22. Zhang Z, et al. *J Mater Sci*. 2021;56:10155-10182

23. *Plastikatlas: Daten und Fakten über eine Welt voller Kunststoff.* 3. Auflage. Berlin: Heinrich-Böll-Stiftung; 2019

24. Jü. Available at: https://commons.wikimedia.org/w/index.php?curid=88900870. Accessed May 9, 2023

25. Smallwood P. *Polymer*. 1986;27:1609-1618

26. Wheeler RN. *Environmental health perspectives*. 1981;41:123-128

27. Ebnesajjad S, et al. *Fluoropolymer Applications in the Chemical Processing Industries: The Definitive User's Guide and Databook*. Burlington: Elsevier Science; 2004. Plastics Design Library Fluorocarbon. https://www.sciencedirect.com/science/book/9780815515029

28. Roland chem. Available at: https://commons.wikimedia.org/w/index.php?curid=52500492. Accessed May 9, 2023

29. Harry J. Lader , James W. Messerly , William R. Rehman, inventor. Triboelectric powder spray gun with internal discharge electrode and method of powder coating. US5622313A. 3.3

30. Drobny JG. In: *Marianne (Hg.) 2017 – Brydson's Plastics Materials*. Vol. 8:389-425

31. Gujarat Fluorochemicals Limited. Available at: https://www.inoflon.com/pdf/PG_Free%20flow%20granular%20PTFE.pdf. Accessed February 19, 2023

32. Calleja G, et al. *European Polymer Journal*. 2013;49:2214-2222

33. Ebnesajjad S. *Expanded PTFE applications handbook : technology, manufacturing and applications: Technology, manufacturing and applications*. Oxford: Elsevier; 2016. Plastics Design Library. PDL handbook series. http://www.sciencedirect.com/science/book/9781437778557

34. Alewelt W, et al. *Polyamide.* Neuausg. München: Hanser; 1998. Technische Thermoplaste / hrsg. von Ludwig Bottenbruch; 4

35. Knudsen Extrusion. Available at: https://pkkaps.dk/pkk-uk/materialer-uk.html. Accessed April 17, 2023

36. Touris A, et al. *Results in Materials*. 2020;8:100149

37. Salmoria GV, et al. *Polymer Testing*. 2012;31:411-416

38. D·海恩里希, inventor. Polyamide fluidized bed coating powder for fluidized thin-layer coating

39. Schmidt MG, et al. *SLS - Selektives Lasersintern mit Kunststoffen: Technologie, Prozesse und Werkstoffe*. München: Hanser; 2015. Hanser eLibrary

40. Botta A, et al. *J. Appl. Polym. Sci.* 1985;30:1669-1677

41. Zhang R, et al. *Polymers*. 2022;14

42. Schmid M, et al. In: AIP Publishing LLC; 2015:160009. AIP Conference Proceedings

43. Groote P de, et al. *J. Polym. Sci. B Polym. Phys.* 2002;40:2208-2218

44. LEHUY H. *Polymer*. 1994;35:136-139

45. Holden G, et al., eds. *Thermoplastic elastomers.* 3rd edition. Munich, Germany, Cincinnati, Ohio: Hanser Publishers; Distributed by Carl Hanser Verlag; Hanser Gardner Publications; op. 2004

46. Prisacariu C. *Polyurethane elastomers: From morphology to mechanical aspects*. Wien: Springer; 2011. http://gbv.eblib.com/patron/FullRecord.aspx?p=763186

47. BASF Forward AM. Available at: https://forward-am.com/material-portfolio/ultrasint-powders-for-powder-bed-fusion-pbf/tpu-line/. Accessed February 9, 2023

48. Menard KP. *Dynamic mechanical analysis: A practical introduction.* 2nd ed. Boca Raton: CRC Press; op. 2008. http://site.ebrary.com/lib/alltitles/docDetail.action?docID=10228625

49. Pavan M. V. Raja , Andrew R. Barron. Available at: https://chem.libretexts.org/Bookshelves/Analytical_Chemistry/Physical_Methods_in_Chemistry_and_Nano_Science_(Barron)/02%3A_Physical_and_Thermal_Analysis/2.10%3A_Dynamic_Mechanical_Analysis. Accessed December 7, 2022

50.   Perkin Elmer. Available at: https://resources.perkinelmer.com/lab-
      solutions/resources/docs/app_tgandmeltofpolyethylene.pdf. Accessed
      December 20, 2022

51.   Perkin Elmer. Available at: https://resources.perkinelmer.com/lab-
      solutions/resources/docs/APP_007771B_03_Use_of_Material_Pockets_for_
      Mechanical_Analysis_of_Powders.pdf. Accessed December 20, 2022

52.   TA Instruments. Available at:
      https://www.tainstruments.com/pdf/literature/TA403.pdf. Accessed December
      20, 2022

53.   Netzsch thermal. Available at: https://analyzing-
      testing.netzsch.com/de/auftragsmessungen/methoden/dynamische-differenz-
      kalorimetrie-dsc. Accessed January 5, 2023

54.   Grellmann W. *Kunststoffprüfung.* 2. Auflage. München: Hanser, Carl; 2011.
      http://www.hanser-elibrary.com/doi/book/10.3139/9783446429703

55.   J. Foreman, S. R. Sauerbrunn, C. L. Marcozzi. Available at:
      https://www.tainstruments.com/pdf/literature/TA082.pdf. Accessed January 5,
      2023

56.   Wetton RE, ed. *Dynamic mechanical thermal analysis of polymers and
      related systems*. London: Applied Science Publishers; 1986. Developments
      series

57.   Creative Proteomics. Available at: https://www.creative-
      proteomics.com/support/dsc-based-analysis-service.htm. Accessed January
      5, 2023

58.   Karoline Carvalho Dornelas, Diego José Araújo Bandeira, Raimundo Calixto
      Martins Rodrigues. *International Journal of Development Research*. 2022;
      12:57772-57777

59.   Schulze D. *Powders and bulk solids: Behavior, characterization, storage and
      flow*. Berlin: Springer; 2010

60. Hassanpour A. *Powder flow: Theory, characterisation and application.* 1st ed. Cambridge: Royal Society of Chemistry; 2019. https://ebookcentral.proquest.com/lib/kxp/detail.action?docID=5835627

61. Oluwatosin Oginni, et al. *Contribution of Particle Size and Moisture Content to Flowability of Fractionated Ground Loblolly Pine*; 2014

62. Ripp M, et al. *Particulate Science and Technology*. 2015;33:494-502

63. rheologylab. Available at: https://www.rheologylab.com/services/powder-rheology-flow-testing/. Accessed May 4, 2023

64. Berry RJ, et al. *Proceedings of the Institution of Mechanical Engineers, Part E: Journal of Process Mechanical Engineering*. 2015;229:215-230

65. Ruggi D, et al. *Powder Technology*. 2020;370:288-297

66. Wieleba W. *Wear*. 2005;258:870-876

67. Beaucage G, et al. *J. Polym. Sci. B Polym. Phys.* 1993;31:319-326

68. Lazić Ž. *Design of experiments in chemical engineering: A practical guide*. Weinheim: Wiley-VCH; 2004

69. Park K, et al. *Journal of Materials Processing Technology*. 2004;146:221-227

70. Montoro SR, et al. In: Borges Silva M, ed. *Design of Experiments - Applications*: InTech; uuuu-uuuu

71. Azaria M, et al. *IEEE Trans. Acoust., Speech, Signal Process.* 1984;32:280-285

72. Divergentdata. Available at: https://commons.wikimedia.org/w/index.php?curid=57768455. Accessed April 26, 2023

73. Kojio K, et al. *J Polym Res*. 2020;27

74. Shirinbayan M, et al. *Int J Mater Form*. 2021;14:143-152

75. C. G. Delides. Available at: https://www.researchgate.net/post/Whats-the-difference-between-measuring-Glass-Transition-Temperature-from-Storage-Modulus-Loss-Modulus-and-Tan-d-for-a-PMC-Which-is-more-

reliable/5a660cc5b0366d595272de02/citation/download. Accessed May 9, 2023

76. Adekunle K, et al. *J. Appl. Polym. Sci.* 2011:n/a-n/a

77. Jansen J. A. Available at: https://madisongroup.com/determining-glass-transition-temperature-using-dma/. Accessed May 9, 2023

78. Askadskii A, et al. *AMR*. 2013;864-867:751-754

79. Santiago-Calvo M, et al. *Polymers*. 2021;13

80. Gogolewski S, et al. *Colloid & Polymer Sci*. 1980;258:1130-1136

81. Henri V, et al. *Polymer Degradation and Stability*. 2020;171:109053

82. G.M. Nasr, et al. *Life Science Journal*. 2014;11:127-134

83. Olejarczyk M, et al. *Applied Sciences*. 2020;10:6184

84. Soe SP, et al. *Polymer Testing*. 2014;34:103-112

85. Svetlana T, et al. *Int J Adv Manuf Technol*. 2021;117:2041-2048

86. Ma N, et al. *e-Polymers*. 2020;20:346-352

87. Dr.Stefan Schmölzer , Claire Strasser. Available at: https://analyzing-testing.netzsch.com/_Resources/Persistent/8/2/0/b/820bf1c7b7ff9e481461a524ba2210b8e754321a/AN%20246_Complete%20Thermal%20Characterization%20of%20PTFE.pdf. Accessed May 1, 2023

APPENDIX

Appendix 1: Amplitude Sweeps

Figure 55: Amplitude sweep of TPE (solid) conducted at 23 °C and 1 Hz. The red line indicated the chosen strain while the blue line indicates the upper limit of the viscoelastic range.
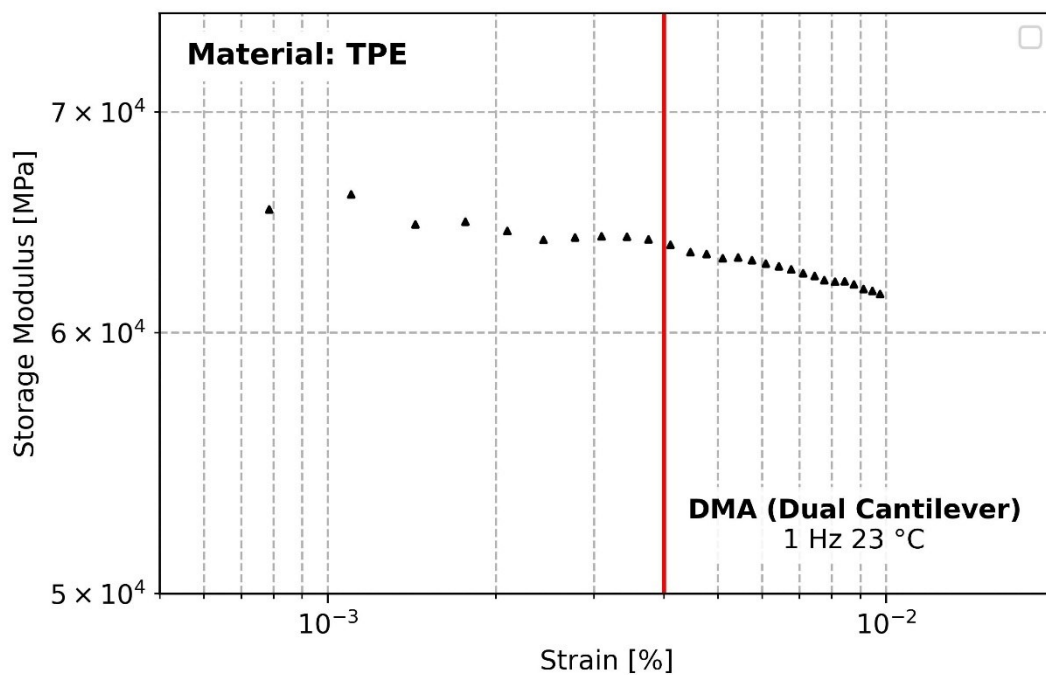
Figure 56: Amplitude sweep of TPE (powder) conducted at 23 °C and 1 Hz. The red line indicated the chosen strain.
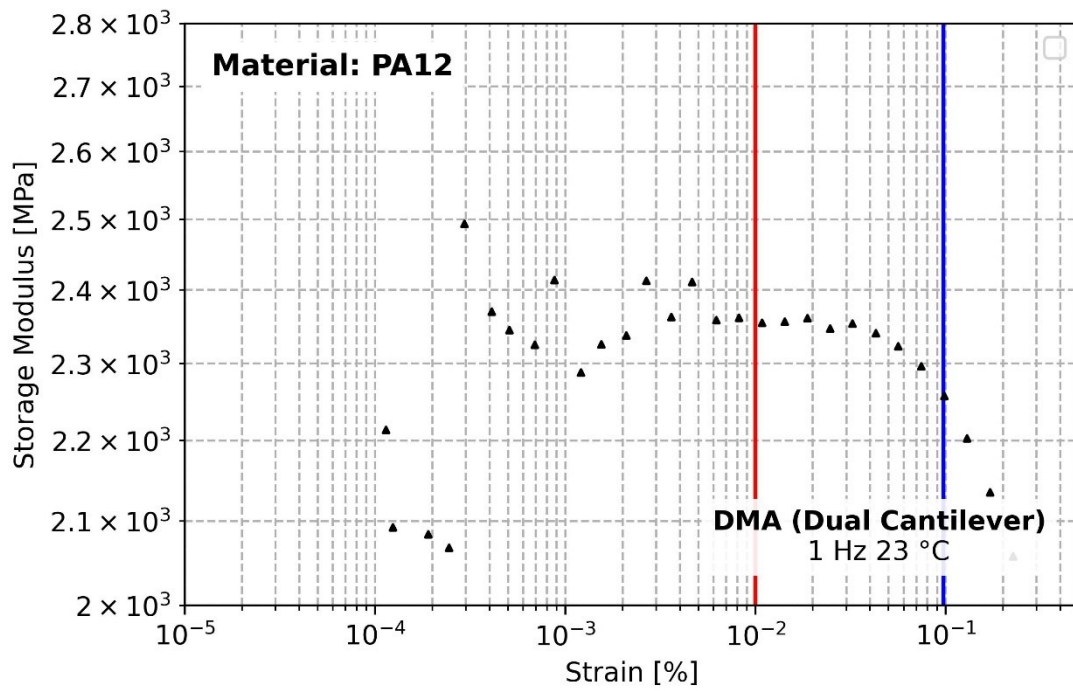
Figure 57: Amplitude sweep of PA12 (solid) conducted at 23 °C and 1 Hz. The red line indicated the chosen strain while the blue line indicates the upper limit of the viscoelastic range.
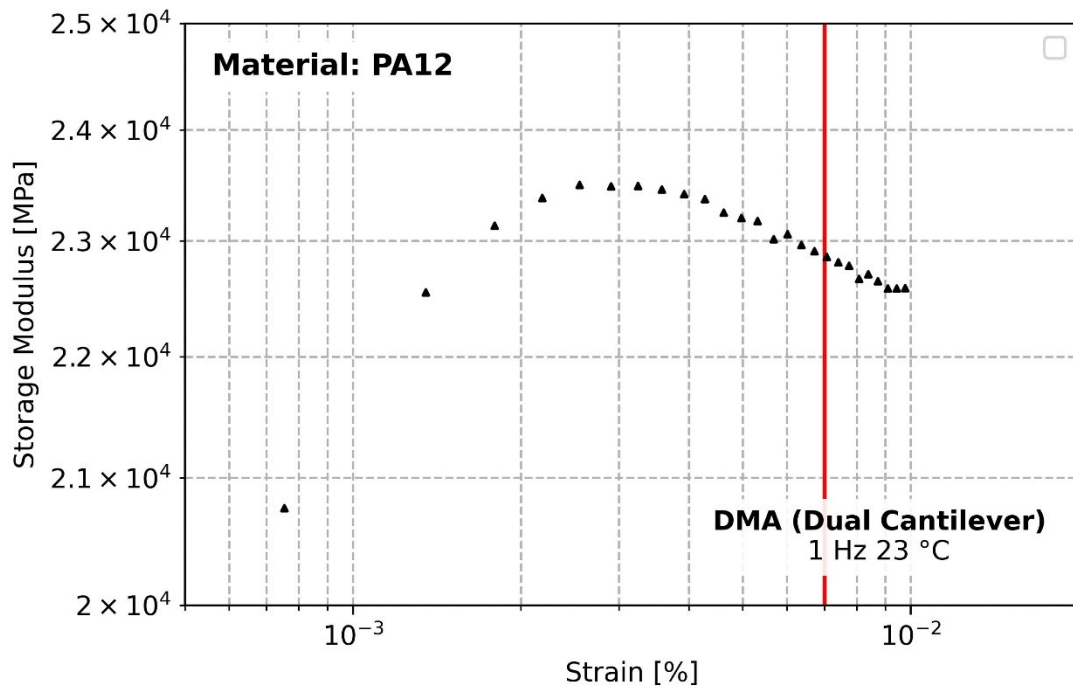
Figure 58: Amplitude sweep of PA12 (powder) conducted at 23 °C and 1 Hz. The red line indicated the chosen strain.
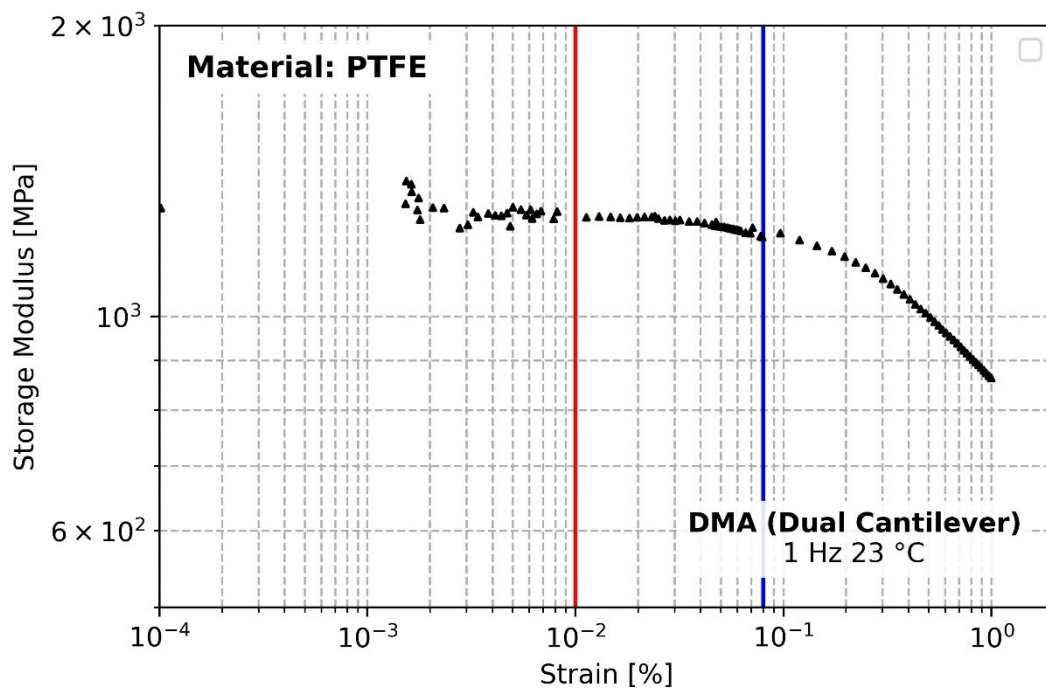
Figure 59: Amplitude sweep of PTFE (solid) conducted at 23 °C and 1 Hz. The red line indicated the chosen strain while the blue line indicates the upper limit of the viscoelastic range.
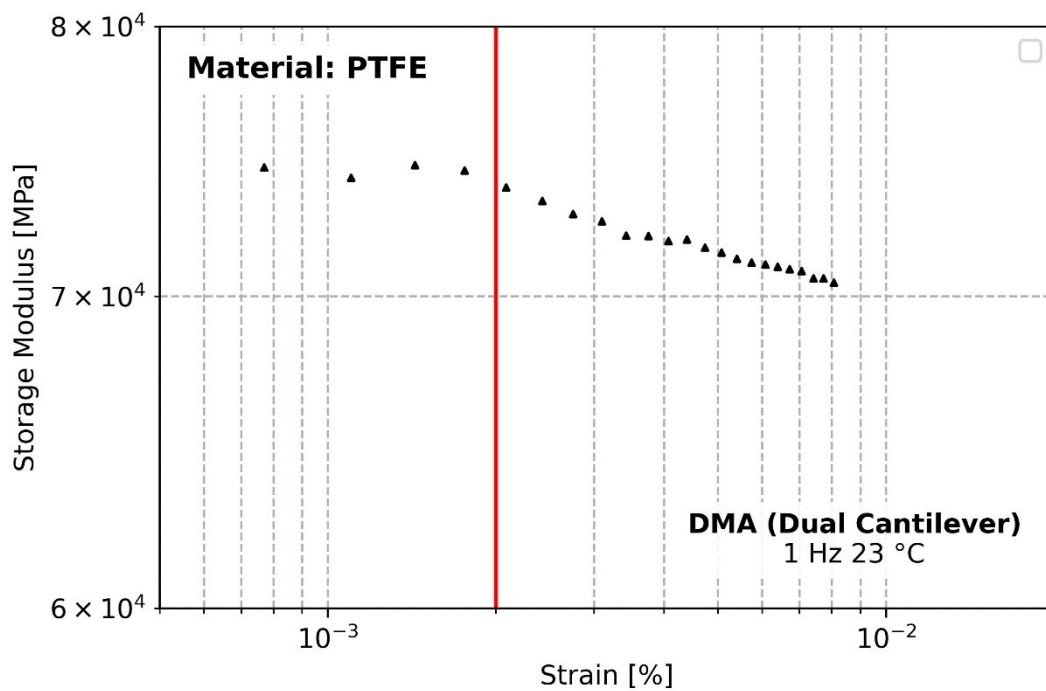
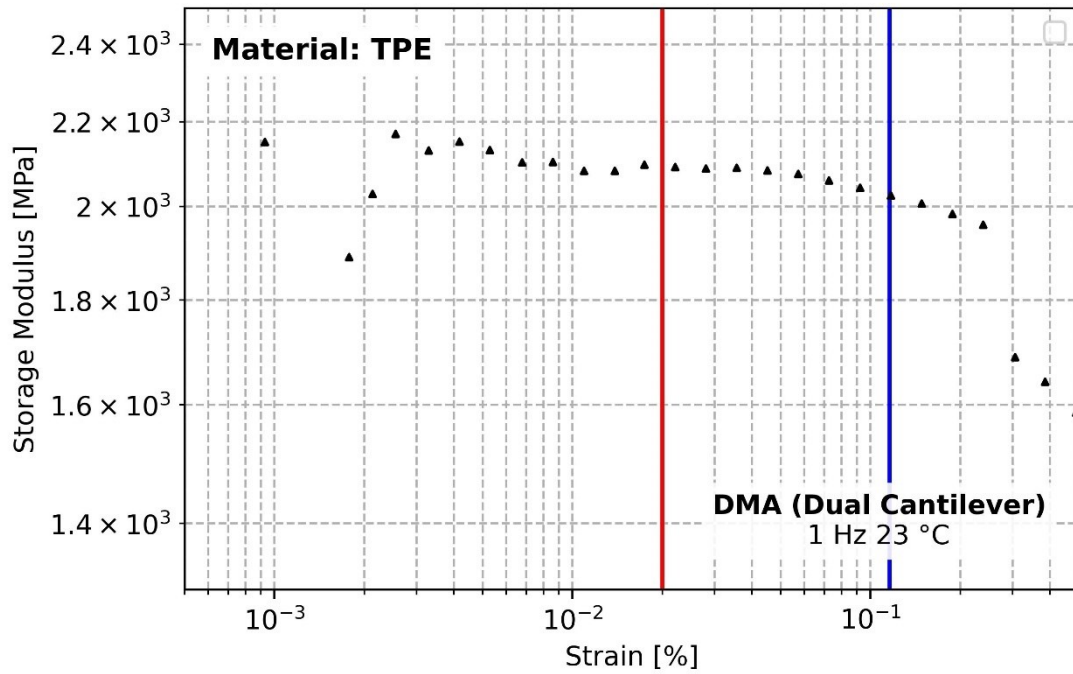
Figure 60: Amplitude sweep of PTFE (powder) conducted at 23 °C and 1 Hz. The red line indicated the chosen strain while the blue line indicates the upper limit of the viscoelastic range.

Appendix 2: Response values used in the DoE

Table 19: Experimental design for DMA measurements

Test Number	Powder Pocket Material	Volume	Distribution	Pre-Compression
1	+1	-1	+1	+1
2	-1	-1	+1	+1
3	+1	-1	+1	+1
4	-1	-1	+1	+1
5	+1	+1	+1	+1
6	-1	+1	+1	+1
7	+1	+1	+1	+1
8	-1	+1	+1	+1
9	+1	+1	-1	-1
10	-1	+1	-1	-1
11	+1	+1	-1	-1
12	-1	+1	-1	-1
13	+1	-1	-1	-1
14	-1	-1	-1	-1
15	+1	-1	-1	-1
16	-1	-1	-1	-1
17	+1	+1	+1	-1
18	-1	+1	+1	-1
19	+1	+1	+1	-1
20	-1	+1	+1	-1
21	+1	-1	+1	-1
22	-1	-1	+1	-1
23	+1	-1	+1	-1
24	-1	-1	+1	-1
25	+1	-1	-1	+1
26	-1	-1	-1	+1
27	+1	-1	-1	+1
28	-1	-1	-1	+1
29	+1	+1	-1	+1
30	-1	+1	-1	+1
31	+1	+1	-1	+1
32	-1	+1	-1	+1

Table 20: Calculated response values for PVC loss factor.

PVC	Loss Factor				
Number	Correlation	Noise	T_g [°C]	ΔT_g [°C]	T_g Lag [°C]
1	0,99	6,5%	89,11	1,64	-2,3
2	0,95	1,1%	90,08	2,61	-3
3	0,97	3,3%	89,1	1,63	-3,7
4	0,94	1,6%	91,11	3,64	-6,1
5	0,99	2,0%	87,11	-0,36	-0,5
6	0,84	1,6%	86,1	-1,37	22,3
7	0,98	1,9%	88,12	0,65	-1,1
8	0,90	1,1%	84,12	-3,35	22,7
9	0,98	1,4%	88,13	0,66	-0,7
10	0,81	1,5%	80,1	-7,37	19,9
11	0,99	2,6%	88,11	0,64	-1,1
12	0,74	2,6%	80,09	-7,38	18,7
13	0,92	1,6%	88,12	0,65	-1
14	0,73	1,2%	86,11	-1,36	2,7
15	0,95	2,6%	88,09	0,62	-0,8
16	0,99	2,2%	91,14	3,67	-4,3
17	1,00	3,4%	88,12	0,65	-0,5
18	0,69	1,9%	86,12	-1,35	21,3
19	0,79	2,1%	88,09	0,62	-2,6
20	0,75	2,9%	89,11	1,64	0,7
21	0,96	2,4%	90,12	2,65	-4,7
22	0,86	3,2%	91,13	3,66	-6,9
23	0,98	7,9%	90,39	2,92	-3,3
24	0,68	2,8%	88,37	0,9	-4,6
25	0,93	9,4%	89,9	2,43	-2,5
26	0,81	2,0%	87,13	-0,34	1,6
27	0,97	2,4%	91,12	3,65	-4,3
28	0,99	1,5%	90,12	2,65	-3,4
29	0,78	1,8%	85,13	-2,34	3,2
30	0,58	1,3%	90,07	2,6	1,2
31	0,72	2,5%	84,1	-3,37	7,1
32	0,95	1,7%	96,13	8,66	25,8

Table 21: Calculated response values for PVC loss modulus

PVC	Loss Modulus				
Number	Correlation	Noise	T_g [°C]	ΔT_g [°C]	T_g Lag [°C]
1	0,87	5,1%	88,11	8,03	-12,2
2	0,98	1,2%	88,08	8	-10,8
3	0,88	3,4%	88,09	8,01	-11,9
4	0,96	2,3%	89,1	9,02	-12,7
5	0,99	2,1%	85,1	5,02	-7,8
6	0,91	1,1%	80,09	0,01	42,2
7	0,99	2,1%	86,12	6,04	-8
8	0,90	1,3%	80,1	0,02	8
9	0,98	1,6%	86,12	6,04	-8,8
10	0,93	1,5%	80,1	0,02	10
11	0,99	2,4%	86,09	6,01	-8,4
12	0,89	2,6%	80,09	0,01	6,2
13	0,99	1,7%	87,11	7,03	-9,5
14	0,94	1,5%	83,11	3,03	-5,7
15	0,96	2,6%	87,1	7,02	-10,1
16	0,98	2,1%	89,13	9,05	-12,1
17	0,94	3,4%	87,12	7,04	-9
18	0,88	2,9%	80,11	0,03	8,2
19	0,85	2,0%	85,09	5,01	-7,1
20	0,85	2,6%	86,1	6,02	-4,9
21	0,91	2,5%	88,12	8,04	-12,7
22	0,77	4,2%	89,12	9,04	-14,5
23	0,92	8,0%	88,38	8,3	-11,9
24	0,90	3,1%	80,38	0,3	42,4
25	0,95	9,1%	88,39	8,31	-11,7
26	0,96	1,8%	84,13	4,05	-6,3
27	0,89	2,5%	88,11	8,03	-13,1
28	0,99	1,7%	88,11	8,03	-10,1
29	0,96	1,8%	82,11	2,03	-4,7
30	0,87	1,4%	80,02	-0,06	4
31	0,96	2,7%	81,1	1,02	-2,1
32	0,98	1,7%	80,09	0,01	42,4

Table 22: Calculated response values for TPE loss factor

TPE	Loss Factor				
Number	Correlation	Noise	T_g [°C]	ΔT_g [°C]	T_g Lag [°C]
1	0,98	2,2%	-61,89	-0,93	2,6
2	0,45	26,3%	-50,88	10,08	-39,2
3	0,93	4,1%	-62,88	-1,92	3,5
4	0,92	2,9%	-65,8	-4,84	10
5	0,98	3,5%	-60,46	0,5	2,1
6	0,89	2,3%	-65	-4,04	15,3
7	0,96	2,8%	-58,78	2,18	-2,9
8	0,89	1,8%	-63,96	-3	7,3
9	0,94	2,8%	-59,31	1,65	-2,5
10	0,64	2,3%	-66,95	-5,99	24,3
11	0,92	2,0%	-50,24	10,72	-6,7
12	0,48	2,8%	-65,39	-4,43	27,5
13	0,80	6,5%	-61,35	-0,39	0
14	0,92	4,5%	-65,62	-4,66	13,9
15	0,90	10,4%	-64,51	-3,55	5,8
16	0,94	3,3%	-61,35	-0,39	7,9
17	0,85	4,0%	-50,27	10,69	-6,8
18	0,96	2,3%	-66,66	-5,7	12,7
19	0,96	3,7%	-52,1	8,86	0
20	0,86	1,3%	-63,47	-2,51	-29,3
21	0,95	5,6%	-63,36	-2,4	8,4
22	0,87	2,5%	-65,45	-4,49	6,7
23	0,94	5,1%	-62,57	-1,61	7,1
24	0,94	3,2%	-68,92	-7,96	14,6
25	0,97	2,9%	-60,34	0,62	-2,6
26	0,87	2,9%	-67,96	-7	14,8
27	0,96	4,0%	-62,39	-1,43	5,3
28	0,86	2,7%	-64,6	-3,64	7,9
29	0,89	2,7%	-56,95	4,01	-6,3
30	0,49	6,3%	-68,33	-7,37	49,3
31	0,95	3,1%	-61,77	-0,81	-0,6
32	0,79	4,7%	-79,67	-18,71	27,4

Table 23: Calculated response values for TPE loss modulus

TPE	Loss Modulus				
Number	Correlation	Noise	T_g [°C]	ΔT_g [°C]	T_g Lag [°C]
1	0,98	2,2%	-65,04	3,3	-8
2	-0,35	14,3%	-60,37	7,97	-8,2
3	0,98	4,1%	-64,83	3,51	-9,7
4	0,98	5,1%	-79,87	-11,53	-3
5	0,97	3,3%	-64,97	3,37	-7,8
6	0,95	3,3%	-79,69	-11,35	-2,6
7	0,96	2,8%	-63,6	4,74	-9,6
8	0,95	2,1%	-74,33	-5,99	1,8
9	0,97	2,9%	-63,11	5,23	-10,1
10	0,94	5,9%	-79,8	-11,46	47,3
11	0,92	2,2%	-64,26	4,08	-9,5
12	0,91	4,5%	-79,93	-11,59	-3,6
13	0,87	5,9%	-64,6	3,74	-7,9
14	0,97	4,2%	-70,36	-2,02	2,6
15	0,90	9,8%	-67,54	0,8	-6,2
16	0,97	2,8%	-66,68	1,66	-2,9
17	0,93	3,7%	-61,38	6,96	-13,4
18	0,97	1,7%	-71,33	-2,99	2,8
19	0,95	3,5%	-64,57	3,77	-6,7
20	0,96	0,8%	-71,34	-3	4,1
21	0,98	5,6%	-64,97	3,37	-5,1
22	0,98	2,6%	-68,78	-0,44	-2,6
23	0,97	4,9%	-65,46	2,88	-7,1
24	0,96	3,0%	-71,82	-3,48	1,4
25	0,93	3,2%	-64,01	4,33	-12,1
26	0,95	2,7%	-70,36	-2,02	-1,9
27	0,97	3,8%	-65,31	3,03	-6,1
28	0,98	3,4%	-66,57	1,77	-4,1
29	0,95	2,8%	-63,83	4,51	-12,2
30	0,94	9,3%	-79,74	-11,4	49,2
31	0,96	3,0%	-64,89	3,45	-8,3
32	0,94	9,0%	-79,67	-11,33	27,1

Table 24: Calculated response values for PA12 loss factor

PA12	Loss Factor				
Number	Correlation	Noise	T_g [°C]	ΔT_g [°C]	T_g Lag [°C]
1	0,95	0,6%	99,55	47,06	-40,3
2	0,95	1,6%	75,88	23,39	-0,3
3	0,91	3,6%	85,83	33,34	-11,1
4	0,93	1,7%	82,86	30,37	-8,9
5	0,89	1,1%	75,78	23,29	0,7
6	0,99	0,8%	40,8	-11,69	72,4
7	0,91	3,4%	79,53	27,04	-4,2
8	0,64	1,1%	58,89	6,4	70,5
9	0,92	1,5%	89,84	37,35	-14,4
10	0,90	1,1%	82,85	30,36	71,9
11	0,99	2,0%	99,85	47,36	-34
12	0,67	0,9%	66,86	14,37	71,9
13	0,94	1,1%	84,08	31,59	-10,4
14	0,90	1,1%	78,09	25,6	-1,2
15	0,91	3,1%	84,5	32,01	-9,3
16	0,88	2,1%	96,86	44,37	-15,6
17	0,86	0,8%	83,77	31,28	-7,3
18	0,61	2,0%	60,86	8,37	71,7
19	0,90	1,6%	85,04	32,55	68,6
20	0,71	1,2%	56,94	4,45	71,7
21	0,93	2,3%	77,9	25,41	2,6
22	0,45	2,1%	89,82	37,33	-6,4
23	0,89	3,3%	84,84	32,35	-8,3
24	0,73	1,3%	84,89	32,4	-9,6
25	0,90	4,1%	96,85	44,36	-6,5
26	0,90	1,3%	89,84	37,35	-11,6
27	0,91	2,6%	84,82	32,33	-11,3
28	0,88	1,3%	90,85	38,36	-16,4
29	0,97	1,1%	93,83	41,34	-27,1
30	0,88	1,5%	95,86	43,37	71,9
31	0,94	1,3%	83,89	31,4	-7,7
32	0,94	1,4%	56,88	4,39	71,9

Table 25: Calculated response values for PA12 loss modulus

PA12	Loss Modulus				
Number	Correlation	Noise	T_g [°C]	ΔT_g [°C]	T_g Lag [°C]
1	0,67	0,5%	51,82	8,03	71,9
2	0,89	1,4%	69,02	25,23	-5,2
3	0,76	3,8%	85,83	42,04	-21,8
4	0,87	1,6%	78,76	34,97	-10,3
5	0,79	1,0%	65,83	22,04	1,1
6	1,00	0,9%	40,8	-2,99	68,2
7	0,84	3,2%	70,84	27,05	-6,2
8	0,81	0,9%	50,98	7,19	49,5
9	0,78	1,3%	86,3	42,51	-21,1
10	0,97	1,2%	57,91	14,12	59,4
11	0,98	1,8%	99,85	56,06	-39,5
12	0,95	1,2%	50,86	7,07	66,6
13	0,92	1,0%	76,09	32,30	-10,5
14	0,80	1,0%	68,19	24,40	-2,8
15	0,77	2,9%	82,32	38,53	-20,1
16	0,77	2,0%	82,65	38,86	-13
17	0,66	0,9%	60,85	17,06	2,9
18	0,87	4,9%	40,96	-2,83	71,7
19	0,94	1,4%	78,04	34,25	55,7
20	0,79	1,4%	49,23	5,44	48,1
21	0,81	2,2%	69,85	26,06	-7,8
22	0,57	2,0%	50,84	7,05	19,7
23	0,76	3,2%	84,84	41,05	-19,3
24	0,89	1,2%	55,86	12,07	71,9
25	0,75	4,3%	87,01	43,22	-15
26	0,73	1,1%	80,7	36,91	71,9
27	0,76	2,5%	84,82	41,03	-21
28	0,67	1,2%	90,85	47,06	-17,1
29	0,94	1,0%	91,85	48,06	68,1
30	0,97	1,5%	49,86	6,07	71,8
31	0,86	1,1%	79,8	36,01	-12,5
32	0,97	1,6%	52,81	9,02	62,6

Table 26: Calculated response values for PTFE's T_g via loss factor.

PTFE	Loss Factor				
Number	Correlation	Noise	T_g [°C]	ΔT_g [°C]	T_g Lag [°C]
1	0,42	8,0%	-	-	40,2
2	0,70	3,7%	-	-	40,2
3	0,61	6,6%	-	-	-11,8
4	0,59	2,8%	-	-	39,2
5	0,63	4,8%	-	-	39
6	0,63	2,4%	-	-	40,2
7	0,73	6,9%	-	-	39,6
8	0,87	2,6%	-	-	40,2
9	0,26	7,8%	-	-	37,8
10	0,62	4,4%	-	-	40,4
11	0,44	6,7%	-	-	39
12	0,60	2,7%	-	-	40,2
13	0,38	8,6%	-	-	30,8
14	0,53	5,0%	-	-	40,2
15	0,39	8,6%	-	-	-21,2
16	0,60	3,4%	-	-	40,4
17	0,41	5,0%	-	-	31,1
18	0,80	3,1%	-	-	40,2
19	0,38	5,5%	-	-	39,1
20	0,67	2,4%	-	-	40,2
21	0,82	6,7%	-	-	-26,1
22	0,57	2,7%	-	-	39
23	0,19	8,8%	-	-	-13,9
24	0,73	3,3%	-	-	40,2
25	0,48	5,6%	-	-	40,2
26	0,31	4,1%	-	-	37,7
27	0,20	8,0%	-	-	9,8
28	0,30	3,3%	-	-	0,6
29	0,21	6,9%	-	-	38,3
30	0,62	4,0%	-	-	40,4
31	0,55	9,7%	-	-	38,5
32	0,61	3,1%	-	-	39,8

Table 27: Calculated response values for PTFE's T_g via loss modulus.

PTFE	Loss Modulus				
Number	Correlation	Noise	T_g [°C]	ΔT_g [°C]	T_g Lag [°C]
1	0,66	7,6%	-	-	34,5
2	0,75	3,4%	-	-	29,2
3	-0,10	6,6%	-	-	-31,2
4	0,89	2,7%	-	-	36,8
5	0,84	4,4%	-	-	22,6
6	0,99	2,8%	-	-	40,2
7	0,86	6,8%	-	-	32,7
8	0,98	2,2%	-	-	33,7
9	0,61	7,2%	-	-	37,5
10	0,86	3,5%	-	-	38
11	0,75	6,4%	-	-	31,5
12	0,95	2,5%	-	-	38,8
13	0,57	8,3%	-	-	-7,7
14	0,78	4,7%	-	-	36,4
15	0,45	8,2%	-	-	40,4
16	0,88	3,1%	-	-	36,4
17	0,80	4,6%	-	-	-17
18	0,95	2,8%	-	-	38,3
19	0,68	5,3%	-	-	20,3
20	0,98	2,2%	-	-	38,7
21	0,66	6,4%	-	-	39,8
22	0,84	2,6%	-	-	33,8
23	0,23	8,5%	-	-	16,5
24	0,93	3,1%	-	-	35,4
25	0,79	5,2%	-	-	38,4
26	0,84	4,0%	-	-	3,5
27	0,26	7,6%	-	-	-37,2
28	0,58	3,1%	-	-	-37,2
29	0,73	6,5%	-	-	-27,3
30	0,77	3,6%	-	-	38,2
31	0,61	9,3%	-	-	-3,7
32	0,89	3,6%	-	-	27,6

Table 28: Calculated response values for PTFE' secondary relaxation via loss Factor

PTFE	Loss Factor				
Number	Correlation	Noise	T_{gg} [°C]	ΔT_{gg} [°C]	T_{gg} Lag [°C]
1	0,26	8,0%	-72,24	26,02	-0,7
2	0,95	3,7%	-105,26	-7	7,9
3	0,43	6,6%	-89,24	9,02	-8,3
4	0,92	2,8%	-101,3	-3,04	2,1
5	0,68	4,8%	-84,25	14,01	-16,8
6	0,79	2,4%	-94,31	3,95	-4,1
7	0,11	6,9%	-70,17	28,09	-21,2
8	0,93	2,6%	-109,28	-11,02	30,4
9	0,13	7,8%	-80,14	18,12	-42,9
10	0,91	4,4%	-109,29	-11,03	15,9
11	0,32	6,7%	-70,18	28,08	-42,6
12	0,91	2,7%	-109,31	-11,05	41,8
13	0,16	8,6%	-84,24	14,02	-11,6
14	0,67	5,0%	-106,35	-8,09	12,4
15	0,33	8,6%	-96,32	1,94	-42,9
16	0,57	3,4%	-106,24	-7,98	-20,2
17	0,40	5,0%	-71,28	26,98	-35,3
18	0,89	3,1%	-101,16	-2,9	4,6
19	0,47	5,5%	-105,2	-6,94	5,9
20	0,94	2,4%	-109,26	-11	26,1
21	0,07	6,7%	-71,23	27,03	-6,2
22	0,89	2,7%	-109,3	-11,04	9,7
23	0,27	8,8%	-99,27	-1,01	-41,8
24	0,70	3,3%	-109,3	-11,04	4,3
25	0,44	5,6%	-98,28	-0,02	-4,3
26	0,93	4,1%	-109,33	-11,07	24,1
27	0,19	8,0%	-100,21	-1,95	-3,8
28	0,90	3,3%	-109,29	-11,03	25,1
29	0,29	6,9%	-70,17	28,09	-22
30	0,93	4,0%	-109,32	-11,06	30
31	0,11	9,7%	-71,18	27,08	-15,3
32	0,87	3,1%	-109,18	-10,92	15,4

Table 29: Calculated response values for PTFE's secondary relaxation via loss modulus

PTFE	Loss Modulus				
Number	Correlation	Noise	T_{gg} [°C]	ΔT_{gg} [°C]	T_{gg} Lag [°C]
1	0,55	7,6%	-109,37	-5,1	-10,2
2	0,98	3,4%	-105,26	-0,99	0,6
3	0,68	6,6%	-95,29	8,98	-13,3
4	0,97	2,7%	-104,26	0,01	-4,4
5	0,83	4,4%	-87,16	17,11	-20,2
6	0,89	2,8%	-109,3	-5,03	-9,9
7	0,42	6,8%	-70,17	34,1	-24,2
8	0,94	2,2%	-109,28	-5,01	15,1
9	0,14	7,2%	-83,26	21,01	-16,3
10	0,96	3,5%	-109,29	-5,02	7,4
11	-0,22	6,4%	-70,18	34,09	-42,5
12	0,93	2,5%	-109,31	-5,04	12,9
13	0,33	8,3%	-86,14	18,13	-19,2
14	0,89	4,7%	-109,28	-5,01	8,6
15	0,25	8,2%	-98,22	6,05	-9,3
16	0,88	3,1%	-109,24	-4,97	-29,9
17	0,24	4,6%	-78,21	26,06	-36
18	0,97	2,8%	-107,29	-3,02	-5,8
19	0,73	5,3%	-105,2	-0,93	-6,2
20	0,96	2,2%	-109,26	-4,99	13,2
21	0,44	6,4%	-89,21	15,06	-11,3
22	0,95	2,6%	-109,3	-5,03	1,6
23	0,31	8,5%	-98,28	5,99	-7,8
24	0,89	3,1%	-109,3	-5,03	-2,4
25	0,70	5,2%	-99,22	5,05	-9,4
26	0,94	4,0%	-109,33	-5,06	10,5
27	0,55	7,6%	-100,21	4,06	-10,3
28	0,94	3,1%	-109,29	-5,02	13,3
29	0,49	6,5%	-70,17	34,1	-25,1
30	0,94	3,6%	-109,32	-5,05	21,2
31	0,31	9,3%	-70,09	34,18	-18,4
32	0,94	3,6%	-109,18	-4,91	5,1

Table 30: Calculated response values for PTFE's crystalline transition evaluated via loss factor.

PTFE	Loss Factor				
Number	Correlation	Noise	T_c[°C]	ΔT_c [°C]	T_c Lag [°C]
1	0,47	8,0%	-0,19	-23,01	29,3
2	0,28	3,7%	14,82	-8	33,9
3	0,40	6,6%	11,82	-11	29,1
4	0,36	2,8%	13,8	-9,02	35,4
5	0,49	4,8%	15,77	-7,05	21,8
6	0,40	2,4%	30,81	7,99	-1,9
7	0,49	6,9%	15,88	-6,94	27
8	0,46	2,6%	17,78	-5,04	10,1
9	0,59	7,8%	11,91	-10,91	21
10	0,45	4,4%	27,86	5,04	-1
11	0,48	6,7%	15,77	-7,05	17,8
12	0,76	2,7%	26,86	4,04	-0,2
13	0,44	8,6%	9,8	-13,02	23,2
14	0,34	5,0%	-0,14	-22,96	37,4
15	0,39	8,6%	5,76	-17,06	32,1
16	0,31	3,4%	15,81	-7,01	33,8
17	0,30	5,0%	15,79	-7,03	18,8
18	0,53	3,1%	18,82	-4	10,4
19	0,53	5,5%	15,82	-7	28,5
20	0,35	2,4%	17,8	-5,02	13
21	0,49	6,7%	12,82	-10	26
22	0,33	2,7%	12,83	-9,99	33,3
23	0,51	8,8%	11,82	-11	25,2
24	0,36	3,3%	-0,25	-23,07	33,6
25	0,59	5,6%	14,79	-8,03	22,1
26	0,33	4,1%	8,85	-13,97	35,2
27	0,50	8,0%	14,82	-8	25,5
28	0,34	3,3%	-1,22	-24,04	37,5
29	0,48	6,9%	14,8	-8,02	20,8
30	0,37	4,0%	16,88	-5,94	26,9
31	0,40	9,7%	14,79	-8,03	25,3
32	0,30	3,1%	17,84	-4,98	15,8

Table 31: Calculated response values for PTFE's crystalline transition evaluated via loss modulus

PTFE	Loss Modulus				
Number	Correlation	Noise	T_g [°C]	ΔT_g [°C]	T_g Lag [°C]
1	0,92	7,6%	-0,19	-22,99	14,4
2	0,87	3,4%	-10,25	-33,05	12,7
3	0,93	6,6%	-0,22	-23,02	14,7
4	0,89	2,7%	-1,21	-24,01	14
5	0,81	4,4%	14,79	-8,01	13,1
6	0,86	2,8%	30,81	8,01	-5,2
7	0,87	6,8%	15,88	-6,92	17,2
8	0,85	2,2%	17,78	-5,02	6,5
9	0,84	7,2%	-0,03	-22,83	12,2
10	0,89	3,5%	27,86	5,06	-2,6
11	0,88	6,4%	15,77	-7,03	10,2
12	0,78	2,5%	25,86	3,06	-3,4
13	0,93	8,3%	7,79	-15,01	12,7
14	0,87	4,7%	-11,21	-34,01	21,5
15	0,92	8,2%	-0,2	-23,00	12,3
16	0,90	3,1%	15,81	-6,99	10,9
17	0,95	4,6%	15,79	-7,01	10,6
18	0,89	2,8%	18,82	-3,98	6,3
19	0,90	5,3%	-1,19	-23,99	12,2
20	0,82	2,2%	17,8	-5,00	6,6
21	0,95	6,4%	11,82	-10,98	12,6
22	0,89	2,6%	-7,18	-29,98	13,7
23	0,91	8,5%	10,77	-12,03	12,7
24	0,86	3,1%	-0,25	-23,05	14,4
25	0,87	5,2%	-0,19	-22,99	3
26	0,89	4,0%	-0,21	-23,01	14,9
27	0,92	7,6%	-1,21	-24,01	10,6
28	0,90	3,1%	-5,21	-28,01	16,2
29	0,92	6,5%	14,8	-8,00	12,2
30	0,82	3,6%	16,88	-5,92	10,9
31	0,90	9,3%	12,86	-9,94	12,1
32	0,93	3,6%	17,84	-4,96	8,1

Appendix 3: Main effect plots obtained from the DoE:
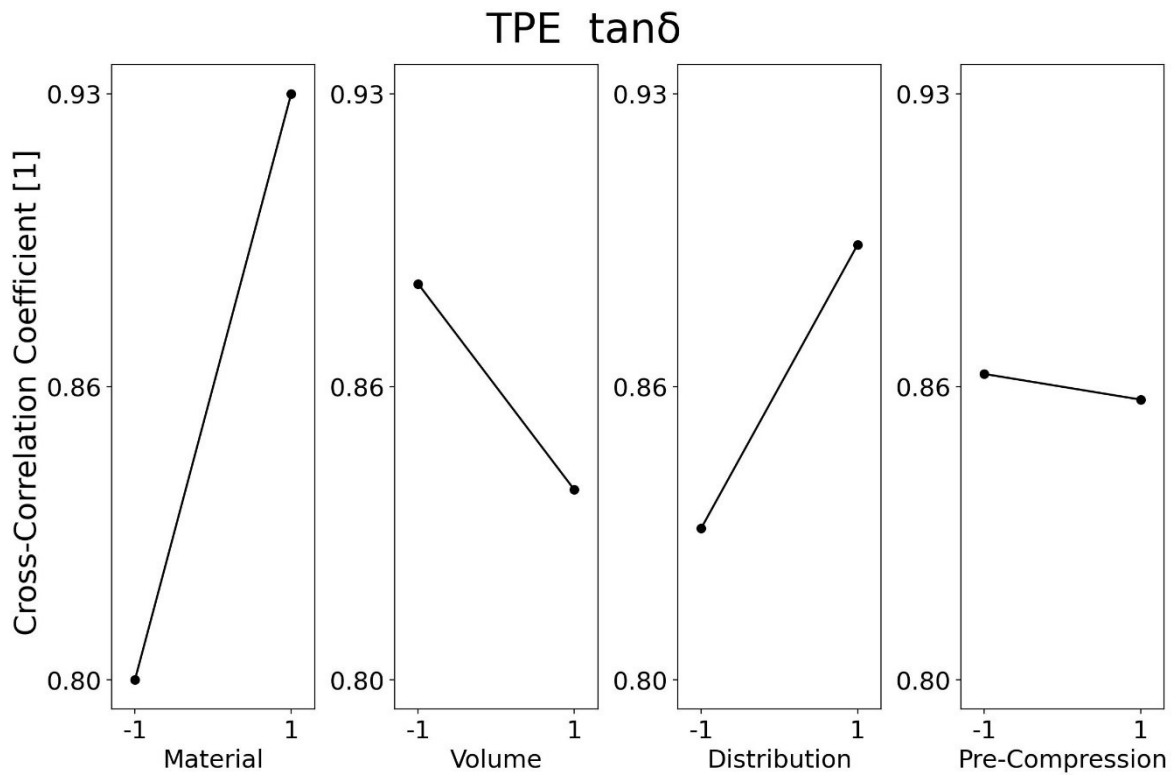
Figure 61: Main effect plot (correlation coefficient) for TPE evaluating tan δ.
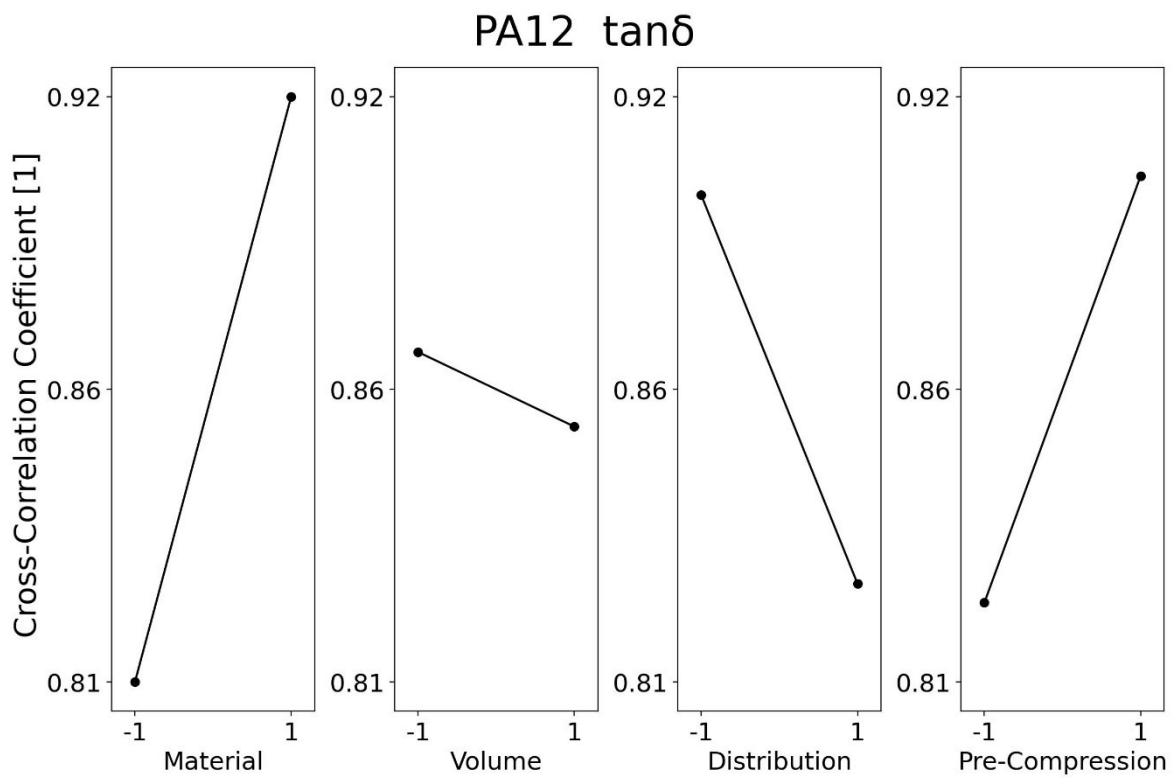
Figure 62: Main effect plot (correlation coefficient) for PA12 evaluating tan δ.
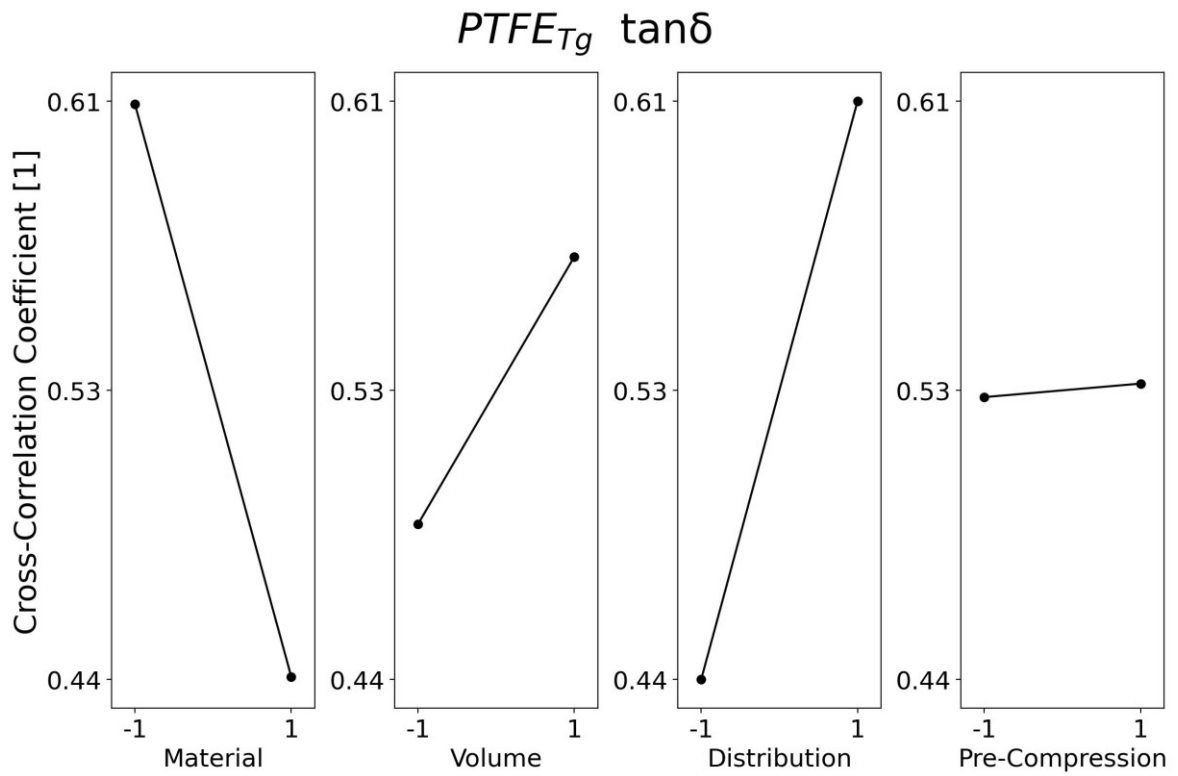
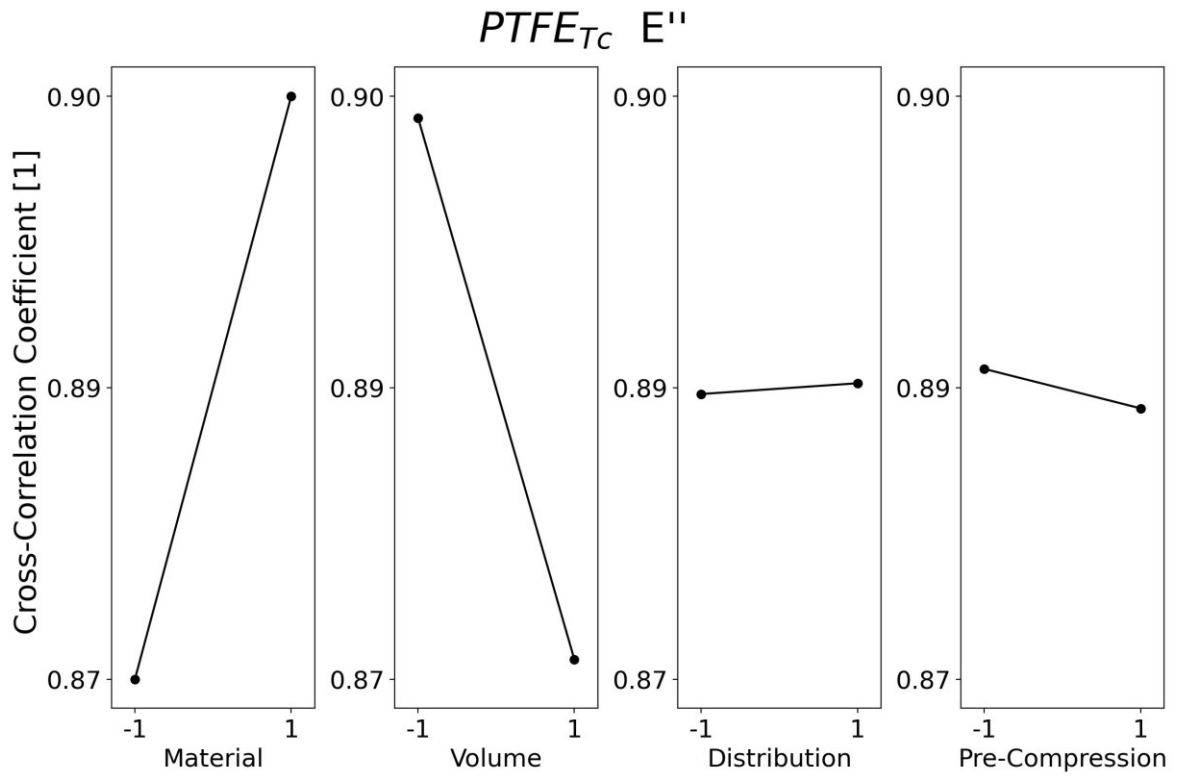Figure 63: Main effect plot (correlation coefficient) of PTFE_Tg evaluating tan δ.
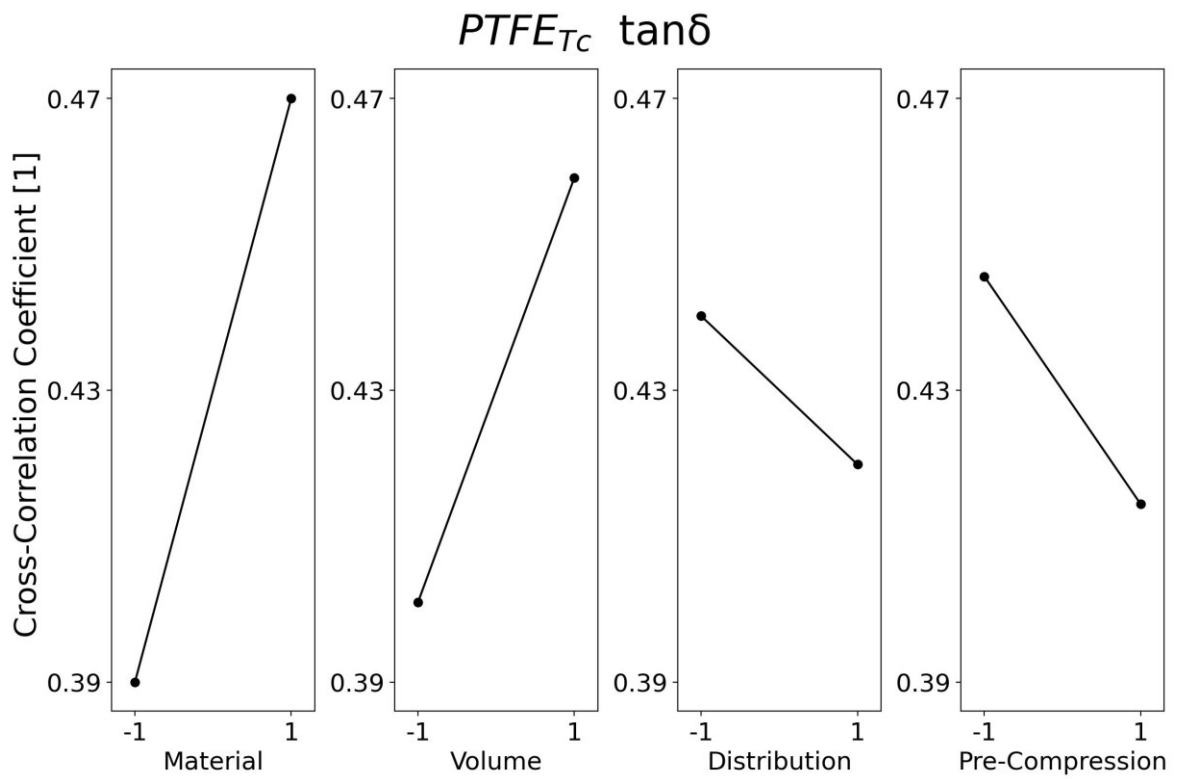
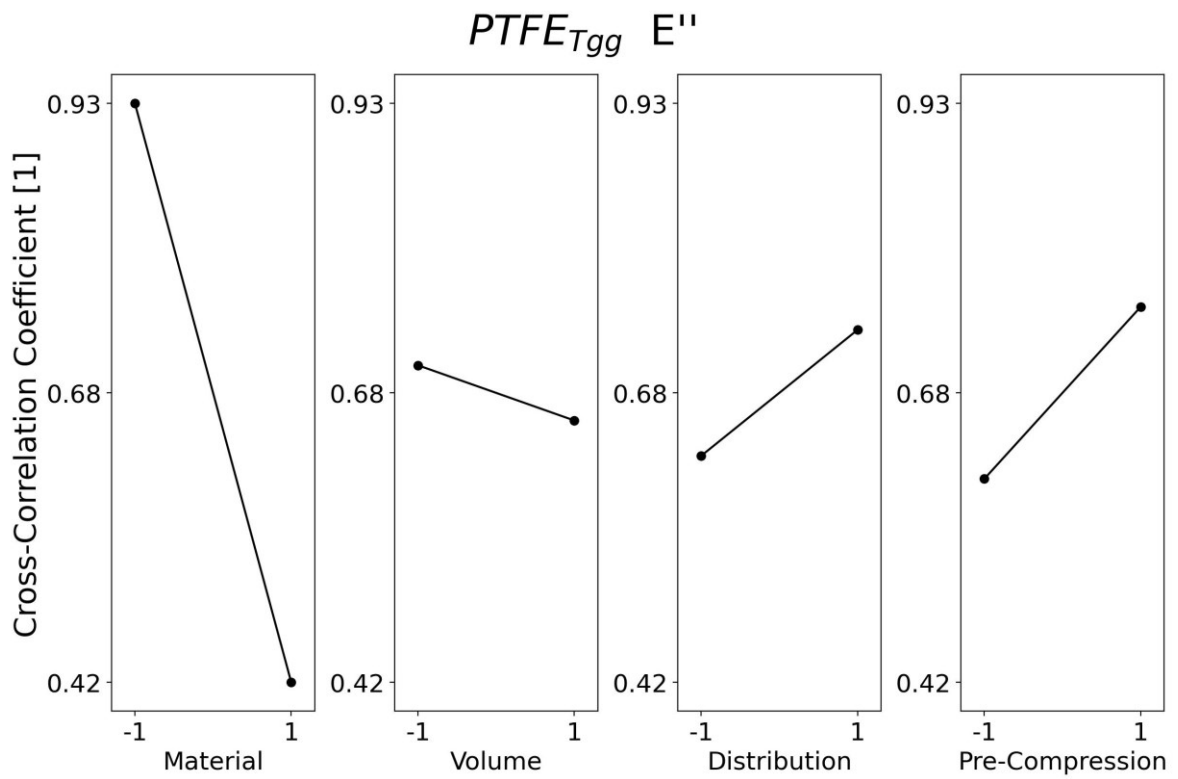Figure 64: Main effect plot (correlation coefficient) of PTFE_Tc evaluating tan δ.
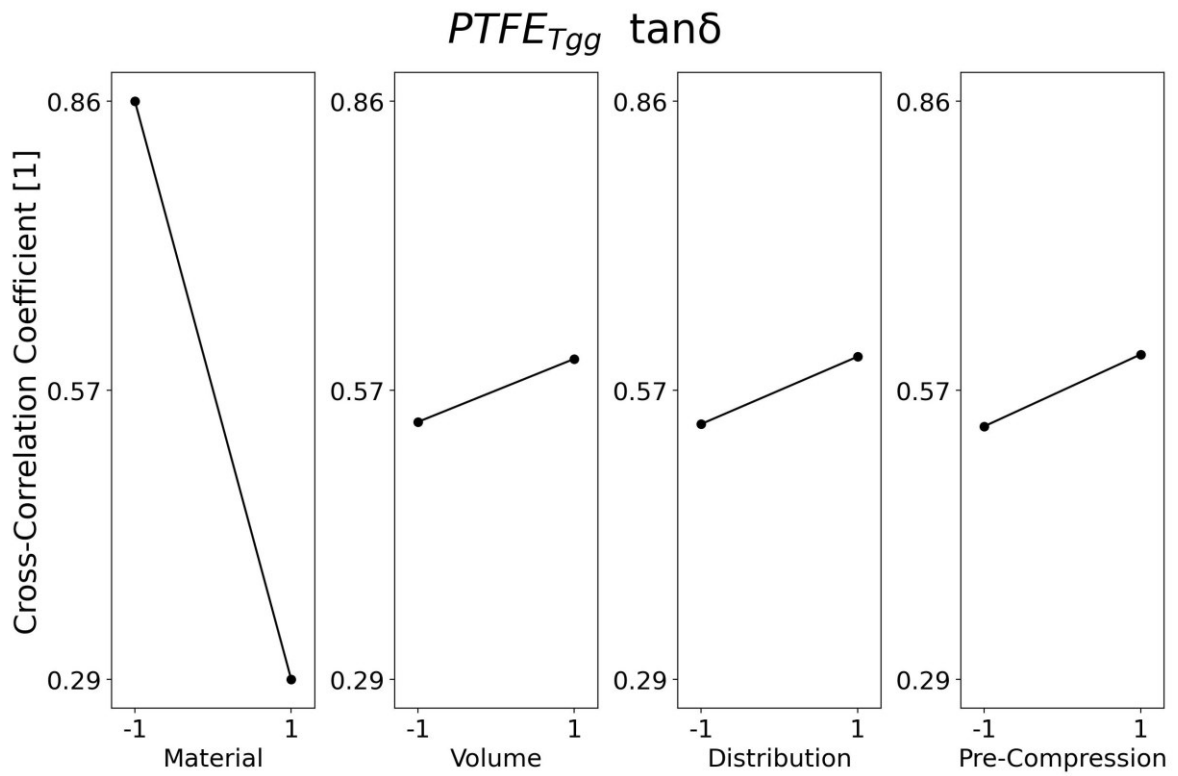
Figure 65: Main effect plot (correlation coefficient) of PTFE$_{Tgg}$ evaluating tan δ.
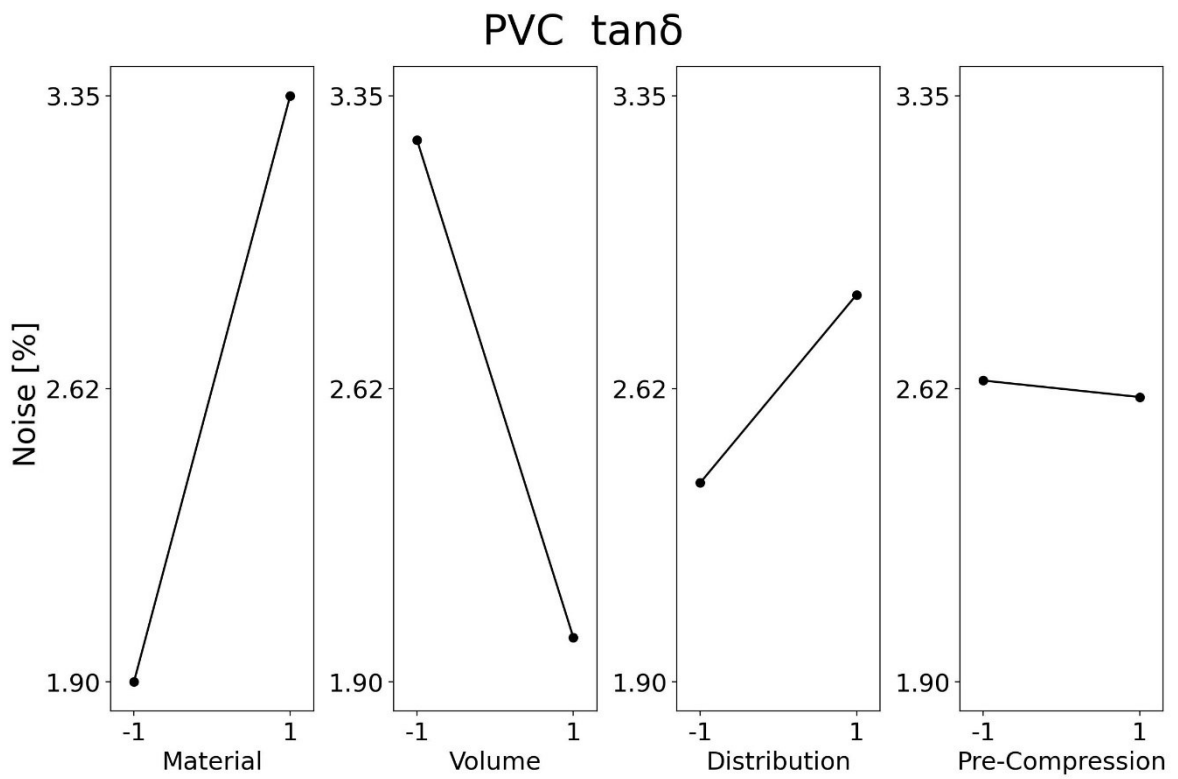
Figure 66: Main effect plot (noise) for PVC evaluating tan δ.
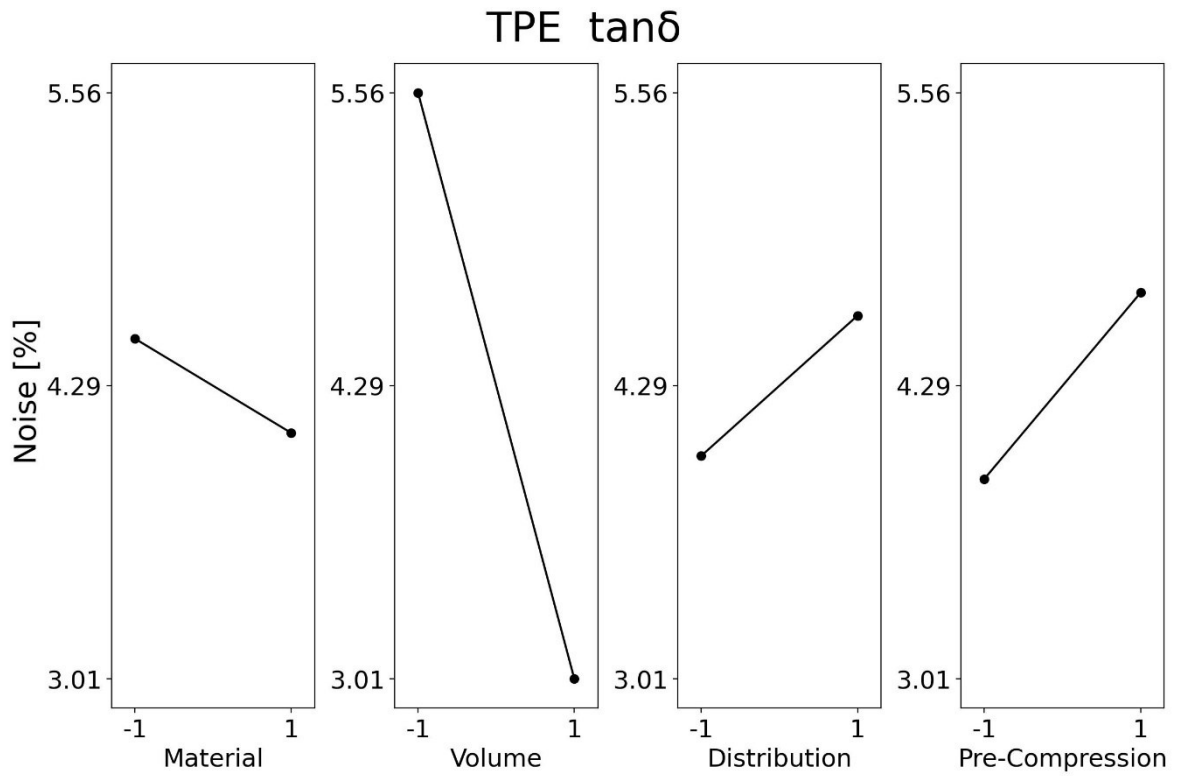
Figure 67: Main effect plot (noise) for TPE evaluating tan δ.
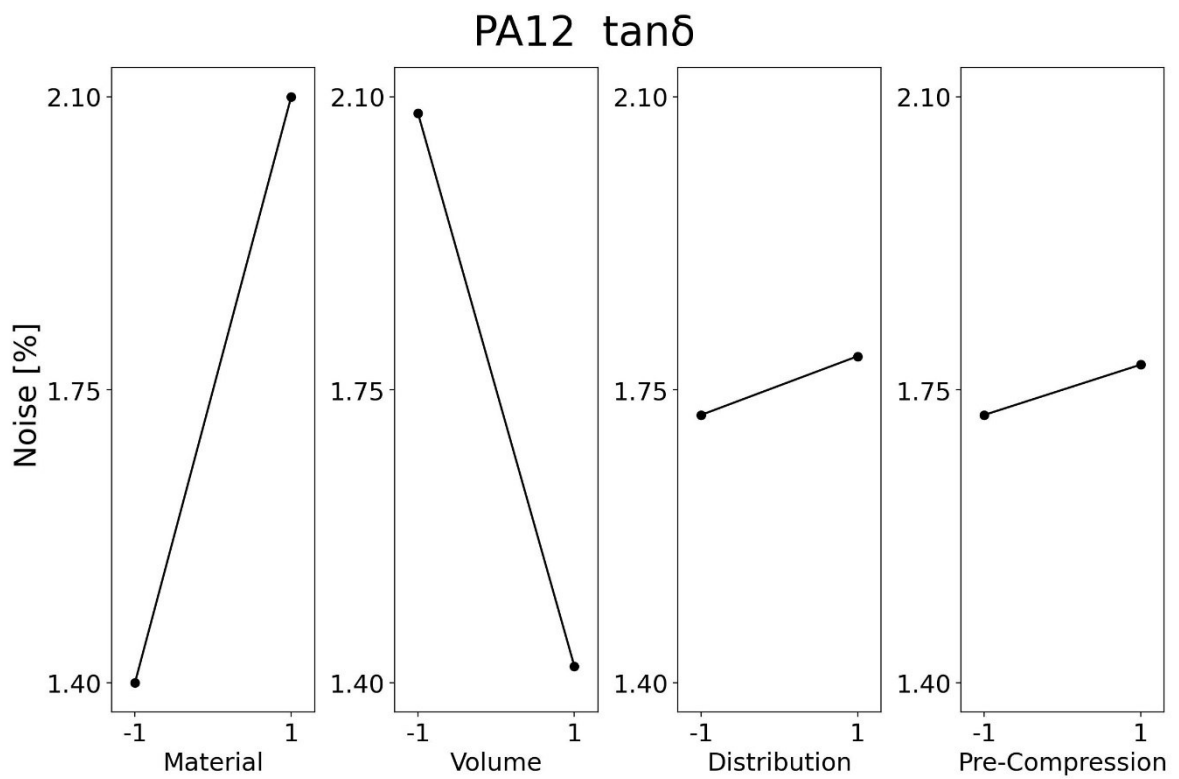
Figure 68: Main effect plot (noise) for PA12 evaluating tan δ.
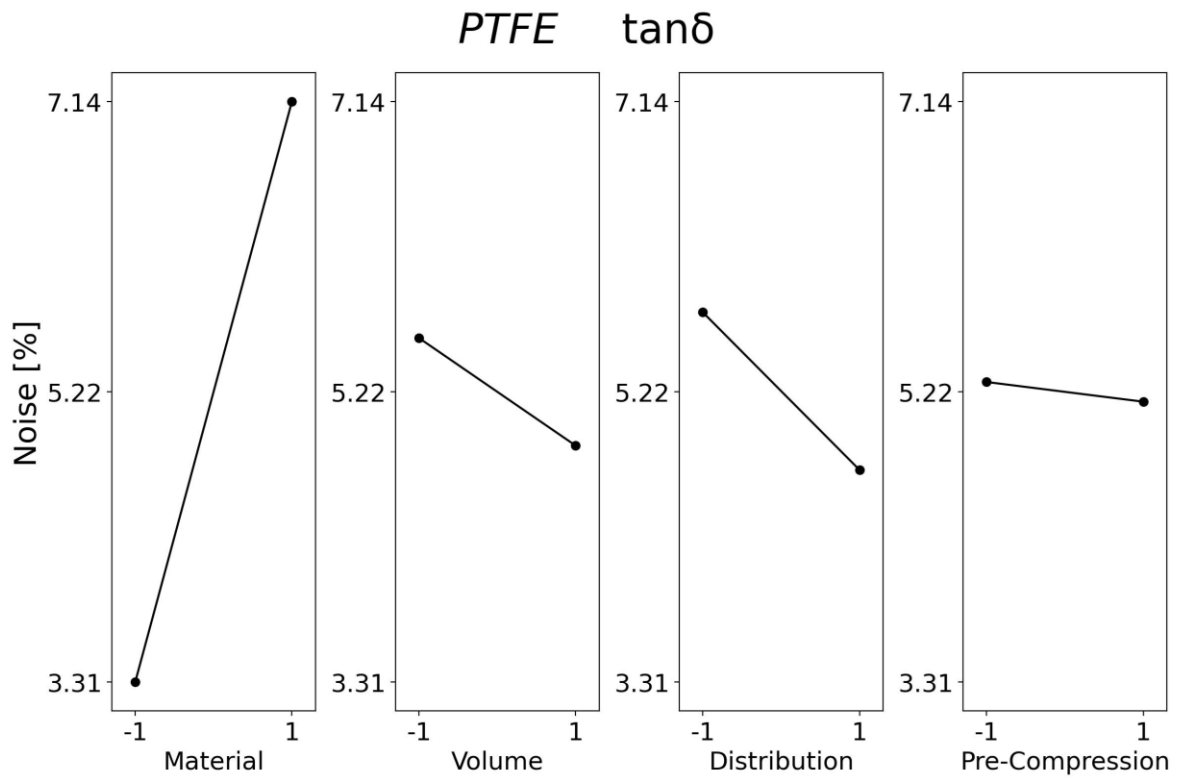
Figure 69: Main effect plot (noise) of PTFE evaluating tan δ.
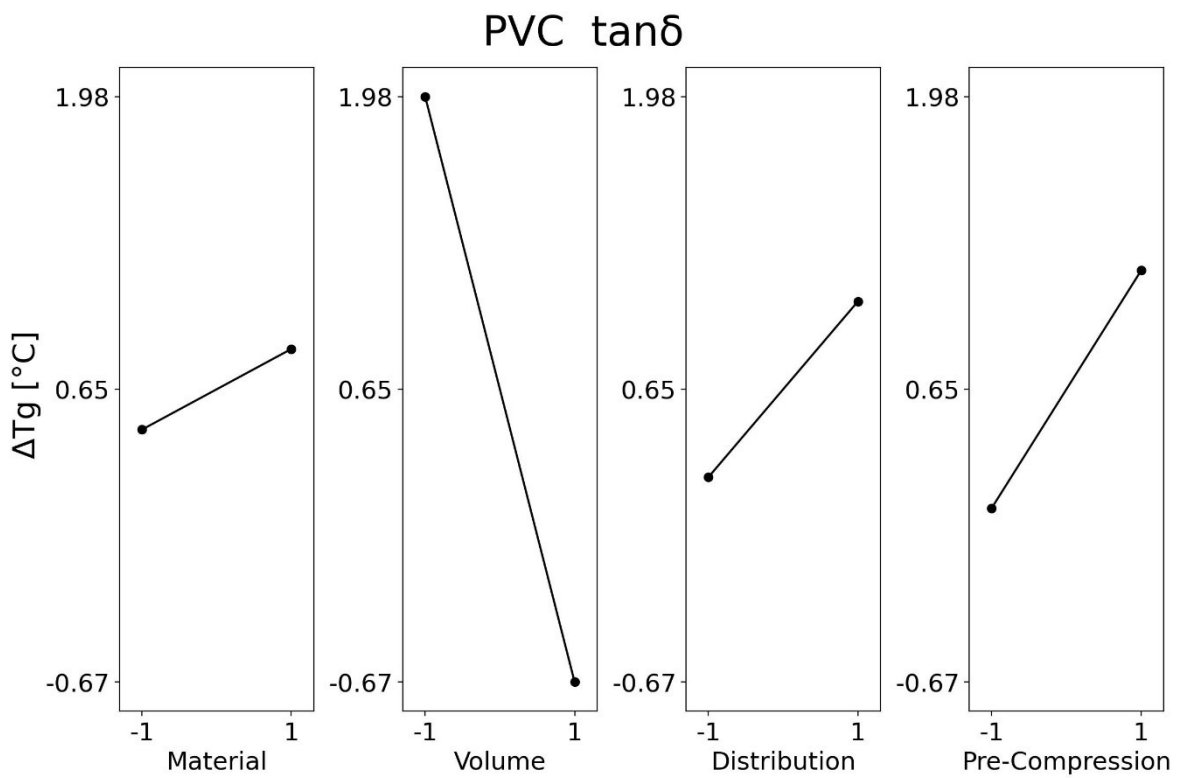
Figure 70: Main effect plot (difference between solid and powder T$_g$) for PVC evaluating tan δ.
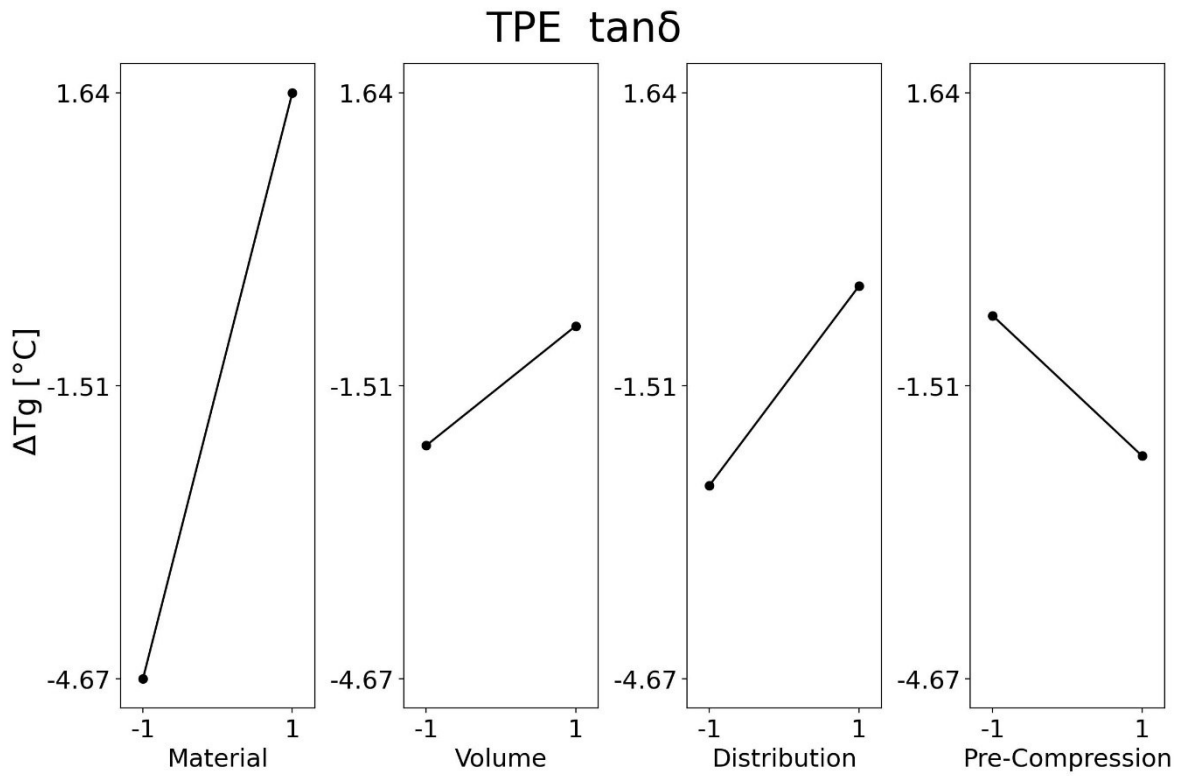
Figure 71: Main effect plot (difference between solid and powder T_g) for TPE evaluating tan δ.
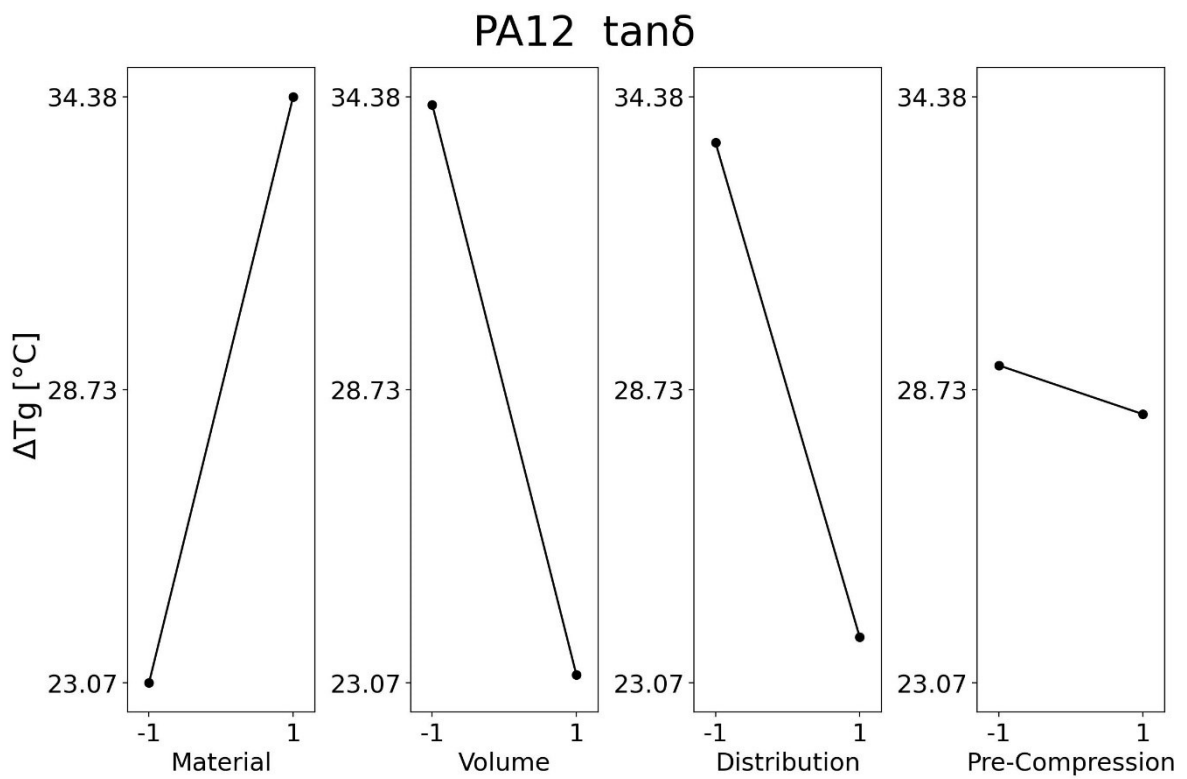
Figure 72: Main effect plot (difference between solid and powder T_g) for PA12 evaluating tan δ.
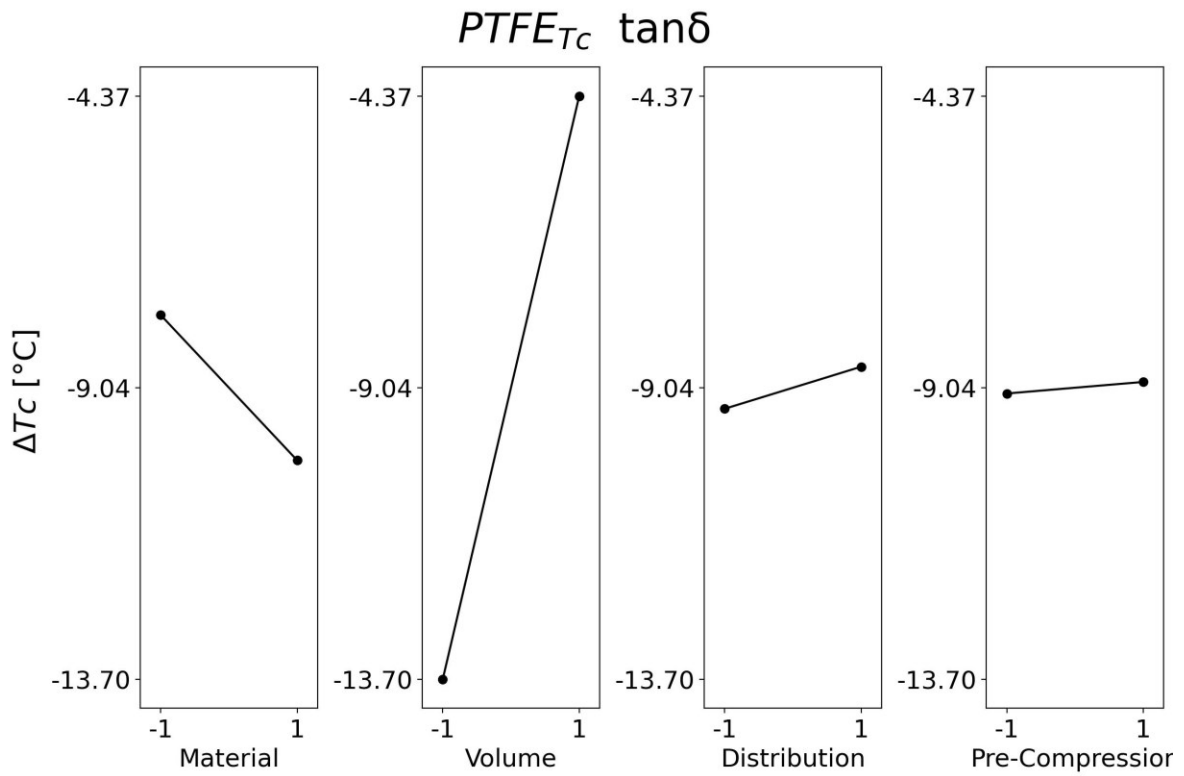
Figure 73: Main effect plot (difference between solid and powder T_c) of PTFE evaluating tan δ.
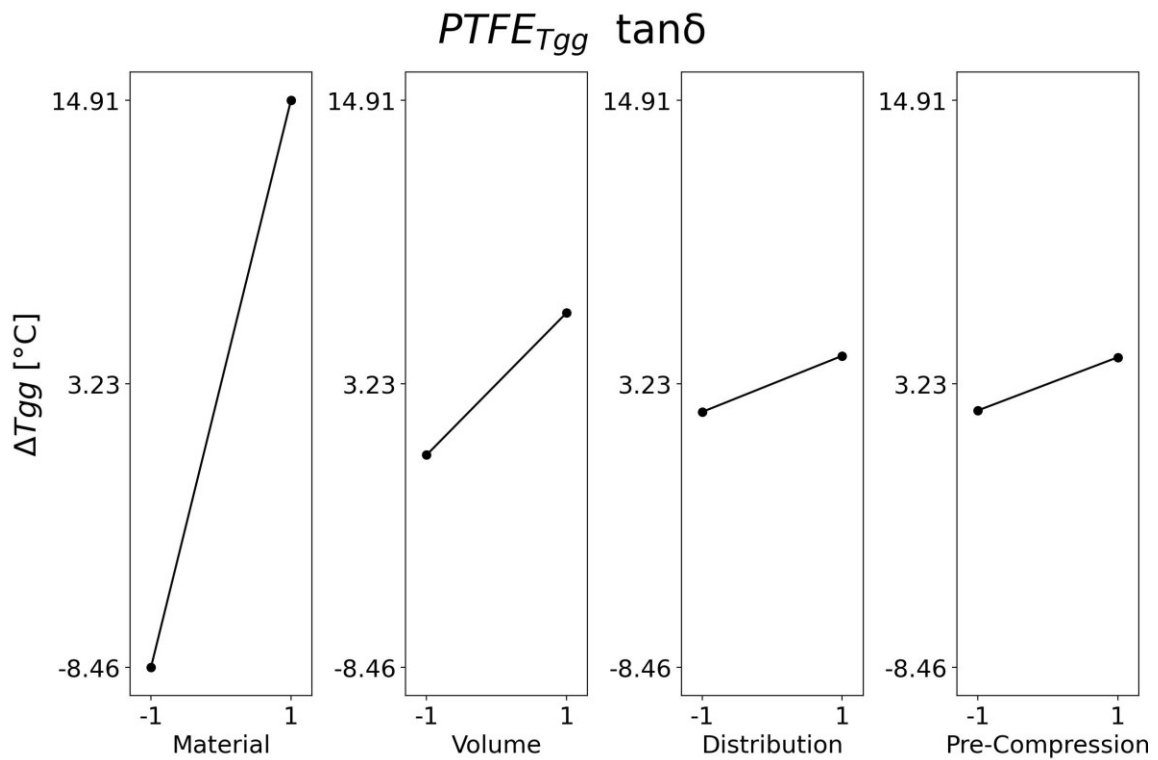
Figure 74: Main effect plot (difference between solid and powder T_{gg}) of PTFE evaluating tan δ.
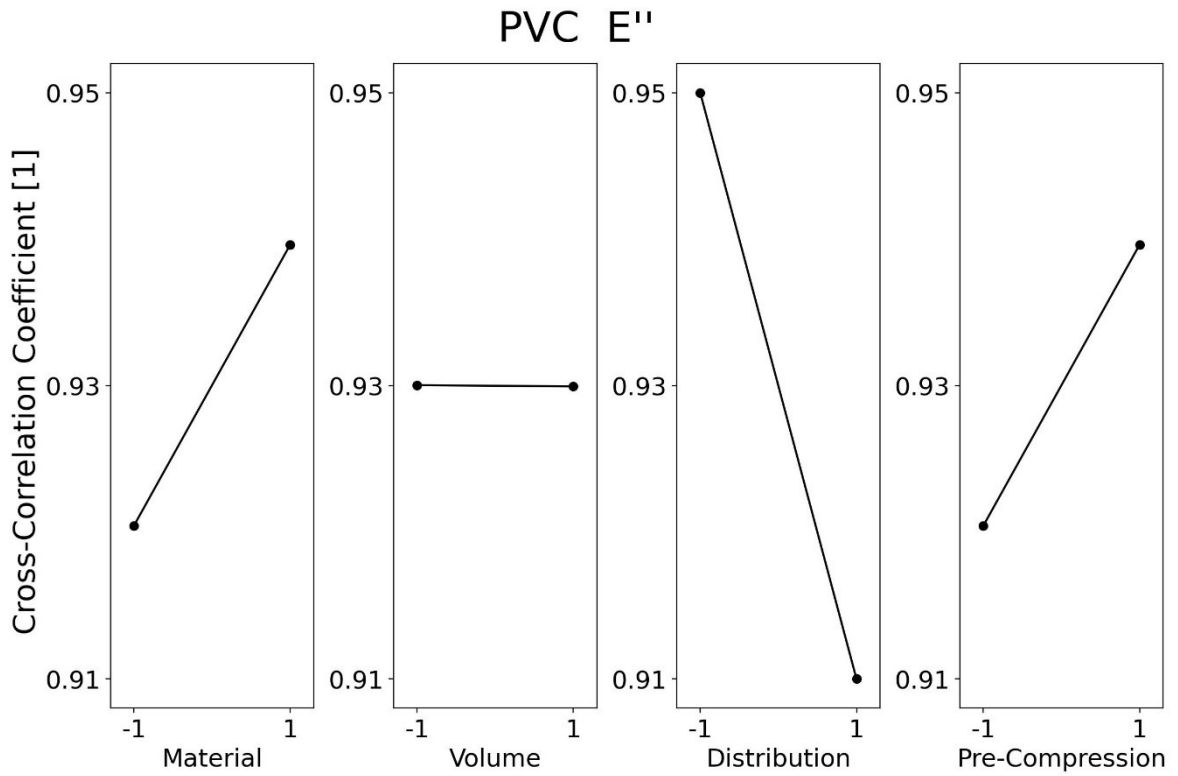
Figure 75: Main effect plot (correlation coefficient) for PVC evaluating E''.
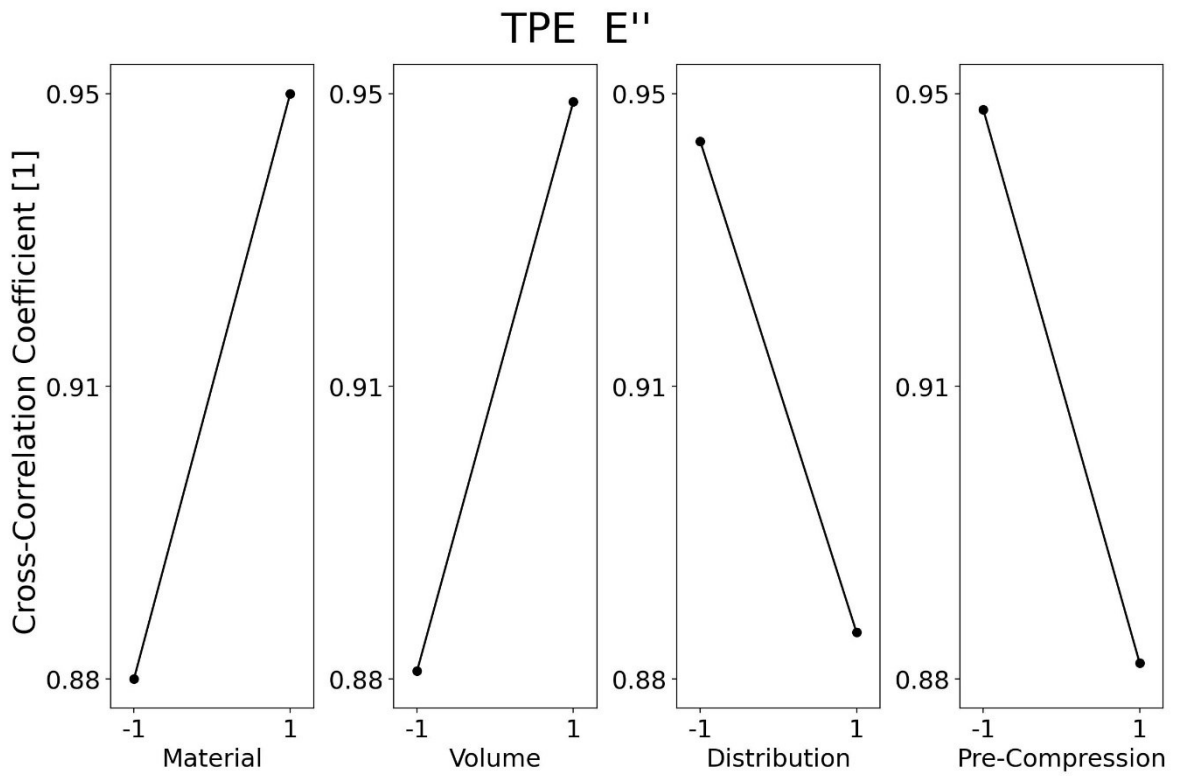
Figure 76: Main effect plot (correlation coefficient) for TPE evaluating E''.
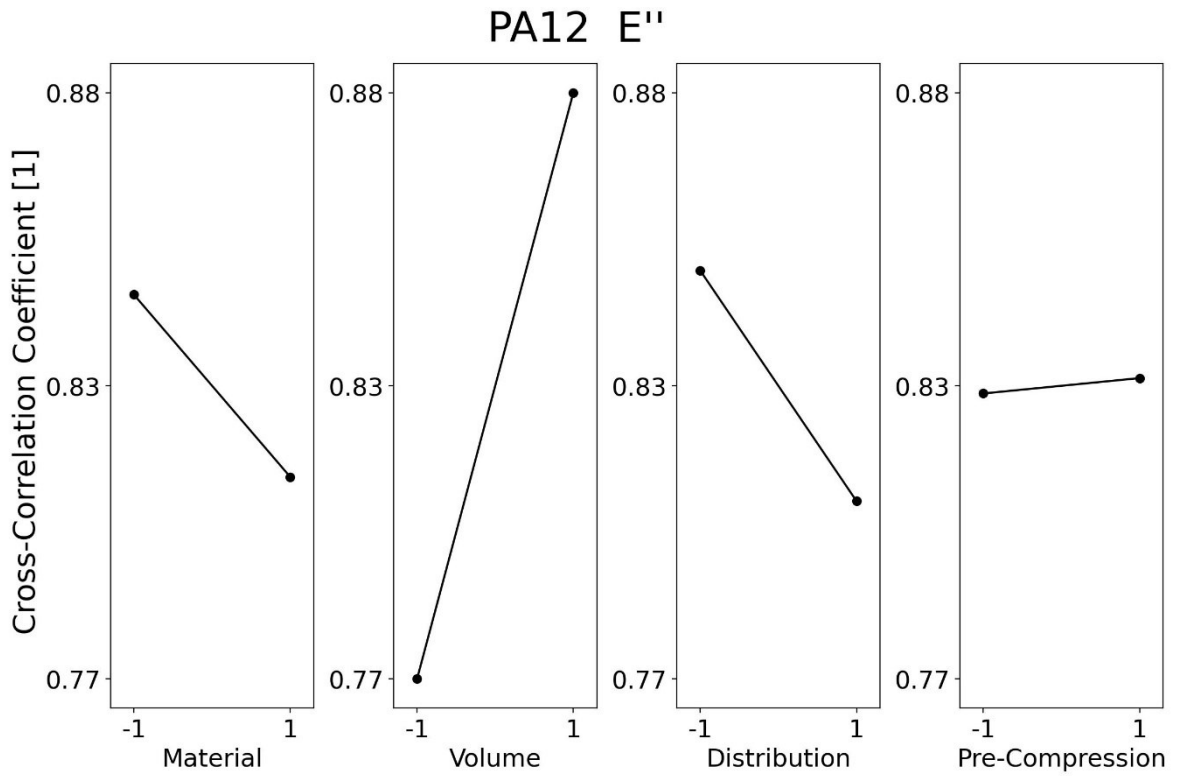
Figure 77: Main effect plot (correlation coefficient) for PA12 evaluating E''.
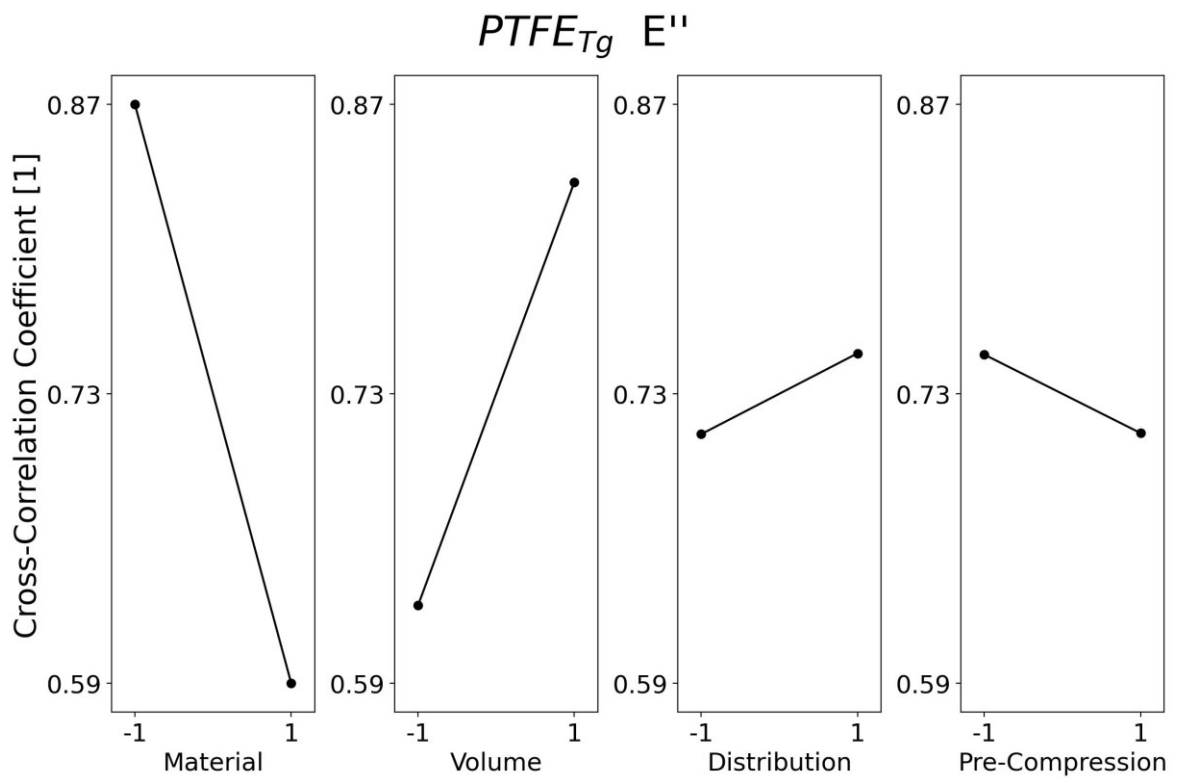
Figure 78: Main effect plot (correlation coefficient) of PTFE$_{Tg}$ evaluating E''.

Figure 79: Main effect plot (correlation coefficient) of PTFE$_{Tc}$ evaluating E''.

Figure 80: Main effect plot (correlation coefficient) of PTFE$_{Tg}$ evaluating E''.
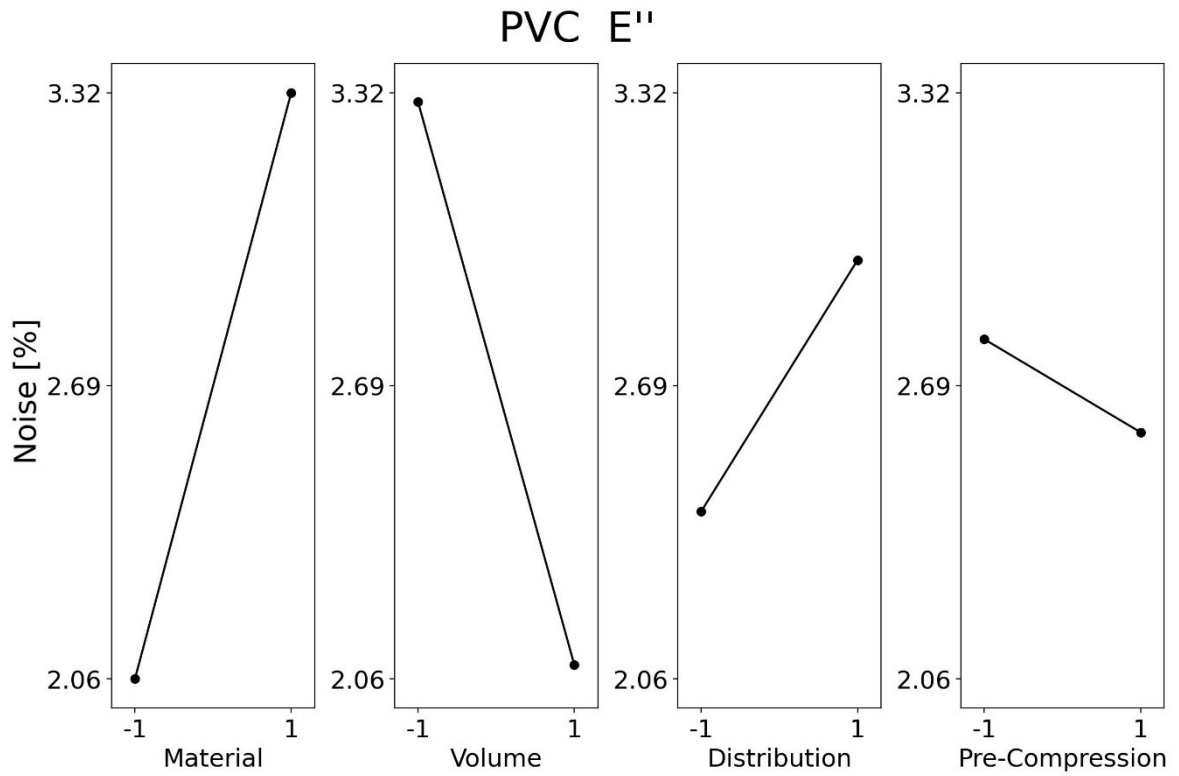
PVC E''

Figure 81: Main effect plot (noise) for PVC evaluating E''.
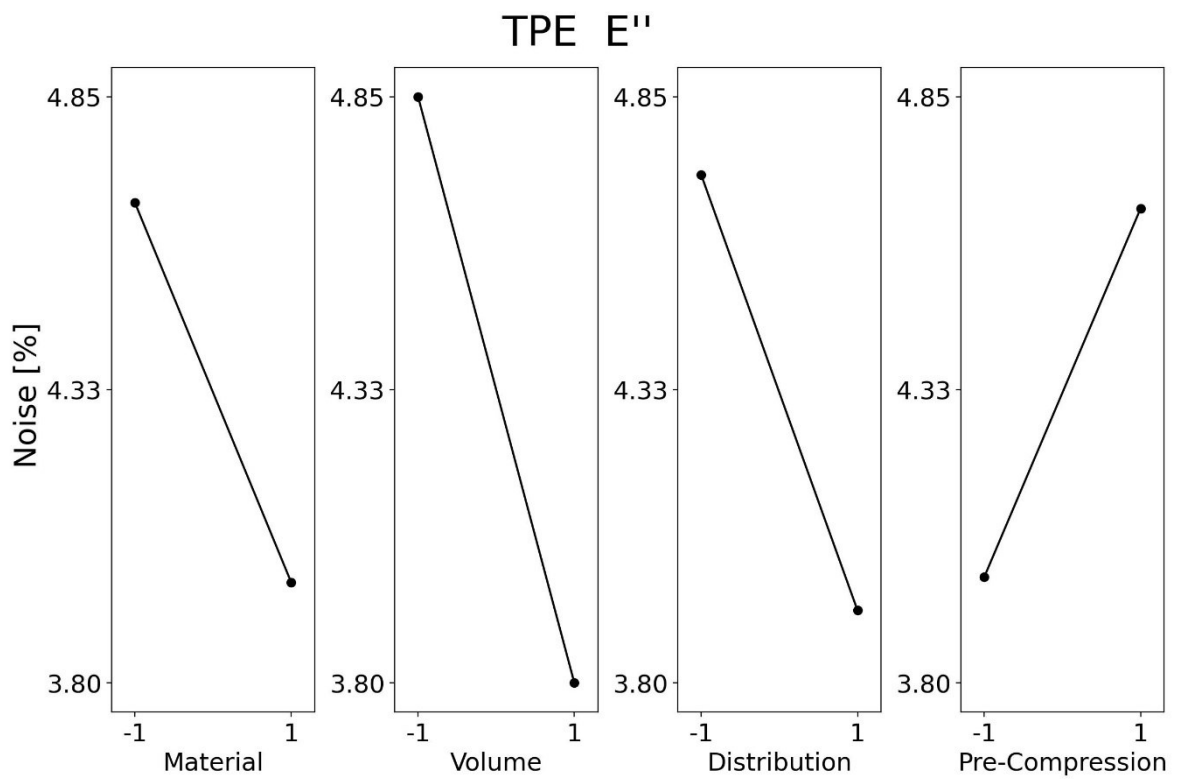
TPE E''

Figure 82: Main effect plot (noise) for TPE evaluating E''.
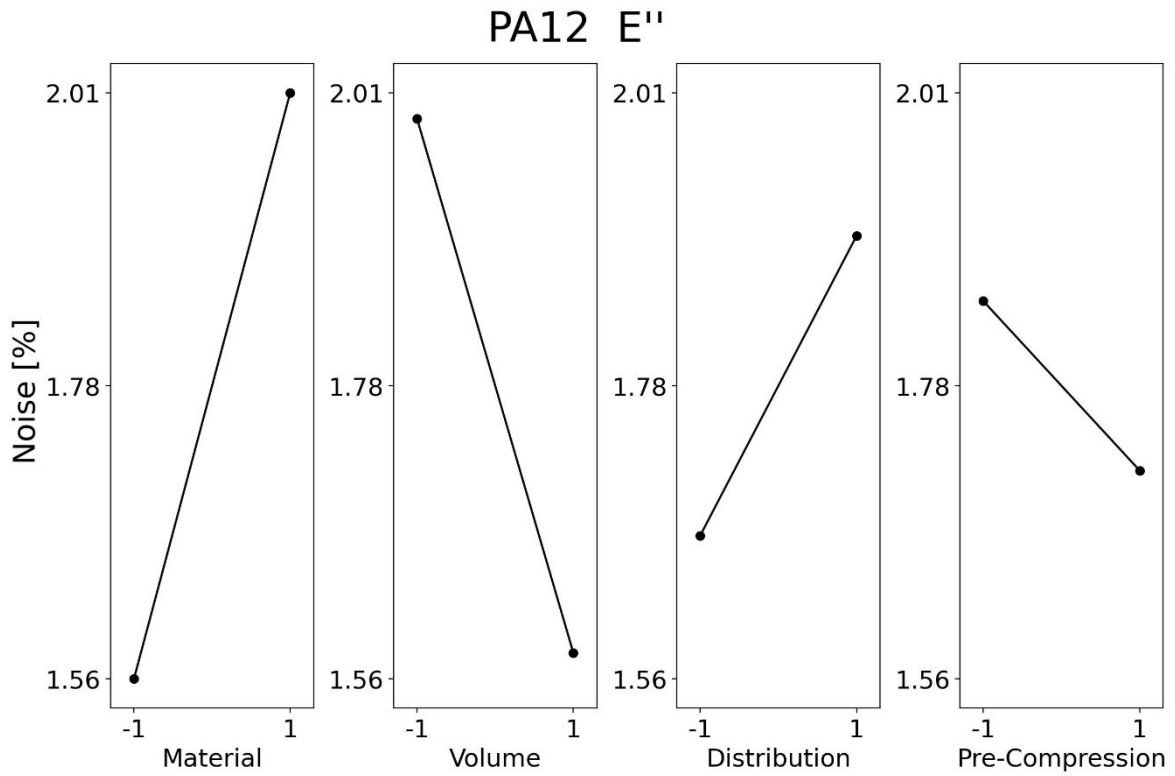
Figure 83: Main effect plot (noise) for PA12 evaluating E''.
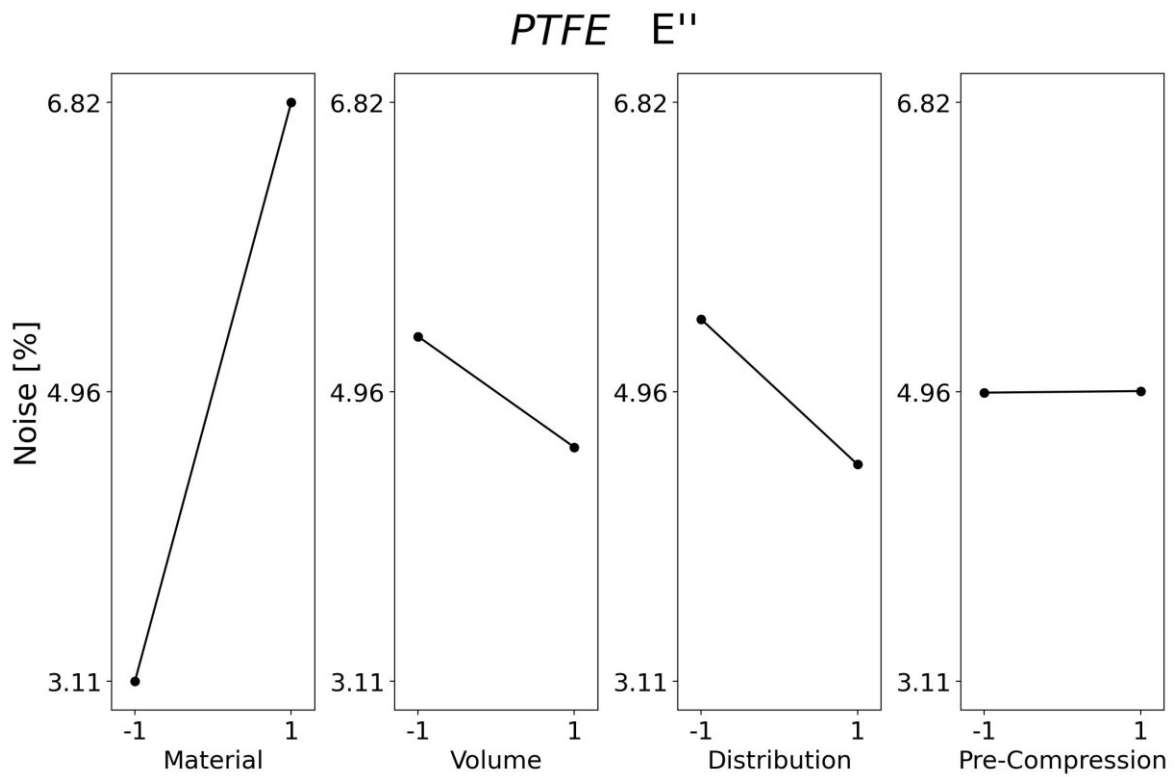
Figure 84: Main effect plot (noise) of PTFE evaluating E''.
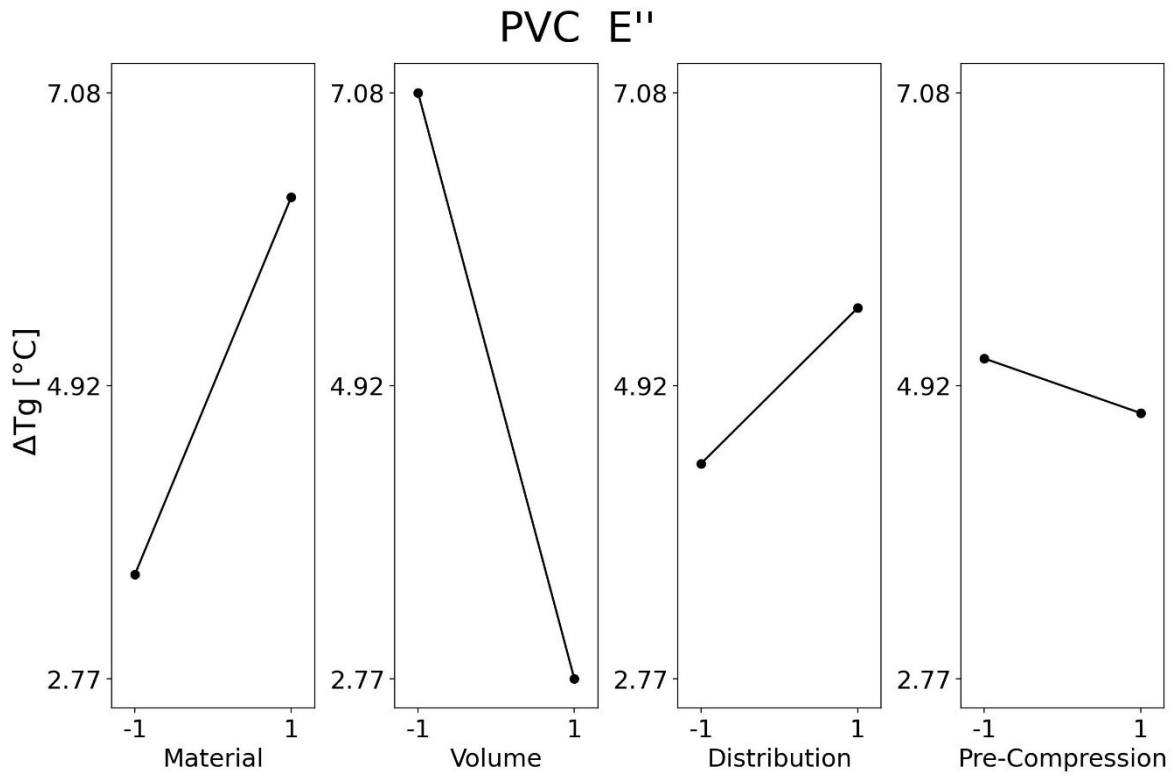
Figure 85: Main effect plot (difference between solid and powder Tg) for PVC.
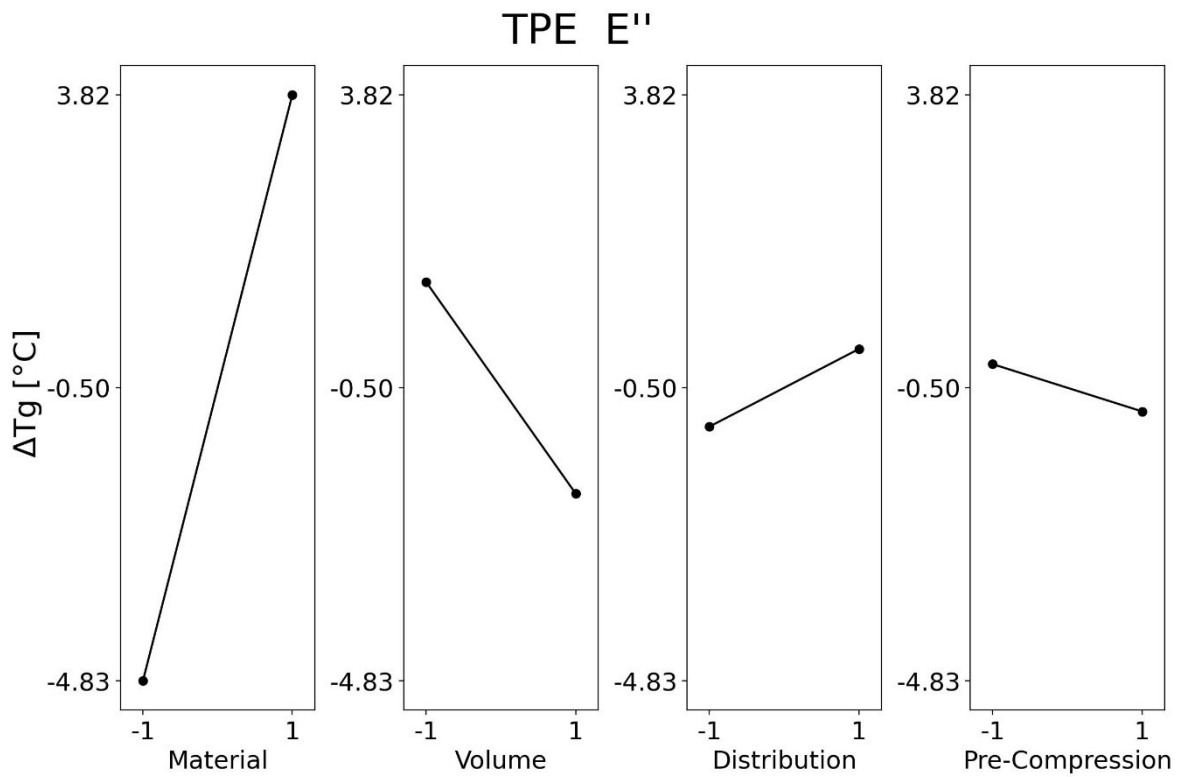
Figure 86: Main effect plot (difference between solid and powder Tg) for TPE.

PA12 E''
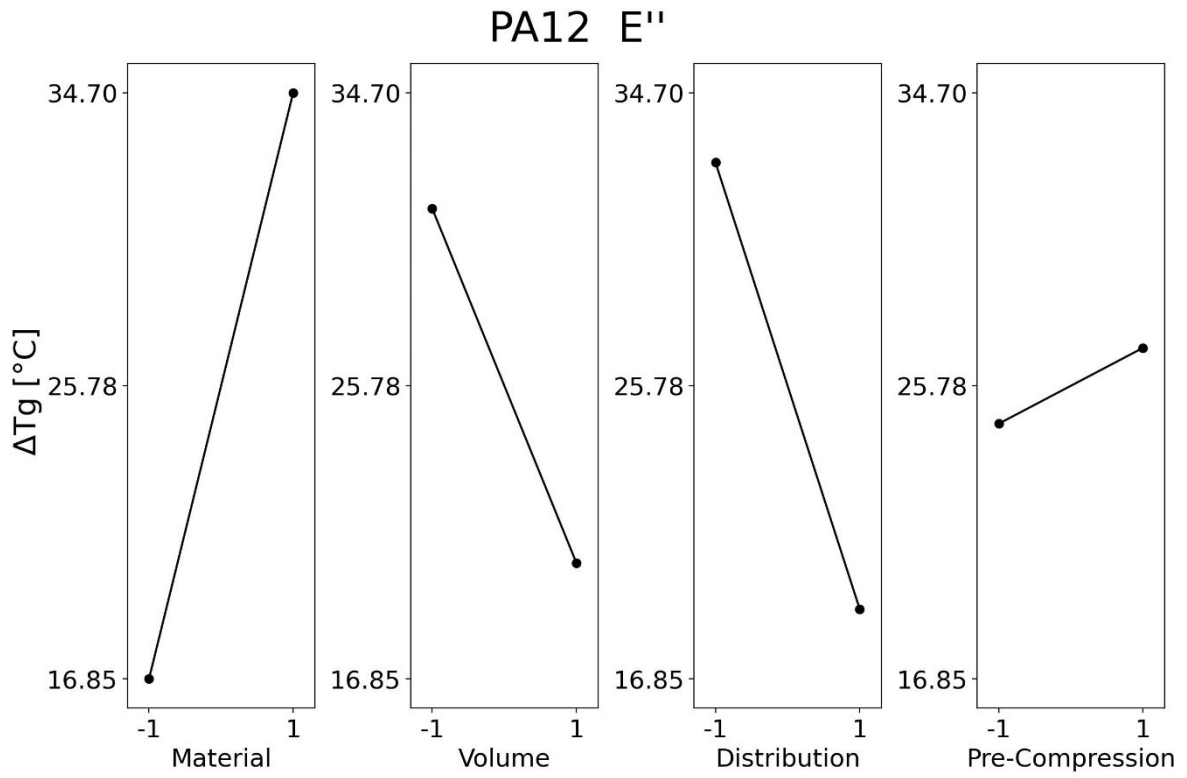
Figure 87: Main effect plot (difference between solid and powder T_g) for PA12.

$PTFE_{TC}$ E''
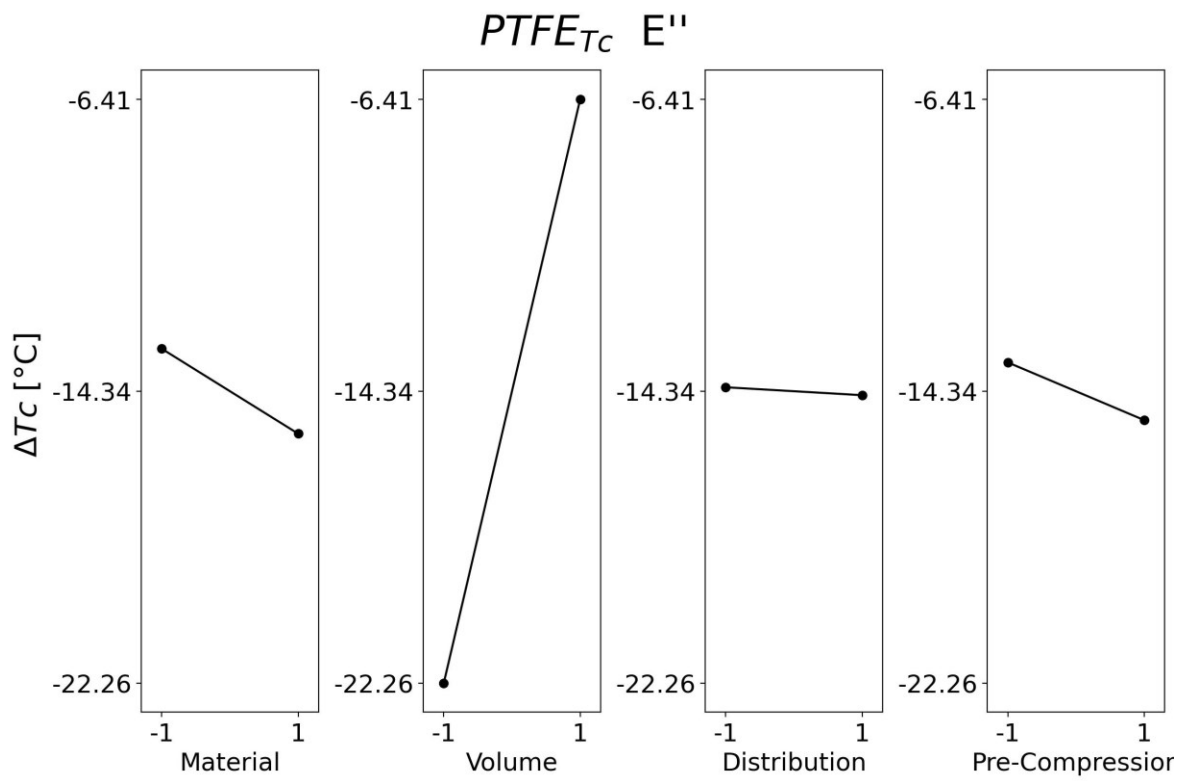
Figure 88: Main effect plot (difference between solid and powder T_c) of PTFE evaluating E''.
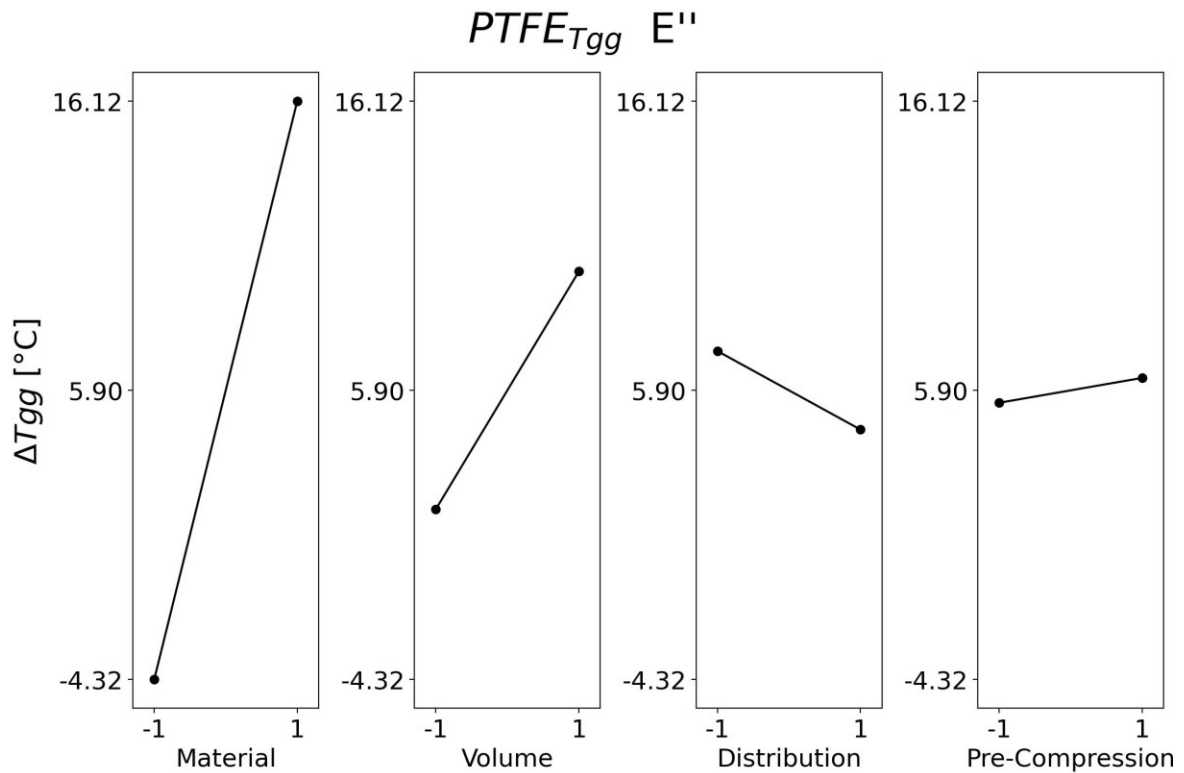
Figure 89: Main effect plot (difference between solid and powder T_{gg}) of PTFE evaluating E''.

Appendix 4: Results from DSC measurements

Table 32: Results obtained from a DSC measurement of PVC.

	1st Run		
Sample	T_g [°C]	T_m [°C]	ΔH_m [J/g]
1	83.7	66.2	0.7
2	83.9	66.9	0.5
3	83.3	66.8	0.8
Average	83.6	66.6	0.7
	2nd Run		
1	83.5	62.5	0.3
2	83.7	62.4	0.2
3	83.6	62.0	0.1
Average	83.6	62.3	0.2

Table 33: Results obtained from a DSC measurement of TPE.

TPE	1st Run					
Sample	T_g [°C]	T_{mSoft} [°C]	T_{mHard} [°C]	ΔH_{mSoft} [J/g]	ΔH_{mHard} [J/g]	x_c [%]
1	-77.9	-6.5	185.3	7.6	12.8	8%
2	-79.5	-6.1	185.9	7.9	13.6	9%
3	-77.7	-6.2	186.7	7.4	12.9	8%
Average	-78.3	-6.3	186.0	7.6	13.1	8%
	2nd Run					
1	-77.4	-0.1	187.4	12.1	9.4	6%
2	-78.1	-0.1	189.3	12.5	9.5	6%
3	-79.0	0.1	187.3	12.1	9.6	6%
Average	-78.2	-0.1	188.0	12.2	9.5	6%

Table 34: Results obtained from a DSC measurement of PA12.

PA12	1st Run		
Sample	T_m [°C]	ΔH_m [J/g]	X_c [%]
1	185.2	98.5	64%
2	185.3	100.7	65%
3	185.2	106.6	69%
Average	185.3	102.0	66%
	2nd Run		
1	177.3	41.5	27%
2	177.3	41.7	27%
3	177.3	42.7	28%
Average	177.3	42.0	27%

Table 35: Results obtained from a DSC measurement of PTFE.

PTFE	1st Run			
Sample	T_c [°C]	T_m [°C]	ΔH_m [J/g]	X_c [%]
1	17.2	340.8	55.4	68%
2	16.4	340.5	58.6	72%
3	16.3	337.8	62.1	76%
Average	16.6	339.7	58.7	72%
	2nd Run			
1	18.1	324.3	24.3	30%
2	18.1	324.3	24.1	29%
3	17.2	324.0	24.9	30%
Average	17.8	324.2	24.4	30%

Appendix 5: Powder rheological properties over temperature
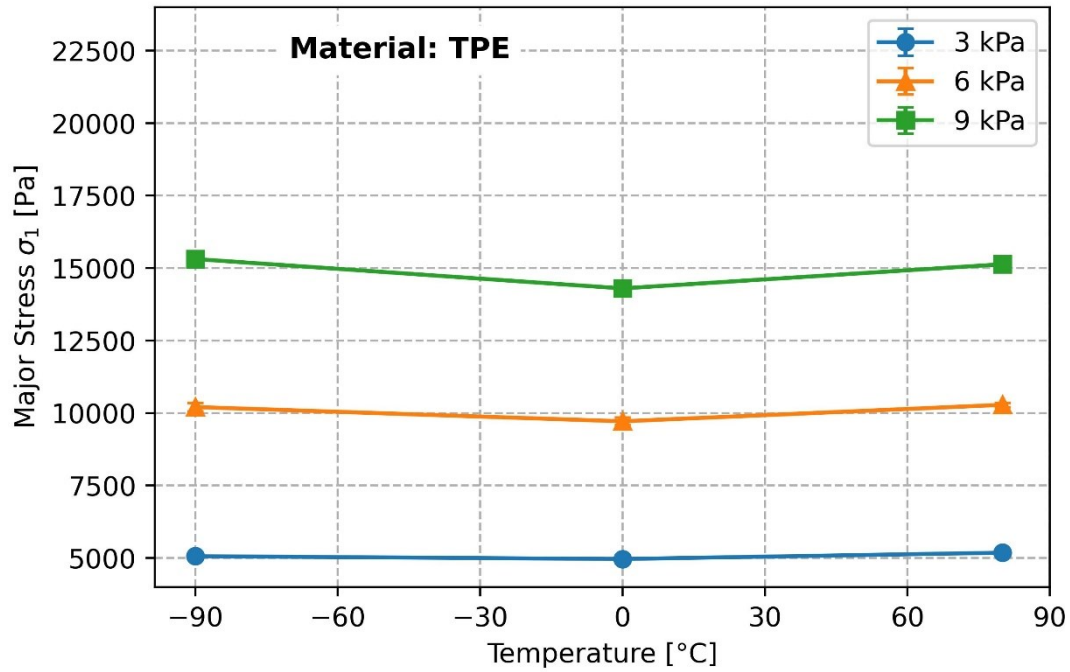
Figure 90: Major Stress σ₁ of TPE over the temperature range -90-80 C°. Three normal stress levels
are depicted.
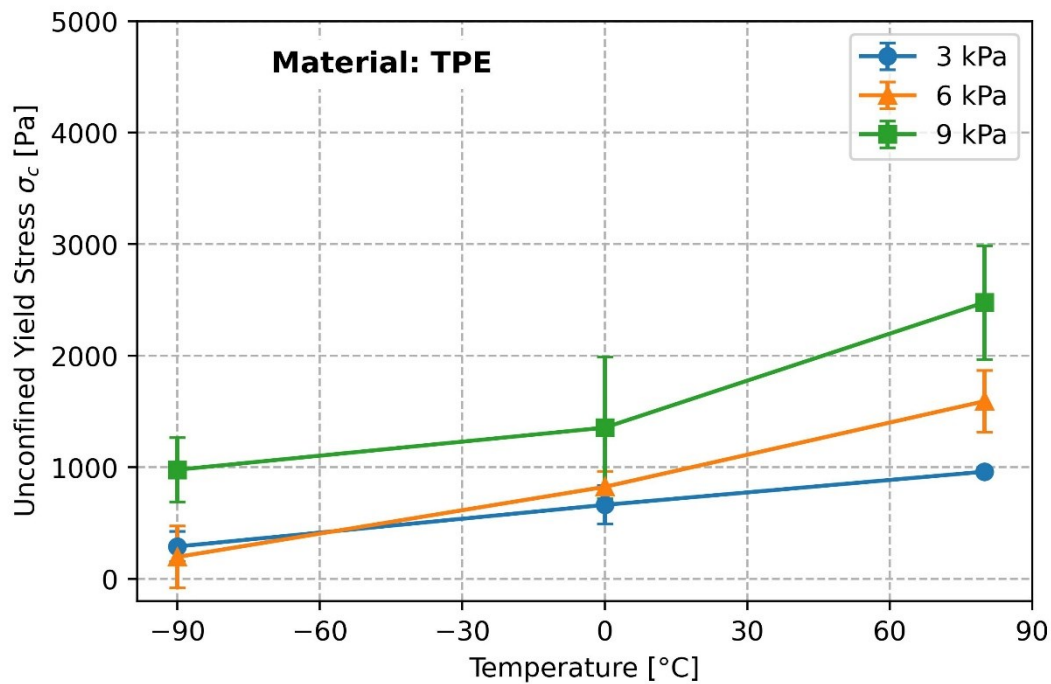
Figure 91: Unconfined Yield Strength σ_c of TPE over the temperature range -90-80 C°. Three normal
stress levels are depicted.
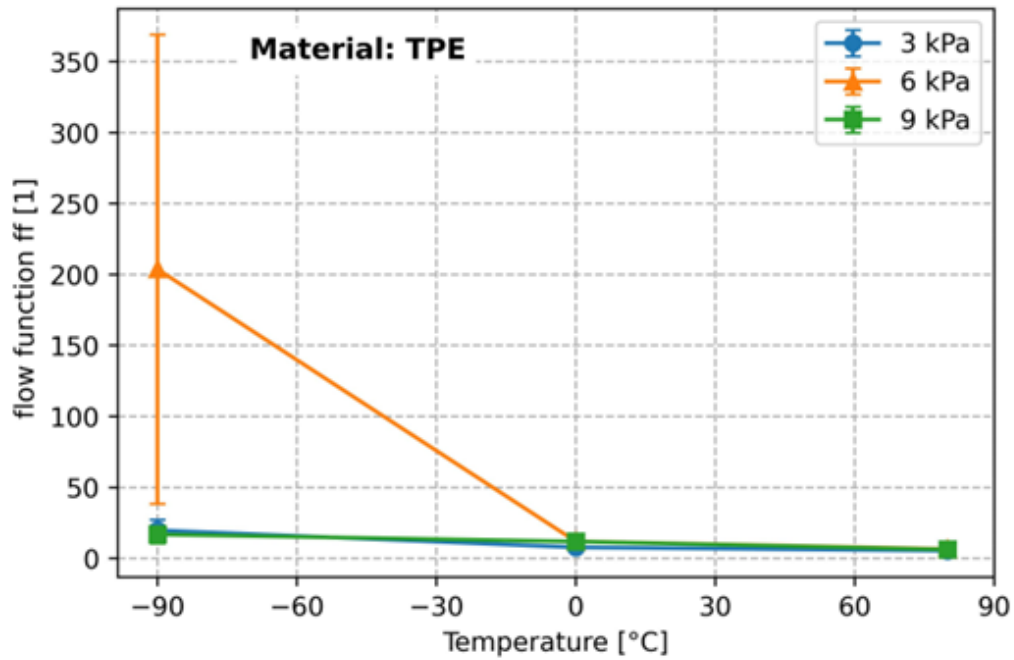
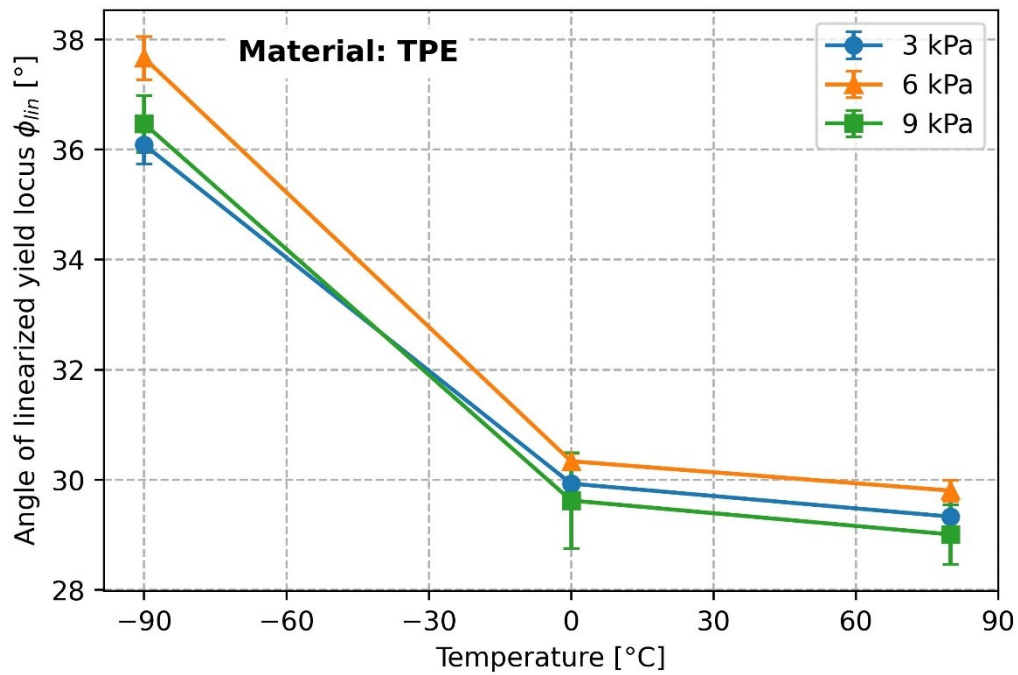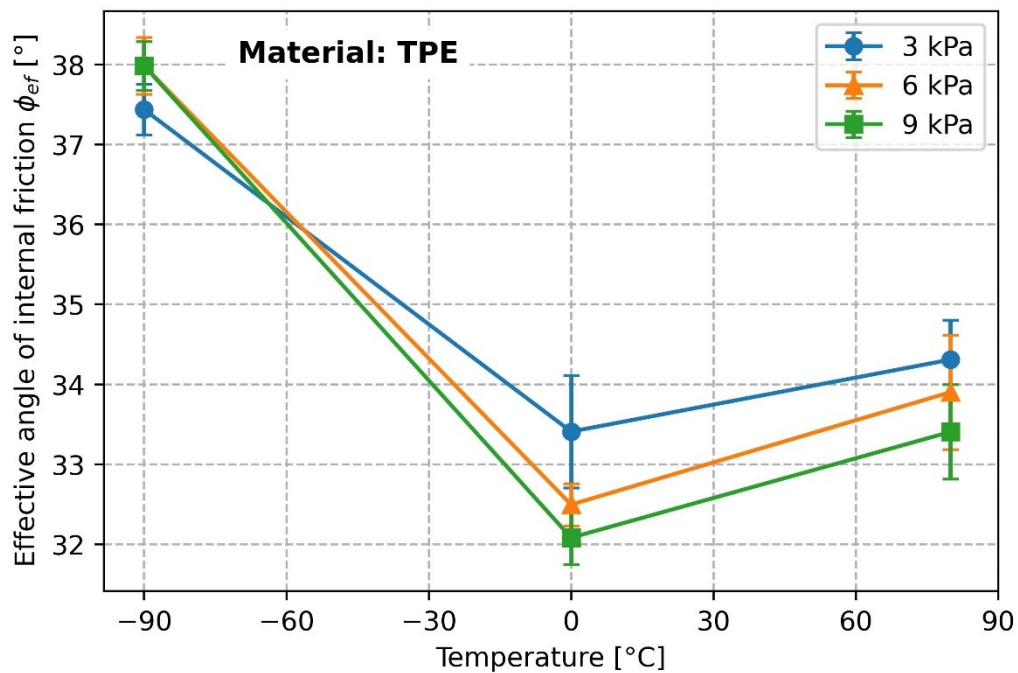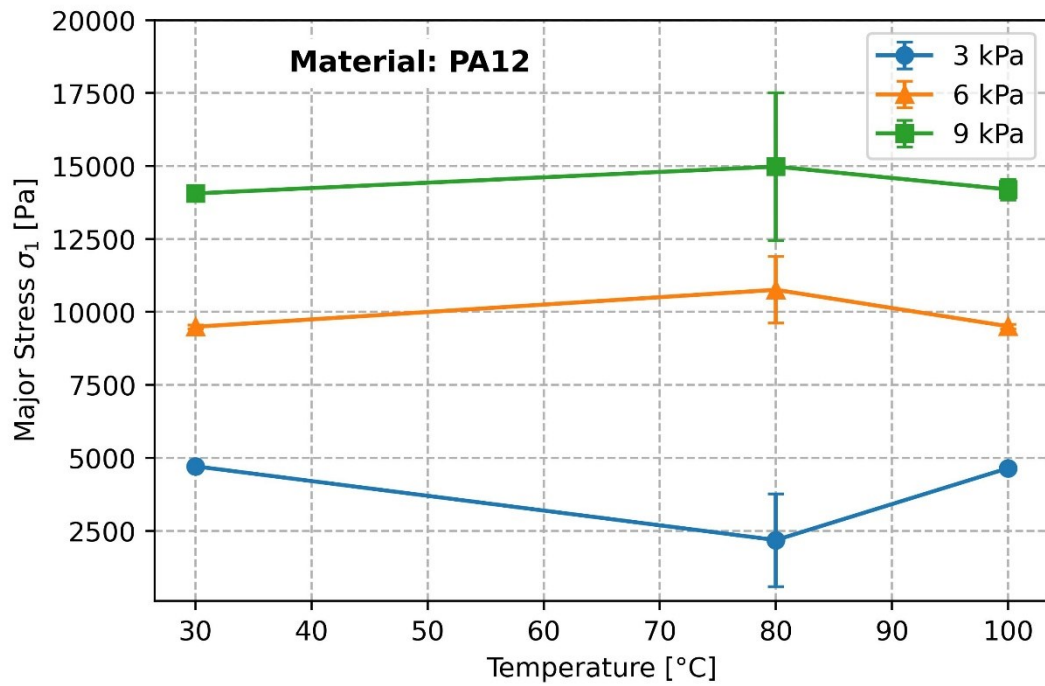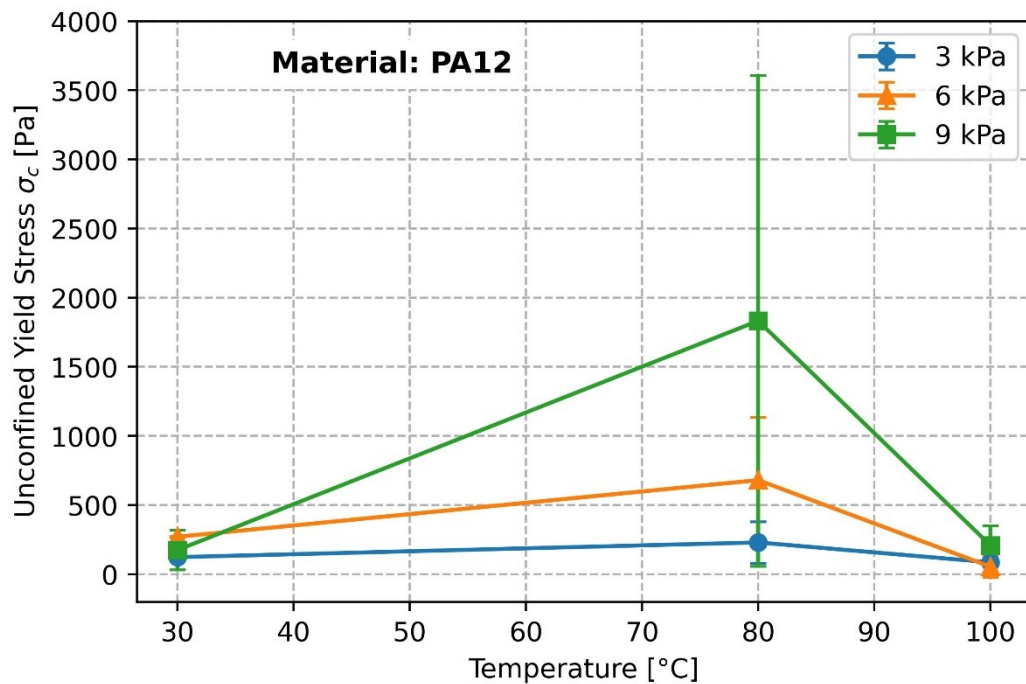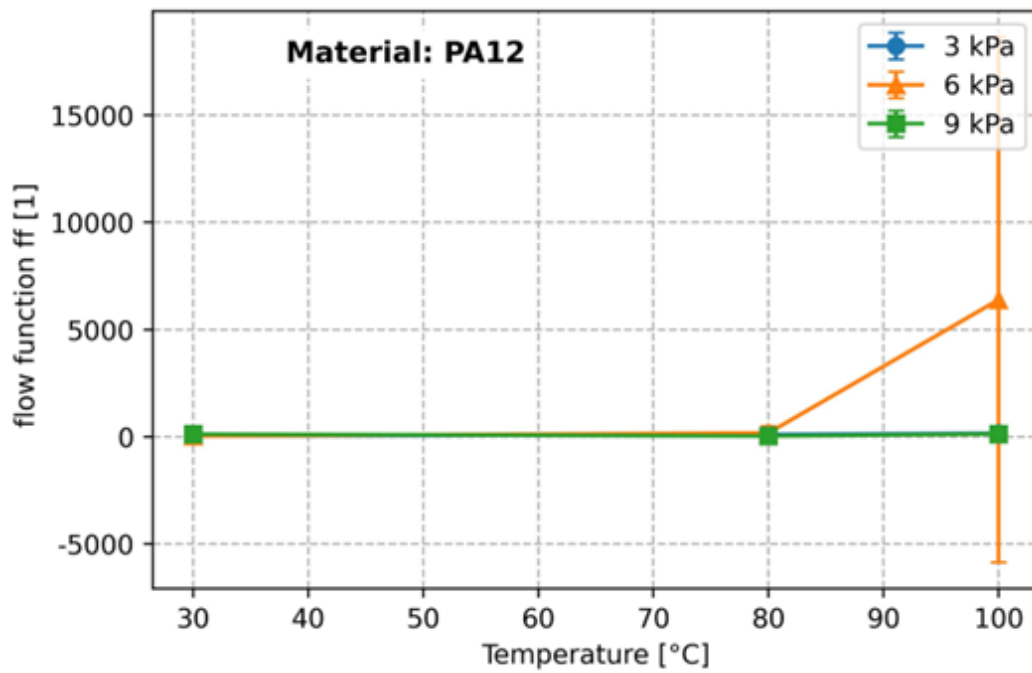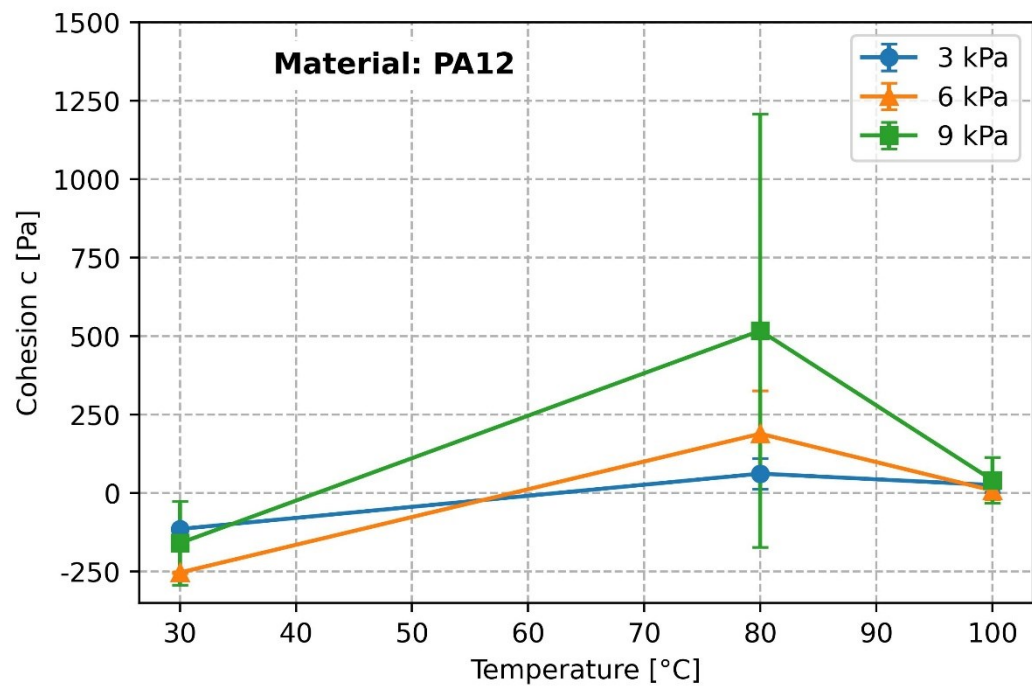Figure 92: Flow function ff of TPE over the temperature range -90-80 C°. Three normal stress levels are depicted.
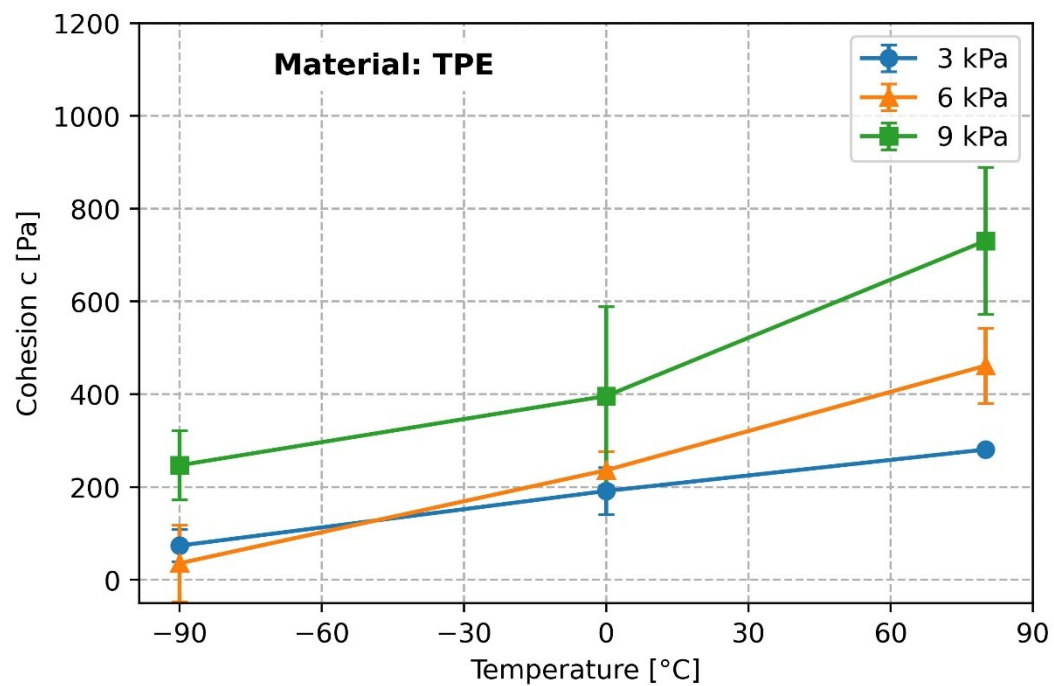
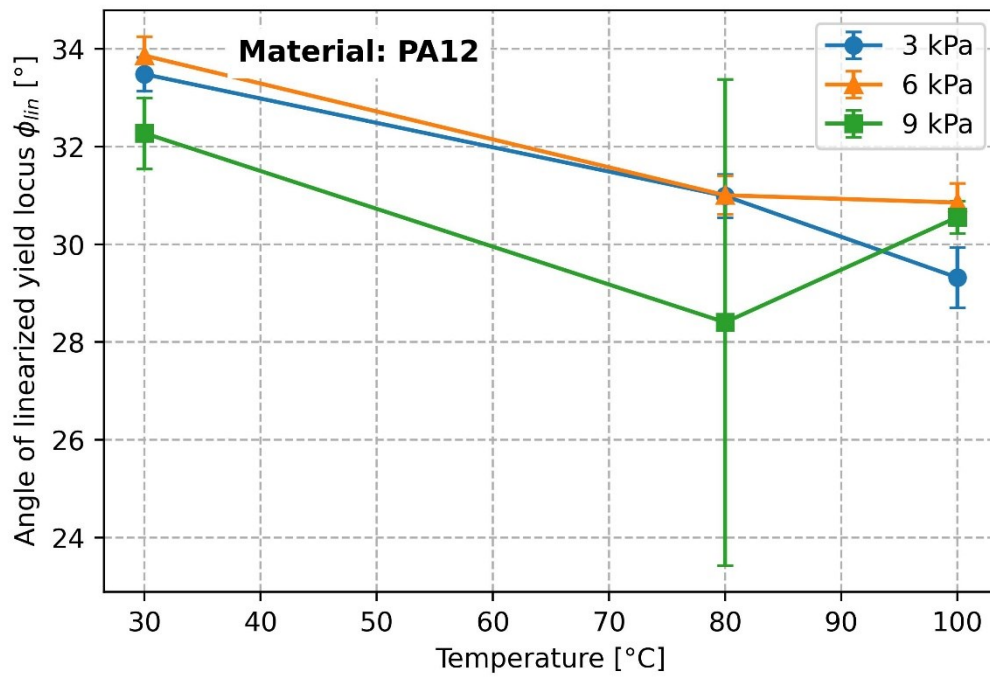Figure 93: Cohesion c of TPE over the temperature range -90-80 C°. Three normal stress levels are depicted.

Figure 94: Angle of linearized yield locus φ_{lin} of TPE over the temperature range -90-80 °C. Three normal stress levels are depicted
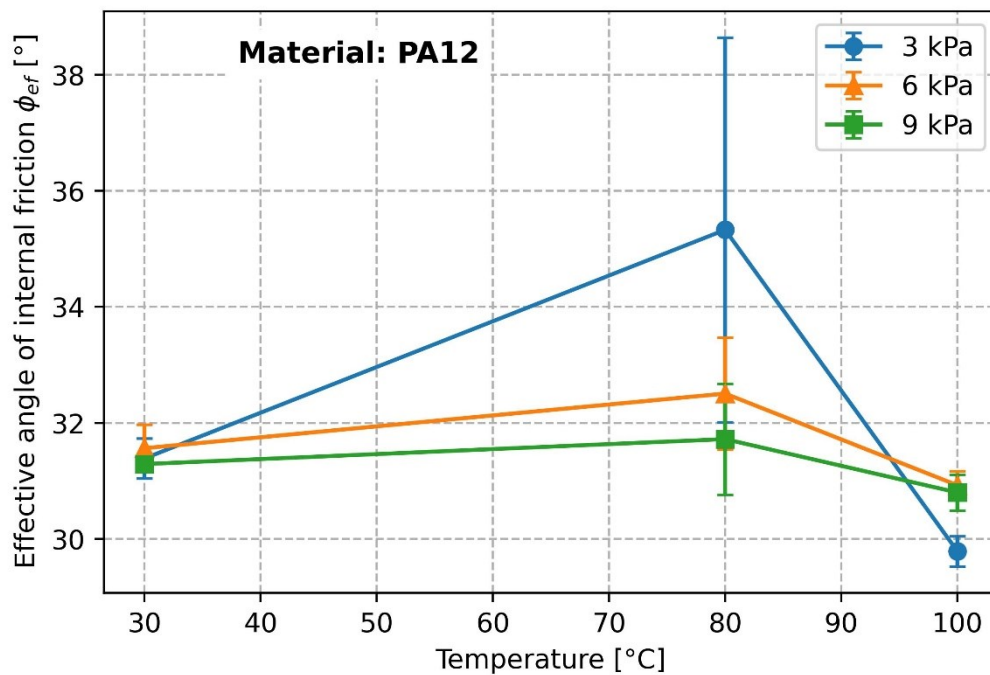

Figure 95: Effective angle of internal friction φ_{ef} of TPE over the temperature range -90-80 °C. Three normal stress levels are depicted

Figure 96: Major Stress σ₁ of PA12 over the temperature range 30-100 C°. Three normal stress levels are depicted.

Figure 97: Unconfined Yield Strength σc of PA12 over the temperature range 30-100 C°. Three normal stress levels are depicted.

Figure 98: Flow function ff of PA12 over the temperature range 30-100 C°. Three normal stress levels are depicted.

Figure 99: Cohesion c of PA12 over the temperature range 30-100 C°. Three normal stress levels are depicted.

Figure 100: Angle of linearized yield locus φ_{lin} of PA12 over the temperature range 30-100 °C. Three normal stress levels are depicted

Figure 101: Effective angle of internal friction φ_{ef} of PA12 over the temperature range 30-100 °C. Three normal stress levels are depicted
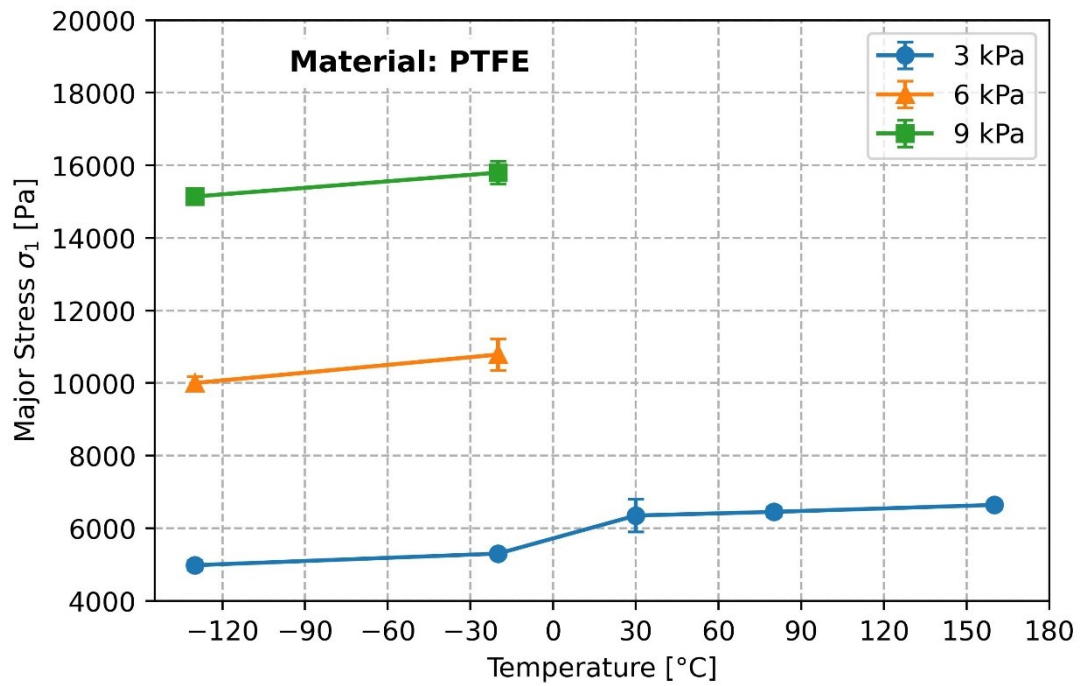
Figure 102: Major Stress σ₁ of PTFE over the temperature range -130-160 C°. Three normal stress
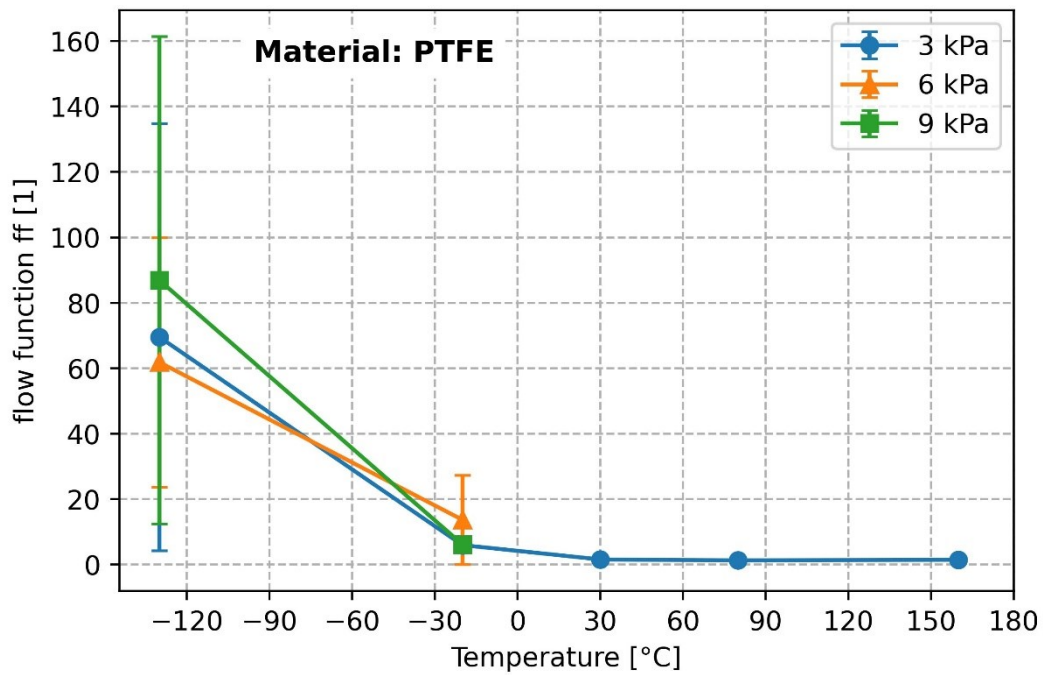levels are depicted.
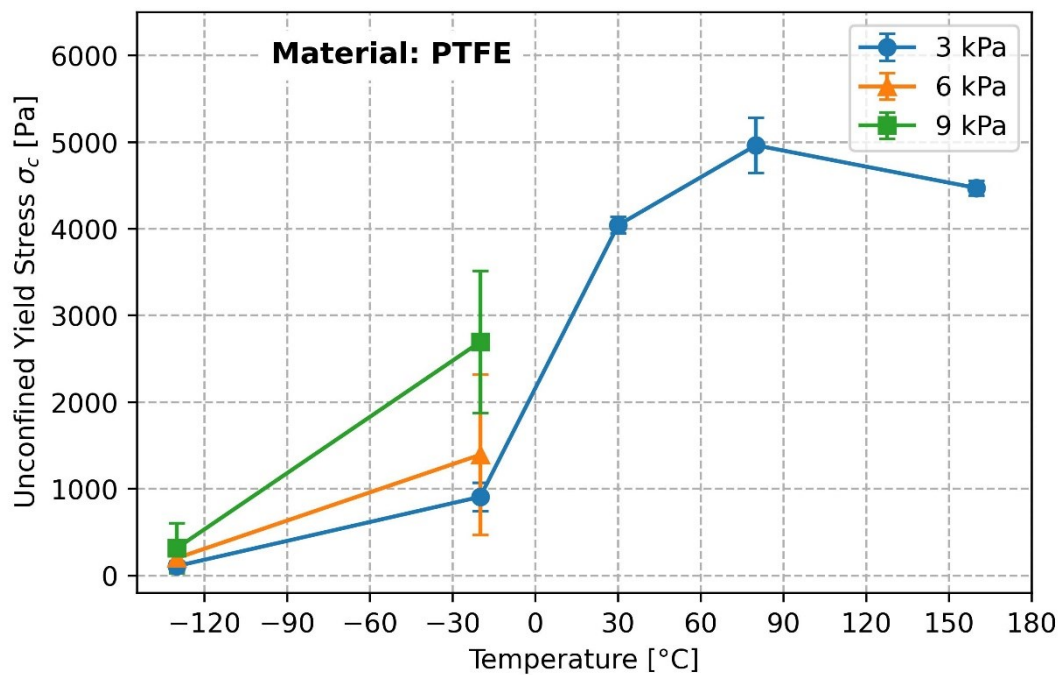
Figure 103: Major Stress σ_c of PTFE over the temperature range -130-160 C°. Three normal stress
levels are depicted.

Figure 104: Flow function ff of PTFE over the temperature range -130-160 C°. Three normal stress levels are depicted.
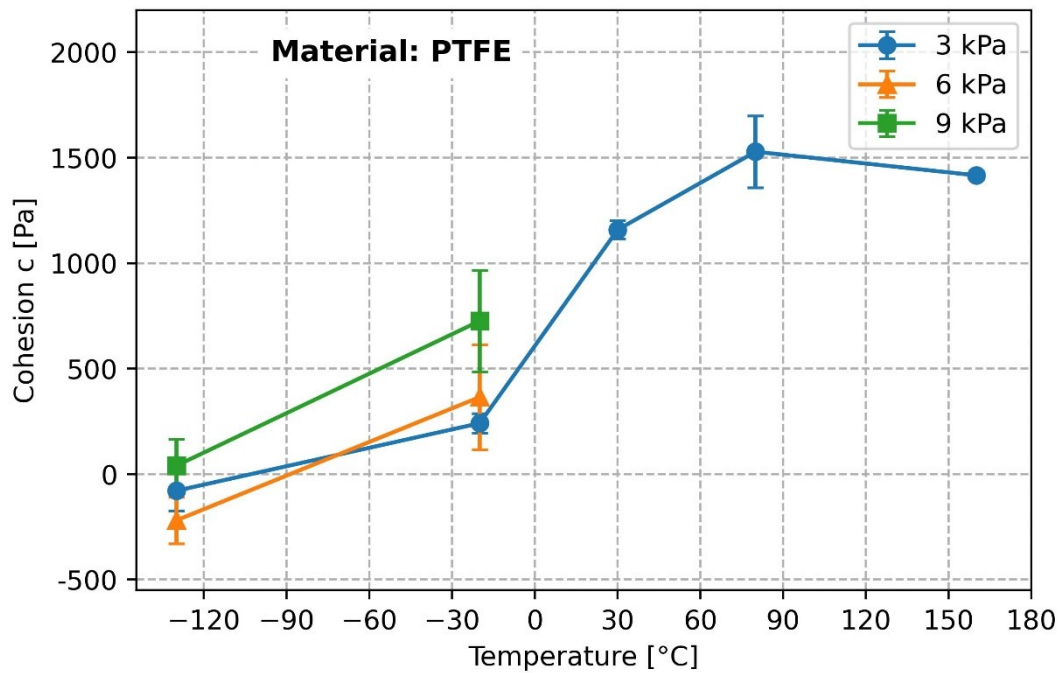

Figure 105: Cohesion c of PTFE over the temperature range -130-160 C°. Three normal stress levels are depicted.
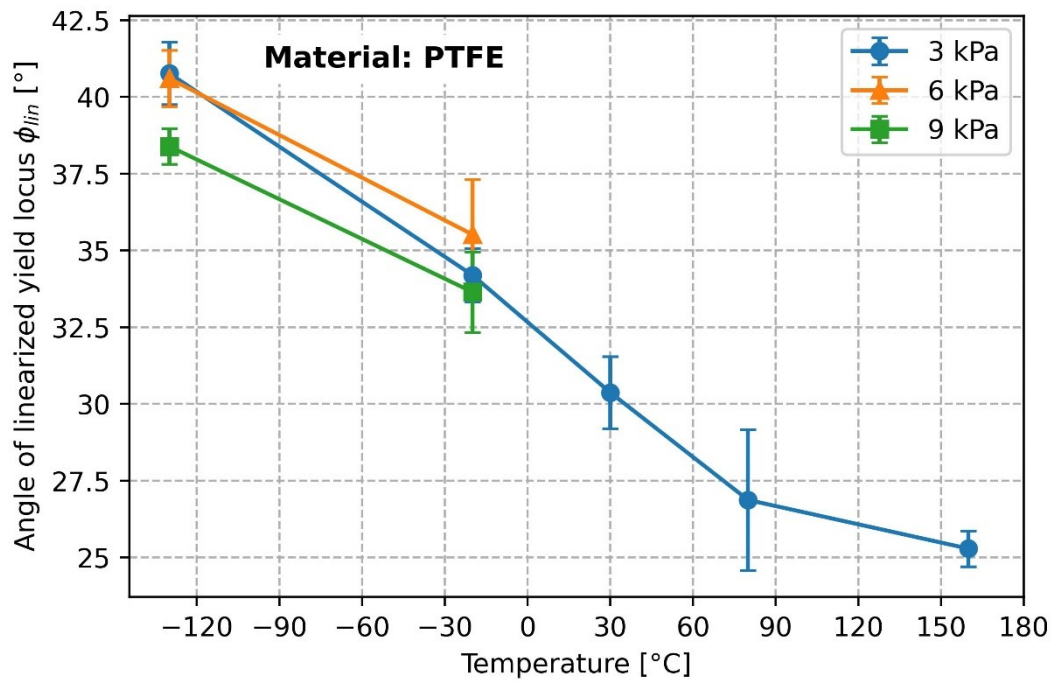
Figure 106: Angle of linearized yield locus φ_{lin} of PTFE over the temperature range -130-160 °C. Three normal stress levels are depicted
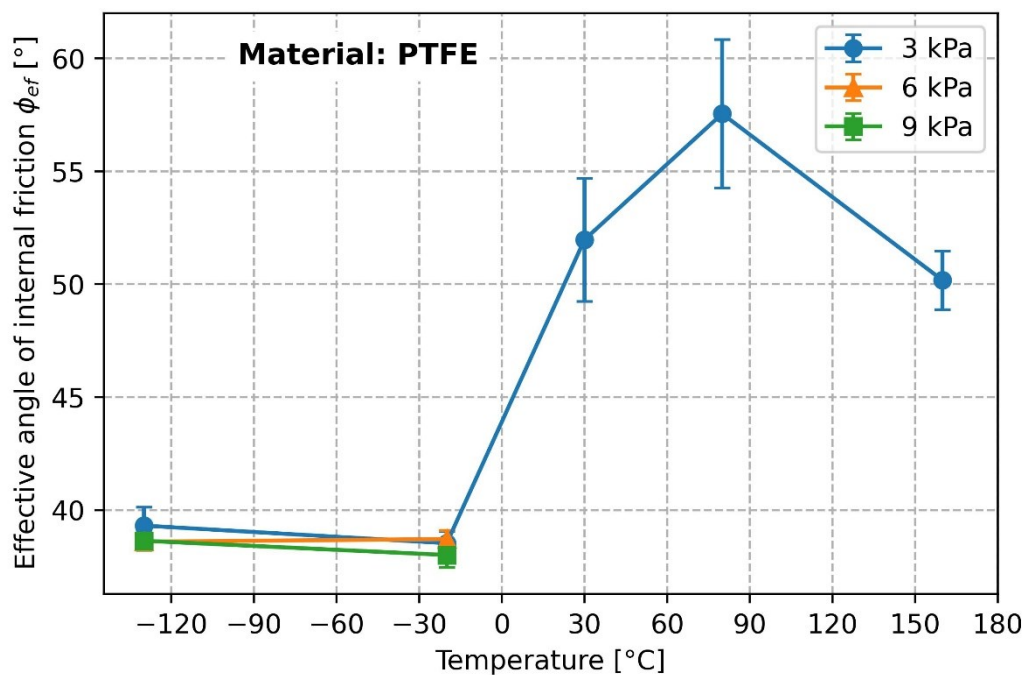

Figure 107: Effective angle of internal friction φ_{ef} of PTFE over the temperature range -130-160 °C. Three normal stress levels are depicted